Investigations to the DNA resection regulation of ion-induced DSBs in G1 cells and the resection limitations of the cells in quiescent state

Untersuchungen zur DNA Resektionsregulation an komplexen DSB in G1 Zellen und die Resektionsbeschränkung in den Zellen im Ruhezustand

Dem Fachbereich Biologie der Technischen Universität Darmstadt zur Erlangung des akademischen Grades eines Doctor rerum naturalium vorgelegte Dissertation von Diplom Biologin Tatyana Syzonenko aus Kiew

Nothing in life is to be feared,
it is only to be understood.
Now is the time to understand more,
so that we may fear less.

Marie Curie

TECHNISCHE UNIVERSITÄT DARMSTADT

Investigations to the DNA resection regulation of ion-induced DSBs in G1 cells and the resection limitations of the cells in quiescent state

Untersuchungen zur DNA Resektionsregulation an komplexen DSB in G1 Zellen und die Resektionsbeschränkung in den Zellen im Ruhezustand

Vom Fachbereich Biologie

der Technischen Universität Darmstadt

zur Erlangung des Grades

Doctor rerum naturalium

(Dr. rer. nat.)

Dissertation

von Tatyana Syzonenko

Erstgutachterin: Prof. Dr. Gisela Taucher-Scholz

Zweitgutachter: Prof. Dr. Marco Durante

Darmstadt 2018

Syzonenko, Tatyana: Investigations to the DNA resection regulation of ion-induced DSBs in G1 cells and the resection limitations of the cells in quiescent state

Darmstadt, Technische Universität Darmstadt,
Jahr der Veröffentlichung der Dissertation auf TUprints: 2018
URN: urn:nbn:de:tuda-tuprints-73560

Tag der mündlichen Prüfung: 23.01.2018

Content

List of figures

List of tables

Abbreviations:

53BP1	P53 binding protein 1
α	Alpha
A	Ampere
AG1522D	Normal human fibroblasts cell line
Alt-NHEJ	Alternative Non-homologous end joining
ATM	Ataxia-telangiectasia mutated
Appr.	approximately
APS	Amoniumpersulfat
ATP	Adenosintriphosphat
β	Beta
BLM	Bloom syndrome helicase
bp	Base pair
BRCA1	BReast CAncer type 1 susceptibility protein type 1
BRCT	BRCA1 C terminus domain
BSA	Bovine serum albumin
c	Centi/Speed of light
c.	chapter
CDK	Cyclin dependent kinase
Chk 1/2	Checkpoint kinase
c-NHEJ	Classic Non-homologous end joining
δ	Delta
D	Dose
Da	Dalton
DAPI	4′,6-Diamidin-2-phenylindol
DDR	DNA damage response
DMEM	Dulbecco's minimal essential medium
D-loop	Displacement loop
DNA	Deoxyribonucleic acid
DNA-PK	DNA-dependent protein kinase
DNA-PKcs	DNA-dependent protein kinase catalytic subunit
DSB	Double strand break
dsDNA	Double stranded DNA
E	Energy
e.g.	For example
EC	Euchromatin
ECL	Enhanced chemoluminescence

EDTA	Ethylenediaminetetraacetic acid
ELISA	Enzyme-linked immunosorbent assay
eV	Electron volt
Exo1	Exonuclease 1
F	Fluence
FCS	Fetal calf serum
FEN1	Flap endonuclease-1
γ	Gamma
Gy	Gray
h	Hour
H3K9Me3	Histone 3 lysine 9 three-methylation
H3K27Me3	Histone 3 lysine 27 three-methylation
HC	Heterochromatin
HR	Homologous recombination
HRP	Horseradish peroxidase
HUWE1	HECT, UBA and WWE Domain Containing Protein 1
IF	Immunofluorescence
IR	Ionizing radiation
IRIF	Ionizing radiation induced foci
J	Joule
k	Kilo
kb	Kilobasepair
kg	Kilogram
λ	Lambda
LET	Linear energy transfer
LMDS	locally multiply damaged sites
μ	micro
m	milli
M	Molar/Mega
min	Minute
mm	Millimeter
MMEJ	Microhomology mediated end-joining
Mre11	Meiotic recombination protein
MRN	Mre11-Rad50-Nbs1 complex
ν	Nu (frequency)
n	nano
Nbs1	Nijmegan breakage syndrome-1
NHEJ	Non-homologous end joining
OD	Optical density

R	Radius
PAGE	Polyacrylamidgelelectrophoresis
PARP	Poly(ADP-ribose) polymerase
PBS	Phosphate buffered saline
PLD	Potentially lethal damage
PLK1	Polo-like kinase 1
PLK3	Polo-like kinase 3
PTIP	Pax2 transactivation domain-interacting protein
PVDF	Polyivylidenfluorid
RBE	Relative biological effectiveness
RIF1	Rap interacting factor 1
RNA	Ribonucleic acid
RPA	Replication protein A
rpm	Rounds per minute
RT	Room temperature
S	Clonogenic survival
SD	Standard deviation
SDS	Sodium dodecyl sulfate
SEM	Standard error of the mean
SIS	Heavy ion Synchrotron
SLD	Sub-lethal damage
SRA	SET-and-RING-finger associated domain
SRR	Survival recovery ratio
SSB	Single strand break
ssDNA	Single stranded DNA
TBS	Tris buffered saline
TCA	Trichloracetic acid
TEMED	Tetramethylendiamin
u	nucleon
UHRF1	Ubiquitin-like, with plant homeodomain (PHD) and Really Interesting New Gene (RING) finger domains 1
UNILAC	Universal linear accelerator
v	velocity
v/v	Percent by volume
w/v	Weight per volume
XRCC 1/4	X-ray-complementing Chinese hamster gene 1/4

Summary

Complex DNA double-strand breaks (DSB) are the most severe DNA damage in that they represent an enormous challenge for the cell to repair faithfully as well as repairing at all. Two main repair pathways are known to repair DSBs: classical non-homologous end joining (c-NHEJ) and homologous recombination (HR). c-NHEJ is available in all cell cycle phases whereas the HR pathway functions only in S/G2 when the sister chromatid is available as a template. In addition, a further repair pathway is available to the cells – alternative non-homologous end joining (alt-NHEJ), which can operate on resected DNA break ends. DNA resection is an important step in the cell's decision as to which DSB repair pathway to choose. DNA resection takes place not only in S/G2 cells but also in G1 cells following complex DNA damage induced by heavy ion radiation. The goal of this thesis is to elucidate the mechanism of resection regulation in G1 cells after heavy ion irradiation. It specifically focuses on the role of the resection regulatory factors RIF1 and BRCA1. A useful model to study the mechanism of resection limitation are cells in quiescent state, G0 cells. In this thesis, quiescent human fibroblasts were used due to their limited resection of heavy ion- induced DSBs in comparison to proliferating human fibroblasts in G1 phase. Therefore, the further aim was to investigate the role of quiescent state compared to the proliferating state in the resection regulation after low- and high LET irradiation.

Recruitment of RIF1 to heavy ion induced DSBs in S/G2 and G1 phase cells suggested its involvement in the DNA damage response of complex DNA lesions. RIF1's recruitment to DSB sites is LET dependent in S/G2 cells. However, a direct impairment of DNA resection of ion-induced DSBs by RIF1 was not detected. An RPA-foci formation analysis upon ion irradiation in BRCA1 depleted cells, however, it showed that the RIF1 antagonist BRCA1 is involved in resection regulation of ion-induced DSBs in G1 cells. Moreover, BRCA1 depletion resulted in a strong increase of the number of RIF1 foci in G1 cells after carbon ion irradiation suggesting that RIF1 is, after all, involved in the resection regulation of heavy ion induced DSBs. This was further supported by the observation that RIF1 depletion led to an increase of the BRCA1 foci number in G1 cells.

Co-immunofluorescence staining of BRCA1 and RIF1 showed cell cycle dependent overlap of the BRCA1 and RIF1 foci, which was more pronounced in G1 than in S/G2 cells. The observed overlap of BRCA1 and RPA foci was also cell cycle dependent, yet was greater in S/G2 compared to G1 cells suggesting that BRCA1 is more active in the resection promotion after heavy ion radiation in S/G2 than in G1 cells.

UHRF1 is as an interaction partner of BRCA1 in removing RIF1 from DSBs. Therefore, UHRF1 was considered as a positive resection regulator and hence was depleted in U2OS cells to analyze its influence on resection of ion-induced DSBs. Surprisingly, UHRF1 depletion strongly decreased the fraction of resection positive G1 and S/G2 cells indicating a significant role of UHRF1 in the resection regulation of complex DSBs.

Normal human fibroblasts in G0 phase showed a smaller number of resection positive cells than fibroblasts in G1 phase. To analyze the cause of decreased resection in human fibroblasts a

protocol to enrich the cells in G1 or G0 phase was established. The biochemical characteristics of human fibroblasts in G1 and G0 phase as well as DSB repair-kinetics after X-ray irradiation showed essential differences between these two cell cycle states. The examination of repair factors that promote resection by Western analysis revealed that BRCA1 and CtIP were strongly reduced in quiescent cells. Moreover, the resection antagonists 53BP1 and Ku80, which protect the DSB ends from resection to promote c-NHEJ, were available. Interestingly, RIF1, which represents another resection antagonist, was not detectable in quiescent cells. The RIF1 downregulation is in line with its recently discovered role in the DNA replication machinery. Furthermore, together with the decreased fraction of resection positive cells after heavy ion irradiation, G0 cells showed slower repair kinetics of X-ray induced DSBs than fibroblasts in G1 phase. A 24 h post irradiation G0 cells revealed still 20 - 30 % unrepaired DSBs detected by γH2AX immunofluorescence staining whereas DSBs in G1 cells were virtually all repaired. The possibility that G0 and G1 cells utilize different DSB repair pathways was examined by using DNA-repair pathway inhibitors; a DNA-PKcs inhibitor was employed in order to inhibit c-NHEJ and a PARP inhibitor was used to inhibit alt-NHEJ. The severe repair impairment of X-ray induced DSBs by the DNA-PKcs inhibitor and the lack of influence by the PARP inhibitor indicated that the main repair pathway for both G1 and G0 cells is c-NHEJ to repair this type of damage. Interestingly, the repair kinetics of helium ion-induced DSBs in G1 and G0 cells was identical, suggesting that c-NHEJ represents the main repair pathway.

Analysis of heterochromatin marker trimethylated histone H3 at amino acids lysine 9 (H3K9Me3) and lysine 27 (H3K27Me3) suggested that G0 cells have more compact chromatin than G1 cell. This may well be the reason why G0 cells show different repair kinetics of X-ray induced DSBs compared to G1 cells, as the chromatin status influences the DSB-repair pathway choice and thus repair kinetics.

The comparative analysis by clonogenic survival assay of delayed plated G1 versus G0 cells after ionizing radiation mirrored the repair kinetics after X-ray- and heavy ion irradiation. Post X-ray irradiation G0 cells were more sensitive than G1 cells, whereas after carbon ion irradiation the G0 and G1 cells showed almost the same radiosensitivity.

Taken together this thesis showed, that both G1 and G0 cells can efficiently repair heavy ion induced damage by DNA-PKcs dependent repair pathway. However, a different chromatin structure might be a cause of slower repair kinetics in G0 cells after X-ray irradiation compared to G1 cells. A slower repair kinetics after Helium ion irradiation compared to X-ray irradiation in G1 cells suggests that G1 cells use a resection dependent c-NHEJ to repair complex DSBs.

Zusammenfassung

Komplexe DNA Doppelstrangbrüche (DSB) zählen zu den schwerwiegendsten DNA Schäden. Die Zellen können die DSB über zwei Hauptreparaturwege: die klassische nicht-homologe End-Verknüpfung (c-NHEJ, engl. *classic non-homologous end joining*) und die homologe Rekombination (HR) reparieren. C-NHEJ ist in allen Zellzyklus-Phasen verfügbar, während die homologe Rekombination nur in S/G2-Zellen zur Verfügung steht, wo die Schwesterchromatiden als Vorlagen dienen. Des Weiteren besitzen die Zellen einen alternativen DSB-Reparaturweg – die alternative nicht homologe End-Verknüpfung (alt-NHEJ, engl. *alternative non-homologous end joining*). Dieser Reparaturweg kann auch resektierte DSB-Enden verknüpfen. Durch die initiale DSB-Resektion wird über die Auswahl des Reparaturweges entschieden. Aktuelle Studien zeigen, dass die DSB-Resektion nicht nur in S/G2- sondern auch in G1-Zellen nach Schwerionenbestrahlung auftritt. Das Ziel dieser Arbeit ist den Mechanismus der Resektionsregulation an den DSB nach Schwerionenbestrahlung in G1-Zellen weiter aufzuklären. Dabei stand die Rolle der Resektionsfaktoren BRCA1 und RIF1 im Vordergrund.

Es konnte gezeigt werden, dass RIF1 zu schwerioneninduzierten DSB rekrutiert wird, was auf eine Beteiligung an komplexen DNA Schäden hinweisen könnte. Außerdem zeigte sich eine LET-Abhängigkeit der RIF1-Rekrutierung an DSB in S/G2-Zellen. Ein direkter Einfluss von RIF1 auf Resektion nach Herunterregulierung der RIF1-Expression durch RNAi war jedoch nicht nachweisbar. Eine RNAi-basierter Knockdown der BRCA1-Expression hingegen reduzierte Resektion in S/G2- und G1-Zellen. Eine erhöhte Anzahl an RIF1-Foci in BRCA1-Knockdown-Zellen deutete indirekt auf einen Einfluss von RIF1 auf DSB-Resektion nach Kohlenstoffbestrahlung hin. Die antagonistische Wirkung von BRCA1 und RIF1 zeigte sich weiterhin im Anstieg der BRCA1-Foci nach Kohlenstoffbestrahlung in G1- und S/G2-Zellen, deren RIF1-Expression durch RNAi herunterreguliert war.

Kolokalisationsanalysen in Immunfluoreszenzfärbungen mit BRCA1 und RIF1 zeigten eine Überlagerung der Signale, wobei die Ausprägung dieser Überlagerung in G1- stärker als in S/G2-Zellen war. RPA und BRCA1 zeigten ebenfalls eine Überlagerung der Fluoreszenzsignale, wobei hier die Ausprägung der Überlagerung in S/G2- größer als in G1-Zellen war. Dieses könnte ein Hinweis darauf sein, dass BRCA1 aktiver in der Resektionsregulation in S/G2- als in G1-Zellen ist.

UHRF1 ist ein BRCA1-Interaktionspartner und agiert an den DSB und ist verantwortlich dafür RIF1 vom Schaden zu entfernen. In dieser Arbeit konnte gezeigt werden, dass UHRF1-Knockdown sowohl die Fraktion resektionspositiver S/G2- als auch G1 Zellen nach Schwerionenbestrahlung reduzierte. Dieses Ergebnis zeigt, dass UHRF1 in der Resektions-regulation an den komplexen DSB beteiligt ist.

Es wurde ein kleinerer Anteil der resektionspositiven Zellen nach Schwerionenbestrahlung in humanen Fibroblasten in G0-Phase im Vergleich zu G1-Phase gezeigt. Die Untersuchungen der Reparaturfaktoren und der Reparaturkinetik der DSB nach Röntgenbestrahlung zeigen deutliche Unterschiede zwischen humanen Fibroblasten in G0- und in G1-Phase. Die positiven

Resektionsfaktoren BRCA1 und CtIP waren in G0-Zellen kaum vorhanden. Die Resektionsantagonisten 53BP1 und Ku80, welche die DSB-Enden gegen Resektion schützen, waren vorhanden. Hingegen war der resektionsantagonistische Faktor RIF1 in G0-Zellen nicht nachweisbar.

Neben der verminderten Resektion zeigten die G0-Zellen eine verlangsamte Reparatur-kinetik im Vergleich zu G1-Zellen. 24 Stunden nach der Röntgenbestrahlung zeigten G0 Zellen in einer γH2AX- Immunfluoreszenzfärbung immer noch 20 - 30 % nicht-reparierte DSB, während die DSB in G1-Zellen fast vollständig repariert wurden. Die Frage, ob dieser Unterschied auf der Verwendung unterschiedlicher Reparaturwege in G0- bzw. G1-Zellen beruht, wurde mit geeigneten Inhibitoren gegen c-NHEJ bzw. alt-NHEJ überprüft. C-NHEJ-Inhibition, aber nicht alt-NHEJ-Inhibition, beeinträchtigte die DSB Reparatur deutlich. Den Hauptreparaturweg nach Röntgenbestrahlung sowohl in G0 als auch in G1-Zellen stellt daher der c-NHEJ dar. Im Gegensatz dazu, war die Reparaturkinetik nach der Heliumbestrahlung in G1- und G0-Zellen identisch. Der Hauptreparaturweg war ebenfalls c-NHEJ.

Die Charakterisierung der Chromatinverdichtung mit den Heterochromatinmarkern trimethyliertes Histon H3 an der Aminosäuren Lysin 9 (H3K9Me3) und Lysin 27 (H3K27Me3) deutete darauf hin, dass G0-Zellen eine höhere Chromatinkompaktierung als G1-Zellen aufweisen. Da der Chromatinzustand die Auswahl des DSB-Reparaturweges und somit auch die Reparaturkinetik beeinflusst, kann der Unterschied in der Chromatinkompaktierung zwischen G0- und G1-Zellen ein Grund für die unterschiedliche Reparaturkinetik sein.

Um die Qualität der DSB-Reparatur zu untersuchen, wurden die G1- und G0-Zellen in einem Zellüberlebensexperiment quantitativ analysiert. Die so erzielten Ergebnisse sind im Einklang mit der Reparaturkinetik nach Röntgen- und Schwerionenbestrahlung. Dabei hatten G0-Zellen 24 Stunden nach der Röntgenbestrahlung eine höhere Strahlenempfindlichkeit als G1-Zellen, während die Strahlenempfindlichkeit nach Kohlenstoffbestrahlung bei beiden vergleichbar war.

Zusammenfassend konnte es in dieser Arbeit gezeigt werden, dass die G0- und G1-Zellen eine effiziente Reparatur nach Schwerionenstrahlung durchführen können, wobei beide einen DNA-PKcs-abhängigen Reparaturweg benutzen. Hingegen, könnte der Unterschied in der Chromatinstruktur ein Grund für die verlangsamte Reparaturkinetik nach Röntgenbestrahlung in G0-Zellen im Vergleich zu G1-Zellen sein. Die langsame Reparaturkinetik nach Heliumionenbestrahlung könnte im Vergleich zu Röntgenbestrahlung in G1-Zellen am resektionsabhängigen c-NHEJ liegen.

1. Introduction

Since DNA is a carrier of all genetic information it is essential for the cells to maintain its integrity in order to give this information to the next generation correctly. Constantly exposed to damaging factors DNA can accumulate toxic lesions leading to mutations, cell death and even tumor formation (Jackson and Bartek 2009). To prevent the passing of compromised DNA to the next generation the cells evolved a sophisticated system of repair pathways which maintain DNA integrity. DNA damaging agents can be categorized in two groups: endogenous and exogenous. The endogenous damaging agents are metabolic oxidative stress and replication whereas exogenous agents are ionizing radiation or chemotherapeutics (Ames 1989). Ionizing radiation such as X-ray and heavy-ion radiation is applied for tumor therapy. The therapy with heavy charged particles was proven to be very effective for deep located tumors (Kraft 1990, Kramer, Weyrather et al. 2003). The radiation risk of charged particles is also an essential issue for the human space exploration (Cucinotta and Durante 2006). Hence, it is important to investigate the impact of ionizing radiation and in particular of charged particle radiation on biological target. The most severe DNA damage induced by ionizing radiation are DNA double strand breaks (DSBs). Furthermore, the heavy charged-particle induced DSBs are related to clustering of different DNA lesions in close proximity and hence are more difficult for the cell to repair (Goodhead 1994). These severe DNA damages - described as complex DNA damage - are a subject of investigation of this work.

1.1. Physical characteristics of ionizing radiation

The interaction of ionizing radiation with matter leads to excitation or to ionization. In the state of excitation, the electron is merely raised to a higher energy level while the radiation provides enough energy to repel one or more electrons from the atom shell. This process is called ionization and the radiation which provides enough energy is called ionizing radiation. The energy, which is released per ionizing event is approximately 33 eV which is more than enough to break covalent bonds, as the energy of a carbon-carbon bond is approximately 4.9 eV. Ionizing radiation includes various types of radiation when interacting with matter provides energy high enough to hit electrons from the atom shell. Ionizing irradiation is classified either as electromagnetic or particulate. The electromagnetic waves that contain as much energy as energy is released per ionizing event are X-rays with a wave length of approximately $\lambda \sim 10^{-8}$ m (Hall 2012). These waves move with speed of light (3×10^{8} m/s), which is defined in equation (1.1):

$$c = \lambda \cdot f \qquad (1.1)$$

c : speed of light [m/s]

λ : wave length [m]

f : frequency [s^{-1}]

The energy of photon is defined in equation (1.2):

$$E = h \cdot f \qquad (1.2)$$

E : energy

h : Planck constant

f : frequency

The corresponded photon energy is approximately 124 keV which exceeds the required energy to break a covalent bond of biological molecules.

The second type of ionizing radiation is particle radiation which includes electrons, protons, neutrons, alpha-particles and heavy ions. They are part of galactic cosmic rays (GCR) and sun flares emerged from nuclear decay. They can also be artificially generated at the GSI accelerator facility.

The absorption of these two types of radiation can be further classified in directly ionizing and indirectly ionizing radiation. Particle radiation is directly ionizing since the particles provide enough kinetic energy to break covalent bonds of relevant biological molecules such as DNA. In contrast, electromagnetic X-ray radiation is indirectly ionizing as they do not break the chemical bonds, rather by absorption in matter produces fast electrons that in turn can break the chemical bonds of biological relevant molecules.

The absorption of radiation by matter depends on a photon's energy; it can interact with matter in different ways. When its energy is low (up to 10 keV in water) there is predominately a photoelectric effect (Figure 1.1). The photon transfers its energy completely to matter by interacting with a tightly bound orbital electron of an atom. This electron is ejected from its shell with a kinetic energy passed from incident photon minus its binding energy. This fast electron produces further ionization events in matter. The vacancy left in the atomic shell is filled by another electron from outer shell. The difference in energy is emits as electromagnetic radiation of very low energy photons.

The Compton scattering occurs by high photon energy (from appr. 60 keV in water) (Figure 1.1). The photon energy is partially transferred to matter by interacting with an electron in the outer shell of an atom. The lower energy photon, which is deflected from its original direction, proceeds with reduced energy. The ejected electron from the outer shell can produce further ionizing event in matter.

At very high photon energies (from appr. 10 MeV in water) a process referred to as pair production appears (Figure 1.1). In this case, the photon's energy, which is converted into a

particle mass in close proximity of the atomic nucleus, is radiated as an electron and a positron, which are usually of high energy producing further ionizing events in matter as well.

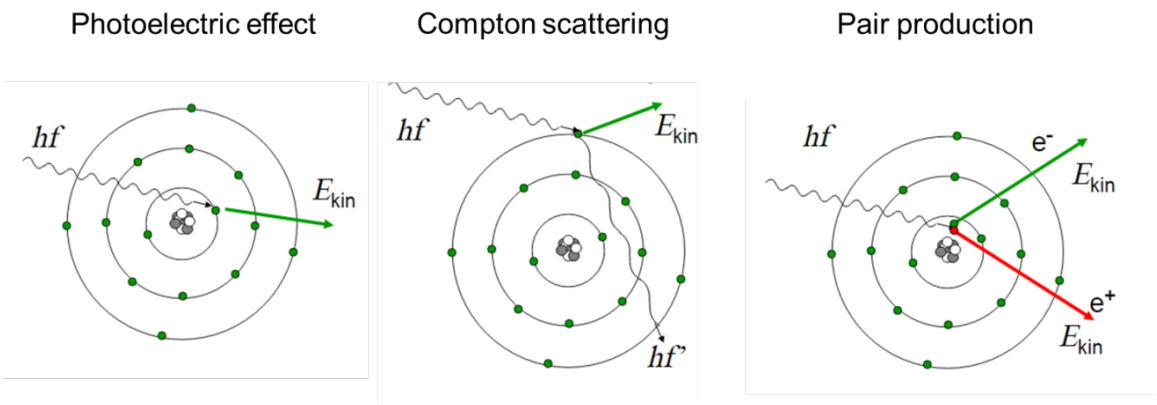

Figure 1.1: Mechanisms of energy transfer by interaction of photons with matter. The energy can be transferred in dependence of the photon energy in three different ways. Photons with low energy transfer its energy by the photoelectric effect. Photons with higher energy (60 keV – 10 MeV) transfer their energy by the Compton Effect where the photon of high energy hit an electron from the outer atom shell. The electron absorbs a portion of photon energy. The photon moves along on its path with reduced energy. By interaction with photon produced fast electron can break chemical bonds on its way and it is expressed as biological damage. At very high photon energy (from 10 MeV) the energy transfer enters as pair production. Electron-positron pair appears from the high photon energy. [Image source: http://slideplayer.org/slide/10468855/]

The photon absorption is not only dependent on the photon energy but also on the nature of absorber. The higher the atomic number the more often the photoelectric effect appears (Figure 1.2).

The sensitive biological target that is principally damaged upon exposure to ionizing radiation is DNA. The absorbed radiation of any form has two possibilities to produce DNA lesions: by direct action or indirect action (Figure 1.3).

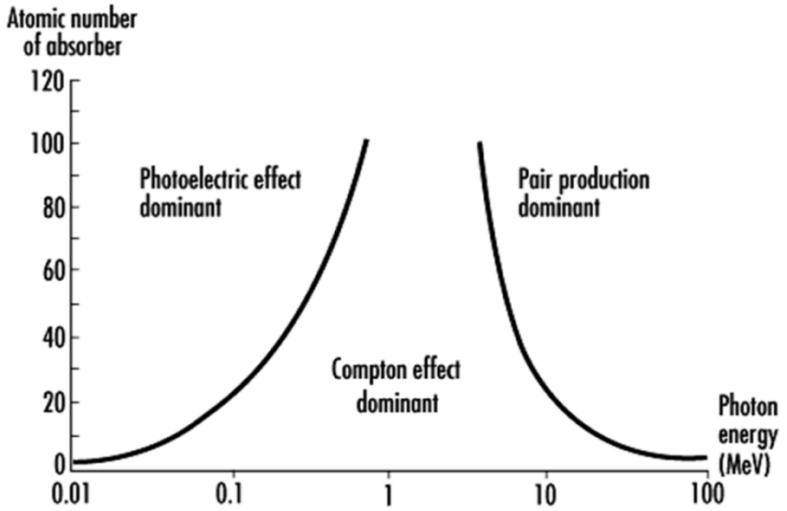

Figure 1.2: Total absorption of the photon energy by matter. Distribution of the energy absorption of different transfer mechanisms is photon energy dependent. [Image source: http://www.ilocis.org/documents/chpt48e.htm].

The sparsely ionizing radiation (e.g. X-rays) usually acts indirectly producing free radicals from the environment molecules (mostly water molecules) resulting with high reactive, charged free radicals. The dominant process for dense ionizing particle radiation is direct action. The atoms of target molecule itself are directly ionized and damaged.

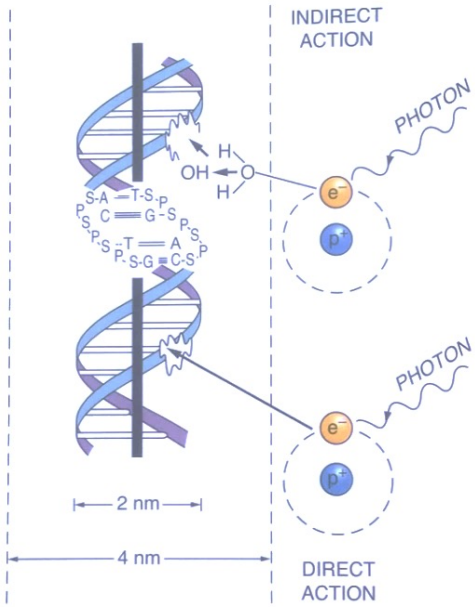

Figure 1.3: Direct and indirect action of radiation on the DNA. In direct action, a secondary electron appearing from photon energy hits directly DNA molecule producing breaks in chemical bonds. In indirect action, secondary electron interacts with environment molecules (e.g. water molecules) producing free radicals, which are chemical active and react very fast with DNA molecule yielding DNA lesions [image source (Hall 2012)].

The radiation energy which is absorbed by matter is referred to as the radiation dose (D). The absorbed dose is defined as deposited energy (E) per unit mass (m). Equation 1.3 defines absorbed dose:

$$D = \frac{E}{m} \qquad (1.3)$$

D: dose [Gy]

E: energy [J]

m: mass [kg]

The unit of absorbed dose is [Gy] and is defined as the deposition of 1 J in 1 kg: 1 Gy = 1 J kg^{-1}.

The distribution of the energy deposition of photons (X- and γ-rays) and charged particles (protons, alpha-particles and heavy ions) is fundamentally different. The energy deposition of X-rays is evenly distributed within the irradiated area and is called sparsely ionizing radiation (Figure 1.4). The energy deposition of heavy ion radiation is tightly concentrated along the ion track; therefore, it is densely ionizing irradiation (Figure 1.4).

The dose decreases within the ion's track from the center to periphery with distance square $1/r^2$ (r – radius of the ion track). In the center of ion track, the dose is very high and decreases on the periphery of the ion track. Equation 1.4 defines maximum range of the δ-electrons:

$$R_{max} = 0.05 \cdot E^{1.7} \qquad (1.4)$$

R_{max} : max range of e^- [μm]

E : energy of ions [MeV/u]

That means that the low energy particles produce secondary electrons with a very low range. Whereas the reverse is true for particles with high energy - the range of their secondary electrons is wider, even if the dose in their ion track core is lower than that of the lower energy particles.

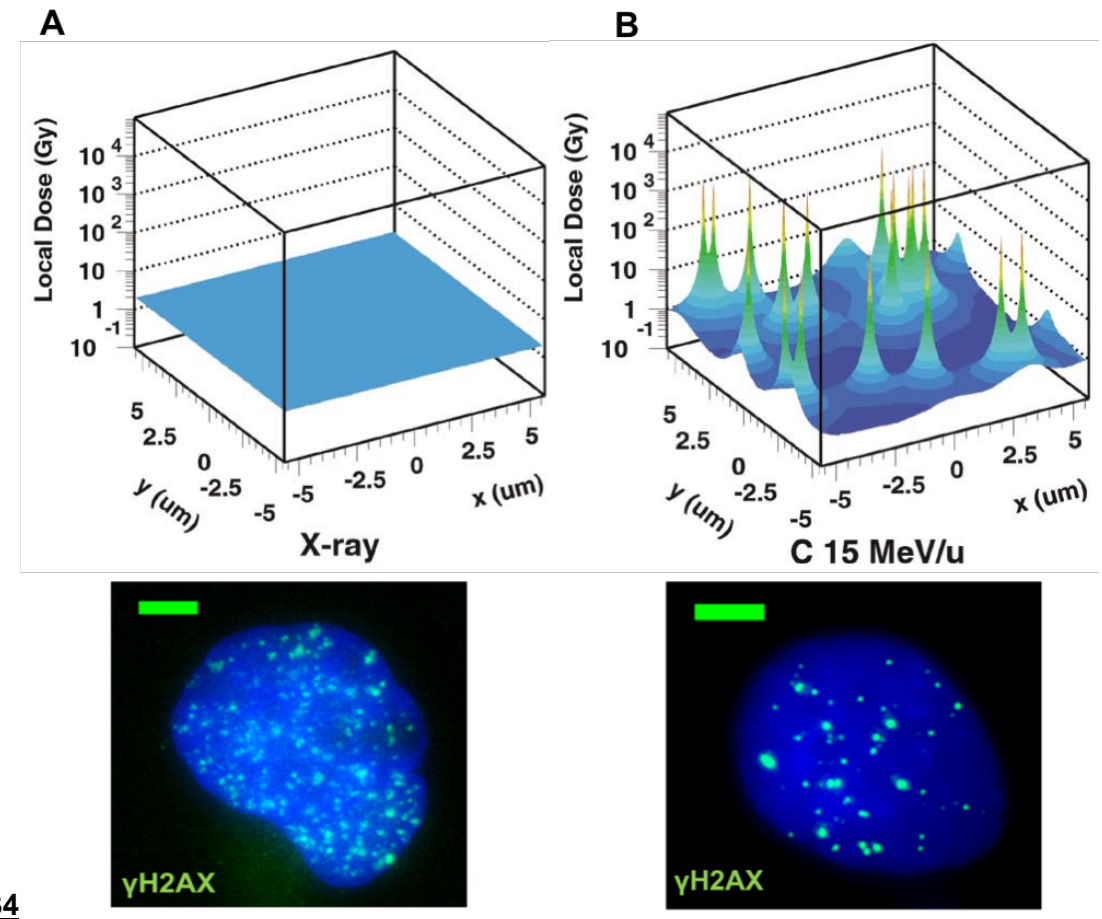

1234

Figure 1.4: Dose deposition on the microscopic level of photons and carbon ions. The image shows a dose deposition profile of X-ray- and carbon ion radiation of the same dose of 2 Gy. **A**: The dose is homogeneously distributed within an irradiated area (e.g. a cell nucleus, bottom) after X-ray (photons) radiation. **B:** Upon heavy ion radiation, the dose distribution is very inhomogeneous. The predominated area of a nucleus of an irradiated cell is not hit by ion (bottom), whereas local dose within ion track is high. DNA is depicted in blue; γH2AX is a DSB marker (green); scale bar 5 µm. [Graphs are from (Krämer, 2003)].

The distribution of ionizing events and the energy deposition within ion track is described with the term of linear energy transfer (LET). LET is defined as energy deposition per unit penetrated depth in matter. LET is dependent on the energy and charge of a particle and described in equation 1.5 (Bethe 1930, Bloch 1933):

$$\mathrm{LET} = \frac{\mathrm{E(keV)}}{\mathrm{dx(\mu m)}} \propto \frac{\mathrm{Z_{eff}^2}}{\beta^2} \qquad (1.5)$$

LET : linear energy transfer [keV/µm]

E : ion energy [keV]

x : distance [µm]

Z_{eff} : charge projectile;

β : relative projectile speed: $\beta = \frac{v}{c}$; v – velocity and c – speed of light

The penetration of a particle in matter is dependent on the kinetic energy of the particle. The higher the particle's energy the deeper it penetrates into the matter and the less it interacts. When the particle loses energy, by traversing the matter, it eventually stops and the remaining energy is released. At a certain depth, the interaction between particle and matter increases as a result of particle energy and velocity decrease. Thus, the LET of a particle increases with penetration providing the highest local dose. The point of a highest dose deposition is referred to as Bragg peak (Figure 1.5). After Bragg peak, the particle stops very quickly loosing charge and energy. Heavy ions are characterized through their special dose-depth profile (Figure 1.5). Moreover, heavy ions generate lots of δ-electrons within their path which produce additional ionizing events damaging DNA more severely (Figure 1.5).

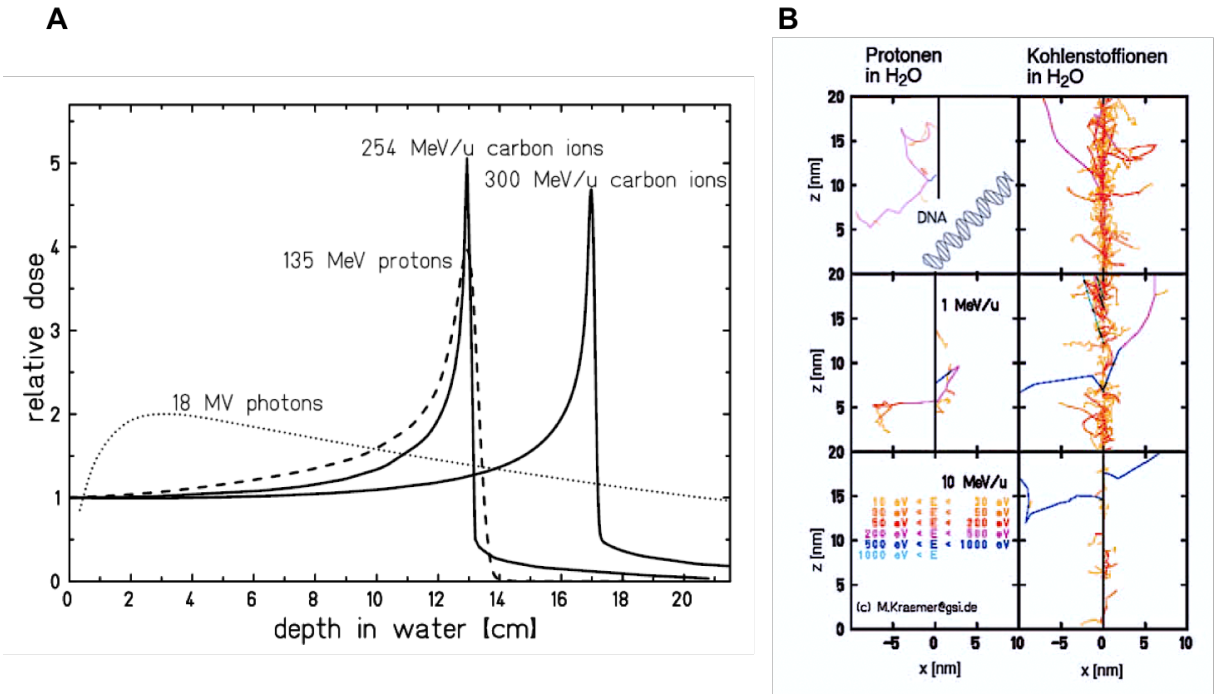

Figure 1.5: A: Depth-range profile of photons and carbon ions of different energies. These characteristics of ions are an advantage in contrast to photons using the tumor therapy, as they deposit low energy in the healthy tissue in the entering channel, but high energy in the tumor core. In contrast, photons provide much more damage to healthy tissue located proximate to the tumor due to their dose-depth profile. Photons release their energy by entering in matter. In contrast, carbon ions have a low energy deposition in the entering channel and high peak shortly before coming to stop. (Weyrather and Debus 2003) **B: Track structure of protons and carbon ions.** Compared to protons, the track structure of carbon ions shows much higher density of ionizing events along the track. The density of ionizing events in a carbon ion track is increased with the depth of penetration (Kraft 2007).

It is important to know the applied dose when using heavy ions in tumor therapy. The applied dose calculation based on the LET and the fluence (F, number of ions per cm^2) is represented in equation 1.6:

$$\mathrm{D(Gy)} = 1.602 \cdot 10^{-9}\left(\frac{\mu m \cdot g \cdot J}{keV \cdot cm \cdot kg}\right) \cdot \mathrm{F}\left(\frac{1}{cm^2}\right) \cdot \mathrm{LET}\left(\frac{keV}{\mu m}\right) \cdot \frac{1}{\rho}\left(\frac{cm^3}{g}\right) \qquad (1.6)$$

Whereas the main component of biological tissue is water, therefore for the density of a biological target the density of water 1 g/cm^3 is used.

1.2. Induction of DNA damage

Ionizing radiation interacts with water molecules when entering biological tissue and thereby generates reactive oxygen species (ROS). An electron is repelled from a water molecule generating a water cation, which reacts with the neighboring water molecule and produces hydronium-cations and hydroxyl-radicals:

$$H_2O \rightarrow H_2O^+ + e^-$$

$$H_2O^+ + H_2O \rightarrow H_3O^+ + OH\cdot$$

The hydroxyl-radicals and other radicals that might be produced with ionizing radiation migrate within the cell in few nanometer range and damage the essential molecular structures in the cell, such as DNA (Hall 2012). The amount of DNA damage derived from ROS is dependent on LET and environment. The with sparsely ionizing radiation produced ROS induces approximately 70 % of DNA damage (Chapman, Reuvers et al. 1973). With increasing LET the fraction of DNA damage induced by ROS decreases (Hirayama, Ito et al. 2009). Treating cells with DMSO (Dimethylsulfoxid), which is a radical scavenger, reduces the portion of indirectly induced DNA damage. On average, radiation with 1 Gy X-rays produces appr. 40 double strand breaks (DSBs), 1000 single strand breaks (SSBs) and >1000 base damages (Ward 1988, Hall 2012). Nevertheless, cells can repair these kinds of damages. However, another type of damage induced by high LET radiation – which is referred to as complex DNA damage - is a challenge for cells to repair (Hada and Georgakilas 2008). These damages are classified as clustered damages (Goodhead, Thacker et al. 1993) or locally multiple damage sites (LMDS) (Ward 1994) and are defined through localization of two or more DSBs within one to two double helix turns. Two SSBs in spatial vicinity usually convert to a DSB. The clustered DNA damage is difficult for the cells to handle compared to spatially separated damages.

The different impact of densely ionizing radiation compared to sparsely ionizing radiation can be seen in survival curves of irradiated cells (Figure 1.6). The survival curve after carbon ion irradiation is steeper than the curve after X-ray irradiation. Thus, the irradiation with heavy ions has a higher relative biological effectiveness (RBE). RBE is defined as the ratio of the reference radiation dose, generally X-ray irradiation (D_γ) to the heavy ion irradiation dose (D_I) by which the same biological effect is achieved (equation 1.7):

$$\mathrm{RBE} = \frac{D_\gamma}{D_I}\Big|_{isoeffect} \qquad (1.7)$$

Figure 6 shows RBE of survival curves after irradiation with different doses of carbon ions or X-rays. As RBE depends on the linear-quadratic X-ray dose-effect curve, it is high for low dose and decreases with increasing dose. With increase of the atomic number the RBE value, however, is not necessarily increased. To adjust the dose of high LET ions their fluence must be decreased and hence, less cells can be irradiated. The targeted cells receive much higher dose than is needed for cell inactivation; thus, the effectiveness of ion radiation therapy decreases. The RBE depends on several different factors such as dose fractionation, oxygen concentration in the tissue and the cell cycle.

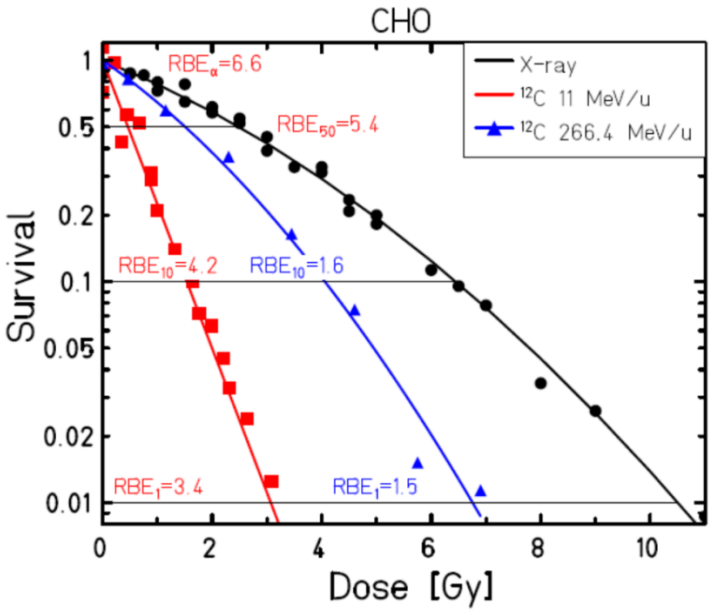

Figure 1.6: Relative biological effectiveness (RBE). Survival curves of a hamster cell line (CHO-K1) irradiated with carbon ions of different LET or X-rays. A given dose of carbon ion irradiation has a much stronger effect than the same dose of X-ray radiation. RBE depends on chosen reference value and the linear-quadratic shape of X-ray dose-effect curve. RBE decreases from 5.4 of 50 % survival to 3.4 of 1 % survival. RBE decreases also with increasing dose of carbon ion radiation [Image source (Kramer, Scifoni et al. 2012)].

1.3. Cell cycle

An important biological paradigm postulated by R. Virchov (1855) is "*Omnis cellula e cellula*", states each new cell originates from a pre-existing cell (Schultz 2008). How two daughter cells emerge from one cell is strictly organized on the so-called cell cycle. The DNA content is doubled only one time during cell cycle. In S-phase of the cell cycle cells start to synthesize the DNA (Figure 1.7). When the replication of DNA is completed the cells enter the G2 phase. In this phase, the cells grow and prepare for dividing, which occurs in M-phase. Here, from one cell originate two daughter cells (G1 phase) with completely identical genetic material. Depending on the environment, nutrition availability and genetic program, the cells continue to grow and to proceed to the cell cycle or they escape the cell cycle and

stop dividing. This state is called G0 phase or resting phase (Alberts 2002). Three different types of the resting phase can be discriminated: first the quiescent state induced by lack of nutrition or genetic programming, second the cell is differentiated and third, the cell is in G0 because of senescence and cannot divide anymore (Yao 2014).

The cell cycle in mammalian cells is a highly regulated process that involves coordinating work of several proteins. When the cells are exposed to DNA damage they arrest their cell cycle processes to gain time for the repair of damaged DNA. The organized interruption occurs at defined sites of the cell cycle, so called “check points”. It is known two check points during the cell cycle G1/S and G2/M; as well as one during S-phase and one during metaphase (M-phase), the actual dividing step (Figure 1.7) (Deckbar, Jeggo et al. 2011).

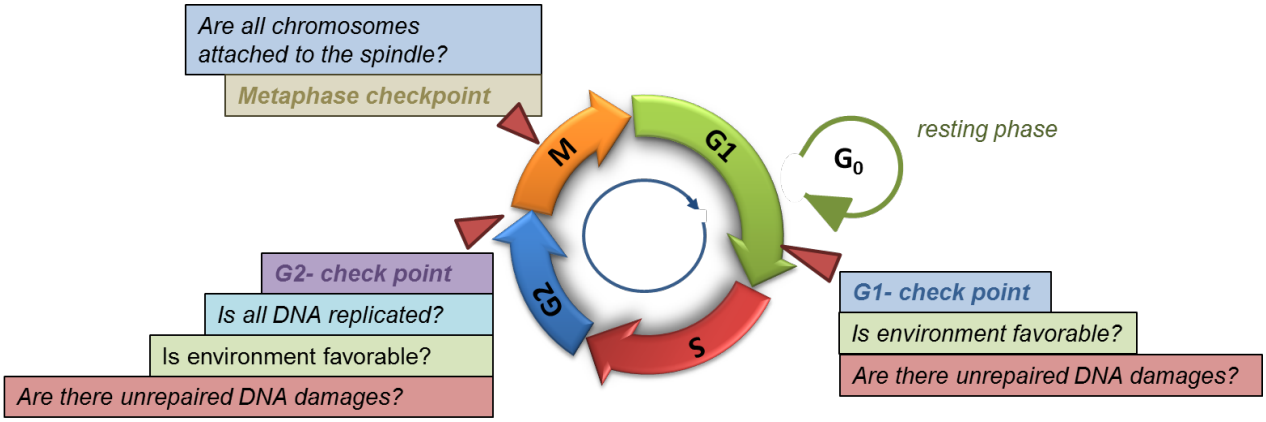

Figure 1.7: Cell cycle of eukaryotic cell and the control system within it. Every cell of eukaryotic organism goes through different phases (G1, S, G2 and M) until it divides into two new daughter cells. Each phase of the cell cycle has a control system (check points) to allow the cell progress within the cell cycle. The cell can exit the cell cycle and proceed in G0 phase, which is also called resting phase.

Most of the human body’s cells persist in a non-proliferating state, G0, outside of the cell cycle (Figure 1.7). Some of these cells cannot re-enter the cell cycle because of senescence or terminal differentiation. A subset of these cells is able to re-enter the cell cycle, these cells are identified as quiescent cells (Figure 1.8). Examples for quiescent cells in the human body are progenitor cells, fibroblasts, lymphocytes, hepatocytes and some epithelial cells (Yao 2014). These cells are fundamental for the mammalian organism to maintain the tissue homoeostasis, its renewal and regeneration. The quiescent state was also shown to be important for stress and toxicity protection in long living organisms (Legesse-Miller, Raitman et al. 2012). For a long time the quiescent state was underestimated as merely passive cellular state, lacking proliferating activity. Yet, recent studies have shown that the quiescent cells are transcriptionally and metabolically active (Liu, Adler et al. 2007, Lemons, Feng et al. 2010).

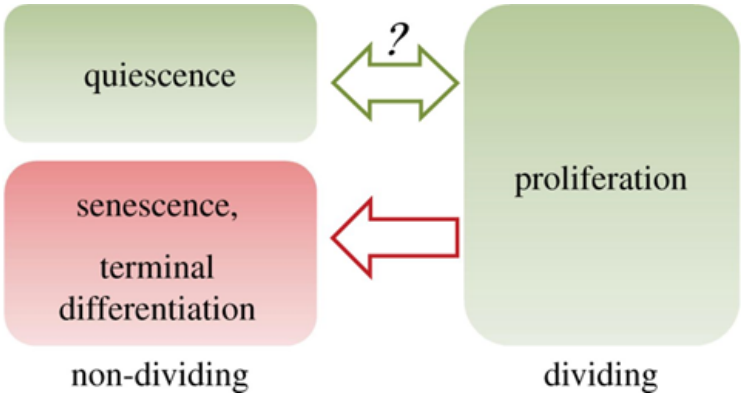

Figure 1.8: The quiescent state differs from other non-proliferating states of the cell as cells can re-enter G1 phase and thus proliferation [image (Yao G., 2014)].

The quiescent cells (G0) are comparable with the cells in G1 phase. G0- like G1 cells originate from M-phase and contain non-replicated DNA content. After re-entering the cell cycle, G0 cells can proceed with entering in S-phase like G1 cells. The distinct characteristic of G0 cells is the significant delay in re-entering in S-phase compared to G1 cells (Zetterberg and Larsson 1985). Moreover, the epigenetic regulation like DNA methylation and histone modification in the quiescent state might modify the chromatin state according to the gene expression (Turner 2007). The unique methylation state and chromatin structure helps the quiescent cells maintaining reversibility into the cell cycle and helps preventing terminal differentiation and senescence (Shrivastav, De Haro et al. 2008).

The quiescent state and its reversibility into the proliferating state in response to environmental signals is very important for the functioning of many tissue types of the human body (Yao 2014). The knowledge about DNA damage response and the DSB repair pathway choice in quiescent cells might be crucial for new therapeutic strategies in cancer particle therapy.

1.4. DNA double strand break repair pathways

DNA double strand breaks are the most severe DNA lesions within the cell. They can occur directly or indirectly by two single strand breaks in close vicinity. They are detrimental to the cell because they can induce genome rearrangements and cell death and are major source of cancer (Aparicio, Baer et al. 2014). To preserve genome integrity, cells evolved several DSB repair mechanisms, of which classical non-homologous end joining (c-NHEJ) and homologous recombination (HR) represent the two most prominent (Figure 1.9). The repair pathway choice is dependent on cell cycle, chromatin structure and complexity of DSBs (Kakarougkas A 2014)

C-NHEJ operates very fast, the two ends of broken DNA in the proximity are joined within a few minutes. This pathway functions in all cell cycle phases in higher eukaryotes (Rothkamm, Kruger et al. 2003). The essential component of this pathway is DNA-PK complex which contains DNA-PKcs, Ku70 and Ku80. The further complex which is important for NHEJ is the LIG4/XRCC4/XLF complex (Wang, Zeng et al. 2001).

The c-NHEJ pathway is considered as an error prone pathway, because the repair process involves processing of the DNA ends at the break sites which can lead to deletions of nucleotides and/or nucleotide exchanges (Betermier, Bertrand et al. 2014). Another problem of the repair by c-NHEJ occurs when the joined DNA ends do not originate from the same DSB. Consequently, chromosomal translocations can occur. Nevertheless, because of the fast rejoining of broken DNA ends the c-NHEJ is considered as the guardian of genomic stability and a suppressor of carcinogenesis (Ferguson, Sekiguchi et al. 2000, Iliakis, Wang et al. 2004).

The second main DSB repair pathway is HR. In contrast to NHEJ, it is very slow, involves more steps and repair factors. HR requires a homologous DNA sequence to remove DSB and restore DNA sequence. The homologous DNA sequence is available after DNA replication; thus, the HR repair pathway is restricted to S- and G2 phases of the cell cycle (San Filippo, Sung et al. 2008). The initial step of HR is resection (Figure 1.10). DNA resection is an enzymatic degradation of one strand at the end of double stranded DNA producing single stranded DNA in order to search for homology (West 2003).

The single stranded DNA is protected from enzymatic degradation by replication protein A (RPA), which is commonly used as a marker for the resected DNA (Figure 1.10) (Wold 1997). The MRN (Mre11, Rad50, Nbs1) and CtIP/BRCA1 complexes support the process of resection (Nimonkar, Genschel et al. 2011, Karanja, Cox et al. 2012). In S/G2 phase of the cell cycle RPA is replaced by Rad51 recombinase after activation of BRCA2 by CHK2 (Bahassi, Ovesen et al. 2008). In the next step of HR, the Rad51 nucleoprotein filament invades the intact DNA of homologous chromatid to search for homologous sequence. The donor DNA, homologous chromatid, forms D-loop (displacement loop). The missing nucleotide sequence is restored by DNA-polymerase I (Li and Heyer 2008). The process is completed by resolvases – enzymes to resolve holiday junctions (Lilley and White 2001). DNA sequence is restored with or without cross-over. The HR is considered error-free because it uses the homologous sequence as repair template.

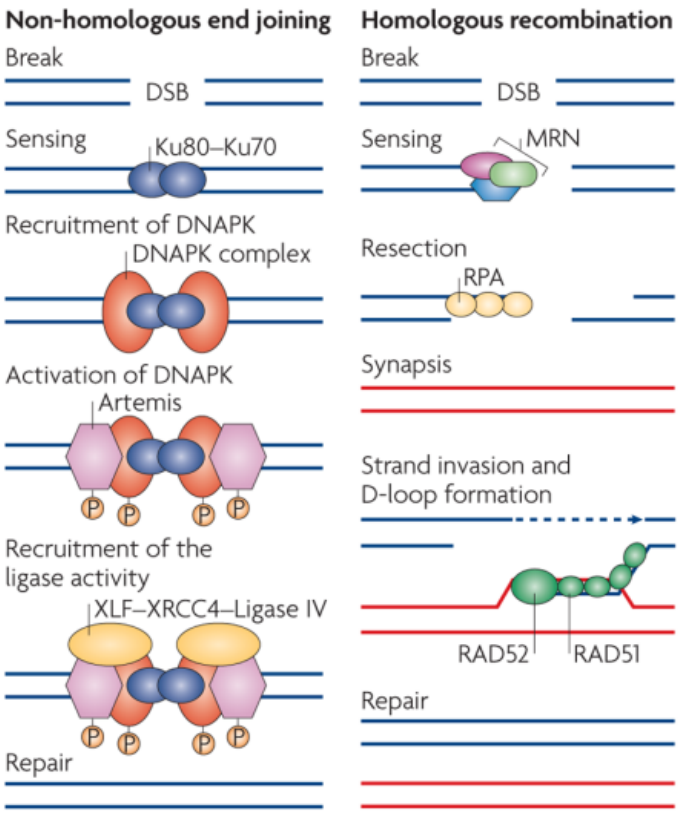

Figure 1.9: Two main DNA double strand break repair pathways NHEJ and HR (simplified). NHEJ: Ku70/Ku80 binds DSB ends, DNA-PKcs is recruited to build DNA-PK complex. Phosphorylated DNA-PK recruits XRCC4, DNA ligase 4, XLF und artemis to ligate the strands. HR: MRN complex binds DSB ends and recruits nucleases to process the DSB. RPA binds ssDNA to stabilize it and then is replaced through Rad51. Rad51 together with Rad52 search for homologous chromatid. D-loop and holiday junctions are formed. Missing DNA strand is synthesized based on template of homologous chromatid. [Image source: (Misteli and Soutoglou 2009)].

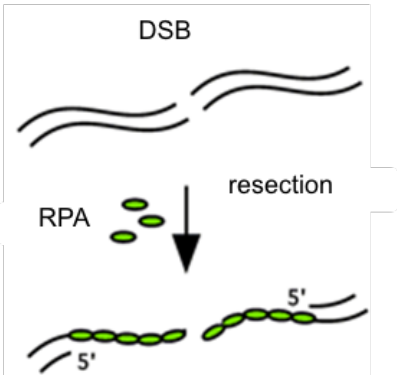

Figure 1.10: Schema of the DNA resection at DSB. The single stranded DNA molecule is cowered with RPA (replication protein A) to stabilize the strand. [Image source: (Zou and Elledge 2003)].

Besides these two main DNA repair pathways there is an alternative pathway, which is a backup form of the c-NHEJ and called alternative NHEJ (alt-NHEJ) (Figure 1.11). This

pathway is thought to operate when c-NHEJ or HR fails (Iliakis 2009). Of note, alt-NHEJ is considered as a slow repair pathway and appears to be a major source of translocations (Iliakis, Wang et al. 2004, Lieber 2010). The main factor involved in alt-NHEJ is poly (ADP-ribose) polymerase 1 (PARP1) (Audebert, Salles et al. 2004), which is also related to the single stranded break (SSB) repair (Fisher, Hochegger et al. 2007). If DSBs are not protected by Ku70/Ku80 complex, the DSB ends are resected by Mre11 and CtIP (Figure 1.11). Thus, alt-NHEJ shares the initial resection step with HR, however, alt-NHEJ does not require either extended resection or homologous sequence of sister chromatid (Mansour, Rhein et al. 2010). The short stretches of ssDNA may by chance contain micro-homologies of few nucleotides (2-4 nt) which probably contribute to alignment of DSB ends for the ligation (Mladenov, Magin et al. 2016). The occurrence of microhomologies promotes the error-prone microhomology-mediated end-joining (MMEJ) which is considered as a form of alt-NHEJ (Figure 1.11) (Durante, Bedford et al. 2013).

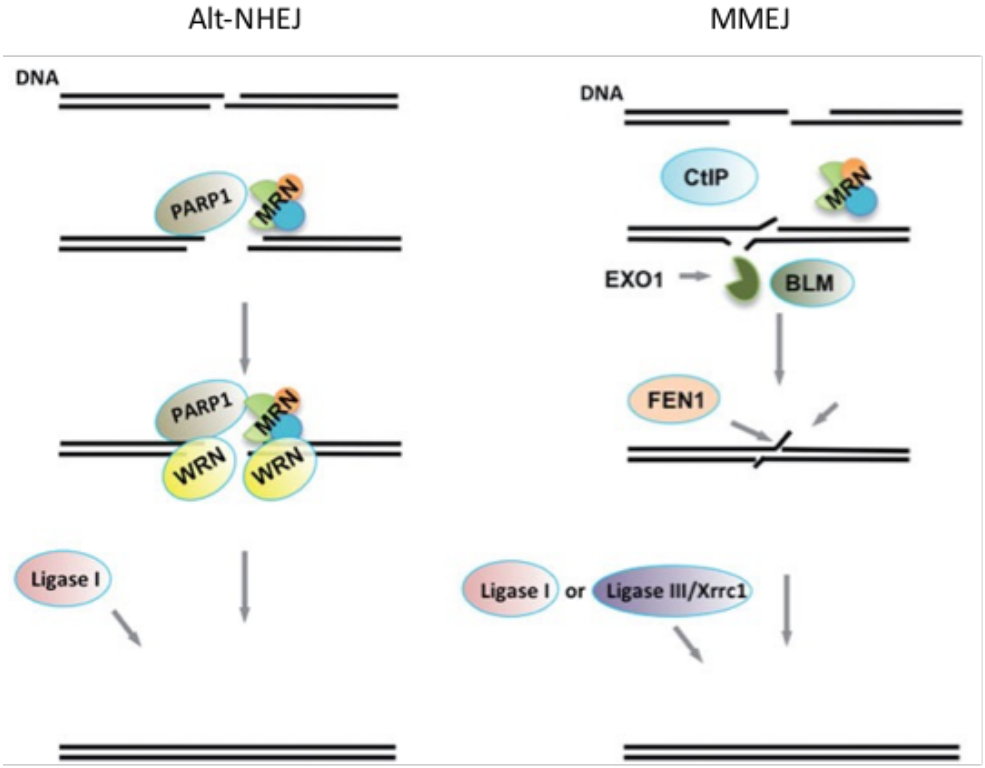

Figure 1.11: Alternative non-homologous end-joining pathways (simplified). The PARP1 and MRN complex bind DSB. MRN complex together with its partner CtIP provide limited resection. The WRN or BLM helicases support alt-NHEJ. FEN1 cuts the ssDNA overhangs. The DSB ends are rejoined either by ligase 1 (without micro-homology) or by ligase 3/XRCC1 complex (with micro-homology) [Image source (Keijzers, Maynard et al. 2014)].

Polymerase θ (pol θ) was shown to be involved in alt-NHEJ by unwinding of double stranded DNA with a helicase domain to open resected ends and to align them with micro-homology sequences (Chan, Yu et al. 2010). The generated template can be used by polymerase

domain of pol θ to re-synthesize the DNA sequence starting from the base-paired region (Chan, Yu et al. 2010). In the final step of the alt-NHEJ the DSB ends are ligated either by ligase 1 or by the ligase 3/XRCC1 complex (Figure 1.11) (Paul, Wang et al. 2013, Soni, Siemann et al. 2014)

Alt-NHEJ can be actively suppressed by Ku complex suggesting a competition between c-NHEJ and alt-NHEJ (Wang, Wu et al. 2006). The role of other components of c-NHEJ in regulation of alt-NHEJ is not known. The alt-NHEJ, similar to c-NHEJ, acts through all cell cycle stages, although the maximum activity is in G2 cells (Figure 1.12).

The availability of repair pathways during the mammalian cell cycle is depicted in Figure 1.12. The relative usage between the pathways within a cell cycle phase is dependent on several factors mentioned above. Although it is a common belief that HR is preferred in S/G2 cells to repair DSBs, the studies based on flow cytometry analysis and repair kinetics in G2 cells showed that c-NHEJ is the predominant pathway in G2 phase just as in G1 phase, while HR represents only a sub-fraction of 15 – 20 % (Mao, Bozzella et al. 2008, Beucher, Birraux et al. 2009). Since c-NHEJ and alt-NHEJ are available in G1 cells and all repair pathways are available in S/G2 cells an important question comes into focus which parameter most dictates the repair pathway choice?

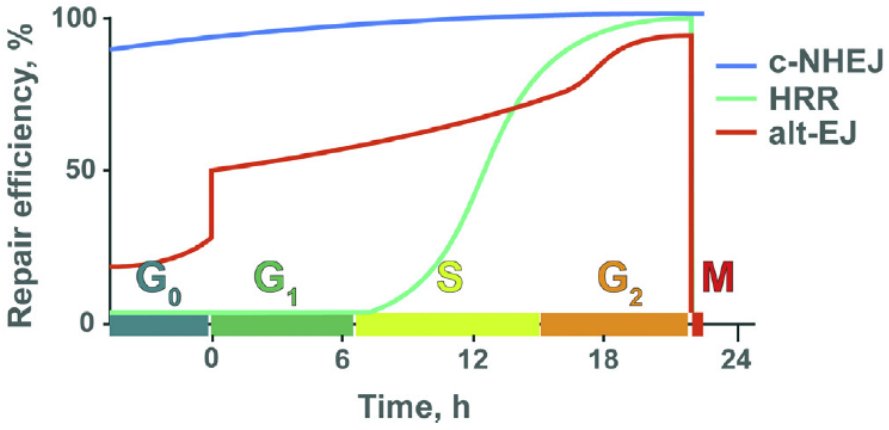

Figure 1.12: **Activity of the repair pathways in dependency on the cell cycle.** C-NHEJ operates during the whole cell cycle. HR can be utilized in S- and G2 phases when sister chromatids are available as a template. Alt-NHEJ occurs in all cell cycle phases. However, it is increased in S/G2 and strongly inhibited in G0 cells (Singh, Bednar et al. 2012) [Image: (Mladenov, Magin et al. 2016)]

1.5. Regulatory mechanisms of repair pathway choice

To maintain genomic integrity, the cells must have a sturdy mechanism to regulate DSB repair pathway choice. The regulation of the repair pathway choice starts with the regulation

of the initial step of HR - DNA end resection (Huertas 2010). Therefore, the DSB resection is highly regulated and responds to various cellular signals. For example, the inhibition of resection in G1 cells is regulated by kinase activity of CDKs which phosphorylate relevant nucleases only in S/G2 cells (Tomimatsu, Mukherjee et al. 2014). Several studies showed that DSB resection is regulated by antagonistic interplay of BRCA1 and 53BP1 (Bunting, Callen et al. 2010, Chapman, Sossick et al. 2012, Croke, Neumann et al. 2013, Bakr, Kocher et al. 2016). Further studies showed that this interplay is cell cycle dependent (Chapman JR 2013, Escribano-Diaz, Orthwein et al. 2013). A hypothetical model of possible resection regulation at DSBs comprises two complexes BRCA1/CtIP and RIF1/53BP1 which oppose each other in a cell cycle dependent manner (Figure 1.13).

RIF1 was identified as a 53BP1 interacting factor which is recruited to DSBs by phosphorylated 53BP1 (Chapman JR 2013, Escribano-Diaz, Orthwein et al. 2013, Zimmermann, Lottersberger et al. 2013). The phosphorylation of 53BP1 by ATM is not required for its recruitment to DSBs but is required for preventing resection (Daley and Sung 2013). It was assumed that the two proteins 53BP1 and RIF1 are involved in the positive regulation of NHEJ pathway (Chapman JR 2013, Zimmermann, Lottersberger et al. 2013).

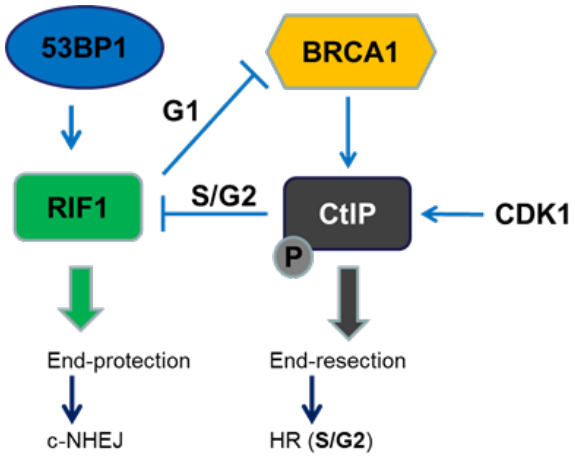

Figure 1.13: Regulation circuit of DNA resection at DSBs. The regulation of resection is cell cycle dependent and is regulated through two complexes anti-resection 53BP1/RIF1 and pro-resection CtIP/BRCA1. [Image based on (Escribano-Diaz, Orthwein et al. 2013)]

The dissociation of the 53BP1/RIF1 complex from DSBs takes place when the cells enter the S-phase and is replaced by the CtIP/BRCA1 complex which promotes resection (Chapman JR 2013, Escribano-Diaz, Orthwein et al. 2013). The formation of CtIP/BRCA1 complex occurs in S/G2 cell cycle phase and is promoted by phosphorylation of CtIP by CDKs in a cell cycle dependent manner (Sartori, Lukas et al. 2007, Escribano-Diaz, Orthwein et al. 2013).

Nevertheless, the heavy ion-induced DSBs showed a fraction of resection positive cells not only in S/G2 phases but also in G1 phase (Yajima, Fujisawa et al. 2013, Averbeck, Ringel et al. 2014). The observed fraction of resection positive cells increased with LET increase (Figure 1.14). It is important to note that the complexity of radiation-induced DSBs increases with increased LET (Ward 1994). The increase of the fraction of resected G1 cells upon high LET irradiation suggests that the DSB complexity forces the pathway choice towards resection-dependent repair. The exact mechanism of the resection regulation in G1 cells upon heavy ion radiation remains to be investigated.

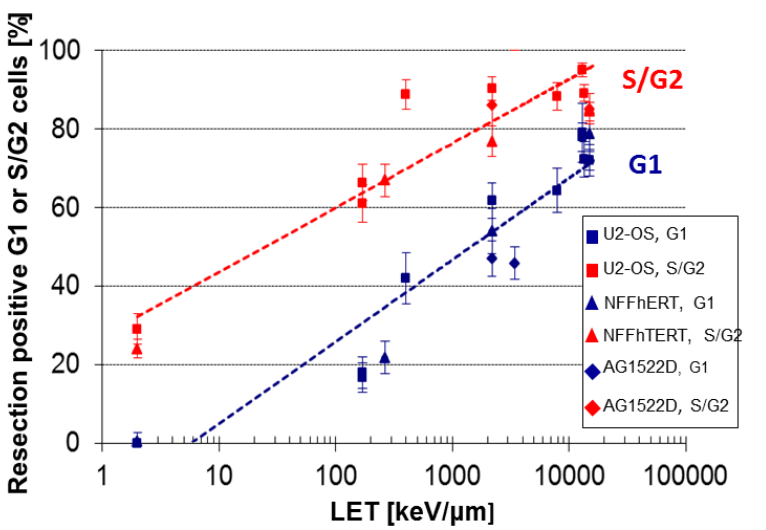

Figure 1.14: The fraction of resection positive cells is LET dependent in all cell cycle phases. The LET increase leads to an increase of resection positive cells. [Image source (Averbeck, Ringel et al. 2014)].

An appearance of the resection positive G1 cells suggests an existence of nuclease activity in these cells (Quennet, Beucher et al. 2011). The study of Averbeck et al. showed that the nucleases such as CtIP, Mre11 as well as EXO1 are important for the resection in G1 cells (Averbeck, Ringel et al. 2014). Furthermore, it was shown in CtIP deficient cells that CtIP is essential for the repair of complex DSBs in G1 cells. Therefore, a resection dependent repair pathway is indispensable for the repair of clustered DSB in G1 cells. The evidence of resection in G1 together with fact that G1 cells do not repair by HR suggests that the G1 cells use alt-NHEJ as a repair pathway for clustered DSBs (Averbeck, Ringel et al. 2014) This idea is supported by the studies of clustered DNA damage in which the accumulation of deletions and flanking microhomologies at rejoined DSB sites was shown (Singleton, Griffin et al. 2002).

1.6. Aim

The aim of this work, as the exact mechanism of DSB resection regulation remains not well understood, was to gain further understanding of this regulation in G1 cells. A recently described putative mechanism of the cell cycle dependent resection regulation comprises two complexes - on the one hand the anti-resection complex 53BP1/RIF1 and on the other hand the pro-resection complex CtIP/BRCA1 (Escribano-Diaz, Orthwein et al. 2013). RIF1 is recruited by 53BP1 to DSBs and represent the effector that prevents resection of DSBs in G1 cells. The CtIP/BRCA1 complex is activated in S/G2 cells through CDKs and thereafter facilitates the DNA resection at DSBs. This model, however, does not explain the appearance of resection in G1 cells, in which the resection regulation was the primary aim of this study. That the resection cannot appear in G1 cells does not conform to the observation that with increasing DSB complexity an increasing fraction of breaks becomes resected even in G1 cells (Yajima, Fujisawa et al. 2013, Averbeck, Ringel et al. 2014). This resection is important for the DSB repair in G1 cells (Averbeck, Ringel et al. 2014). Hence, another aspect of the primary aim of this work was to analyze the role of RIF1, 53BP1, BRCA1 and CtIP in resection of complex DSBs in G1 cells. As it was observed earlier that quiescent cells show far less resection of complex DSBs than proliferating cells do, a further aim was to closer characterize the response of cells in quiescent state to the induction of complex DSBs which are induced upon heavy ion radiation. Heavy ion radiation, moreover, is relevant not only for manned long-term space exploration but also for the tumor therapy utilizing heavy charged particles. The charged particle therapy has gained increasing importance for the treatment of solid tumors. Therefore, an accurate understanding of the repair pathway regulation in dependency of the complexity of DSBs can help in the optimization of tumor treatment. The understanding of the differences between the repair pathway regulations in tumor cells versus normal cells can open the door for future development of drugs which support the treatment using charged particles.

2. Methods

2.1. Cell culture

U2OS cells were cultivated in DMEM medium with 10% FCS at 37°C, 95 % air, 5 % CO_2 and at least 95 % humidity. The passaging of the cells for further cultivating was done two twice a week. After removing the medium, the cells were washed with 1x$PBS^{-/-}$, trypsinized with trypsin-EDTA solution at 37°C up to 5 minutes and resuspend again in medium. The cell concentration in the suspension was determined with a coulter counter (Z2 Coulter Counter, Beckmann coulter, Krefeld) and X cells/cm^2 were seeded in fresh culture dishes. AG1522D cells were cultivated in DMEM medium supplemented with 15 % fetal calf serum (FCS) at 37°C, 95 % air, 5 % CO_2 and 95 % humidity.

The passaging of the AG522D culture was performed every 10 days with once a week medium change. $1*10^6$ cells per 75 cm^2 flask were seeded. The cells, after removing the medium, were washed with 1x$PBS^{-/-}$ and detached with 3 ml accutase solution by 5 minutes incubation at 37°C. To avoid clumping of the cells they were separated by pipetting up and down with 2 mL glass pipette. The suspension was refilled with medium to gain the total volume of 10 ml. The cell-concentration in the suspension were defined with coulter counter and the required volume contained $1*10^6$ cells could be reseeded in the fresh cell culture flask or petri dishes.

All used cell lines in this work were regularly tested for mycoplasma using the PCR Mycoplasma Test Kit (AppliChem, Darmstadt).

2.2. Cryo-conservation of the mammalian cells

Mammalian cells can be stored up to 10 years in liquid nitrogen. The cells were trypsinized and the cell number determined. The suspension was centrifugalized and the cells re-suspended in cryo-solution (30 % BSA and 10 % DMSO or glycerin in DMEM) so that the final concentration was 2 million cells/ml. Thereafter the cells were slowly cooled down (about 1°C/min) in special cryo-boxes at -80°C. Afterwards the frozen cells were moved in liquid nitrogen for long time storage at -196°C.

2.3. Transfection of the eukaryotic cells

Transfection of the cells with siRNA (small interfering RNA) was performed to temporarily block the translation of different target genes. For depletion experiments U2OS cells were seeded 24 h before transfection in Ø 3.5 cm Petri dishes with or without a glass coverslip ($1.1\text{-}1.5*10^5$ cells/dish). The confluency of the cells should be 30-50 % after 24 h plating. The final concentration of siRNA was 10 nM. The siRNA was diluted in 195 µl Opti-MEM and then 8 µl of a transfection agent, INTERFERin, was added. The transfection solution was mixed rigorously and incubated for 10 minutes at room temperature. During the incubation time, the

cell culture medium was replaced with 1.8 ml medium. Petri dish 0.2 ml transfection solution was added and gently mixed. Depending on the target gene the cells were cultivated 48 h or 72 h after transfection before experiment. The used siRNA sequences for the targeted genes are listed in Table 2.1. Efficiencies of the target protein depletion were determined by western analyses 48 hours after siRNA treatment.

Table 2.1: siRNA sequences for the depletion of target proteins

Protein	siRNA sequence	Concentration (final)	Incubation time	Reference
53BP1	GAA CGA GGA GAC GGU AAU A	10 nM	48 h	(DiTullio, Mochan et al. 2002)
BRCA1	AAG GAA CCU GUC UCC ACA AAG	10 nM	48 h	(Bruun, Folias et al. 2003)
CtIP	GCU AAA ACA GGA ACG AAU C	10 nM	48 h	(Sartori, Lukas et al. 2007)
HUWE1	AAU UGC UAU GUC UCU GGG ACA	10 nM	72 h	(Wang, Lu et al. 2014)
RIF1	AGA CUU GUC UCA GAU AU	10 nM	48 h	(Silverman J 2004)
	AAG AAU GAG CCC CUA GGG AAA	10 nM		
UHRF1	GCC UUU GAU UCG UUC CUU CUU	10 nM	48 h	(Zhang, Liu et al. 2016)
	GCA AGA AGA AGG CGA AGA UAA	10 nM		

2.4. Treatment with inhibitors

To inhibit DNA-dependent protein kinase catalytic subunit (DNA-PKcs) activity, normal human fibroblasts were incubated as described above. The medium was collected in a falcon tube and stock solution of the inhibitor NU7026 was added to a final concentration of 10 µM (Table 2.2). The medium enriched with inhibitor was placed back to the cells. The cells were incubated with inhibitor for at least one hour at 37°C prior to the experiment.

Inhibition of PARylation with the PARP inhibitor PJ34 was performed in the same way as the inhibition with the DNA-PKcs inhibitor.

Table 2.2: Inhibitors

Target	Inhibitor	solvent	Concentration [µM]	Incubation time	reference
DNA-PKcs	NU7026	DMSO	10.0	1-2 h	(Peddi, Loftin et al. 2010)
PARP	PJ34	DMSO	10.0	1 h	(Fonfria, Marshall et al. 2004)

2.5. Synchronization of human fibroblasts (AG1522D)

For the synchronization of human fibroblasts (AG1522D) was used on the one hand a starvation method via serum deprivation, which is a common method to withdraw the cells from the cell cycle and enrich them in G0 phase. On the other hand, a contact inhibition method was used, which is based on the fibroblasts' characteristic to stop dividing when they have contact with neighbor cells. According to the starvation protocol described by Lemons et al. (Lemons, Feng et al. 2010) the cells were maintained in DMEM supplemented with 15 % fetal calf serum (FCS) for 7 days to let them proliferate. For the following 7 days, the medium was replaced with DMEM supplemented with 0.1 % serum. In total, the cells were cultivated for 14 days before the experiments. As a control served proliferating culture maintained in DMEM supplemented with 15 % FCS for 3 days.

An alternative non-chemical method to enrich the cells in the G0 phase was a contact inhibition method. Prior to the experiments the cells were cultivated in DMEM supplemented with 15 % FCS for 21 days. Medium was changed once a week. Furthermore, a protocol was established to obtain the cells in G1 phase as a control for the G0 cells. The cells were cultivated for 10 days in normal medium, DMEM supplemented with 15 % FCS and weekly medium change.

2.6. Cell survival

A clonogenic cells survival assay is a basic tool to determine the sensitivity of cells to ionizing radiation or other damaging agents. Every individual cell line possesses a so-called plating efficiency (PE) that has to be determined before the experiment. The plating efficiency is the fraction of cells seeded for clonogenic survival that are able to form a colony from a single cell. The plating efficiency is given by the equation:

$$\mathrm{PE} = \frac{\text{Number of colonies counted}}{\text{Number of cells seeded}}$$

A single colony contains at least 50 cells, i.e. a single cell has to be able to divide at least six times. For the clonogenic survival human fibroblasts AG1522D were used in two different conditions G1 culture and G0 culture conditions, where the PE values were 0.15 and 0.06, respectively. 65,000 cells were seeded per T25 flask, cells for G1 conditions were seeded 10 days before irradiation and cells for G0 conditions were seeded 21 days before irradiation. (Table 2.3) shows the dose in Gy with which the cells were irradiated at different conditions.

Table 2.3: Doses applied for the survival assay to the cells at different conditions

Type of radiation	**X-rays**			**Carbon ions**			
Plating conditions	**immediate**	**delayed**		**immediate**		**delayed**	
Cell cycle phase	**G1/G0**	**G1**	**G0**	**G1**	**G0**	**G1**	**G0**
Dose [Gy]	0.0	0.0	0.0	0.0	0.0	0.0	0.0
	0.5	0.5	0.5	0.2	0.2	0.2	0.2
	1.0	1.0	1.0	0.4	0.4	0.5	0.4
	1.5	2.0	1.5	0.6	0.6	0.6	0.8
	2.0	3.0	2.0	0.8	0.8	1.0	1.2
	3.0	4.0	3.0	1.0	1.0	1.5	1.6
	4.0	6.0	4.0	1.5	1.2	2.0	2.0
	5.0	8.0	5.0	2.0	-	2.5	-
	6.0	10.0	6.0	-	-	3.0	-

The cells were irradiated with carbon ions at the synchrotron SIS or with X-rays. The cells were detached with 1 ml accutase (5 min 37°C) immediately after irradiation or were incubated for 24 hours and then treated with 1 ml accutase to detach the cells from the flask. The cells were re-suspended with additionally 4 ml medium. The 1:10 dilution of the suspension with isotone was used to determine the cell number with the Coulter counter. A volume of the cell suspension, which has to be seeded for clonogenic survival is defined as 100 (expected colony number) divided by the cell concentration times plating efficiency times expected survival (equation 1):

$$\mathrm{I[ml]} = \frac{100}{\frac{\text{cell number}}{\text{ml}} \cdot \mathrm{PE(expected)} \cdot \mathrm{S(expected)}} \qquad (2.1)$$

I : a volume of the cells suspension to be seeded

PE : plating efficiency for G1 0.15 and for G0 0.06

S : expected survival calculated from previous experiments

Equation 2.1: Calculation of the plating volume I [ml].

This calculation is based on the consideration that about 100 cells of the seeded cells have a clonogenic capacity (inclusive the irradiation dose and incubation time of 14 days for AG1522D cells after plating). The calculated volume was seeded in triplicates for each point of each curve. There were used 75 cm^2 culture flasks for this purpose. The flasks were pre-heated to 37°C in the incubator containing fresh medium. Next, the cells were cultivated for 14 days at 37°C, 5 % CO_2 and 95 % humidity. The medium was changed once a week. After 14 days incubation time the medium was removed, the grown colonies were stained with 1x methylenblue for 15 minutes at room temperature. Finally, the methylenblue was removed and the flasks were dried in the hood. The number of colonies was counted with a binocular microscope. The cell survival was calculated with the following equation:

$$S = \frac{\overline{X}}{I[ml] \cdot \text{dilution factor} \cdot \frac{\text{cell number}}{ml}} \qquad (2.2)$$

$\overline{X}$: mean colony number of the triplicates

I : seeded volume

Equation 2.2: Calculation of the cell survival.

The relative survival was defined as the ratio of the cell survival in non-irradiated cells to the cell survival in irradiated cells, whereas the survival in non-irradiated cell is defined as 1 survival:

$$S_{relativ} = \frac{S_{irradiated}}{S_{non-irradiated}} \qquad (2.3)$$

Equation 2.3: Calculation of the relative survival.

2.7. Irradiation of cells

2.7.1. Irradiation with X-rays

The cell irradiation with different doses of X-rays was performed with a voltage of 250 kV and a current of 16 mA using the IV320-13 M1 X-ray tube (Seifert, Germany). The absorbed dose was controlled with a SN4 Dosimeter (PTW, Freiburg). The dose rate was 1-2 Gy min^{-1}. During irradiation, the cells were kept in medium by room temperature. The non-irradiated control cells were treated the same way as irradiated samples, but without irradiation.

2.7.2. Irradiation with heavy ions at the linear accelerator UNILAC

The irradiation with heavy ions was performed at UNILAC – the linear accelerator facility of the GSI (Gesellschaft für Schwerionen Forschung). The ion species choice was mainly

determined by the availability of beam-time at the facility. The ion species that were used in this work are listed in Table 2.4.

Table 2.4: The ion species used by irradiation at UNILAC

Ion species	Energy on target [MeV/u]	LET [keV/µm]	Fluence [particles/cm^2]	Dose [Gy]
Carbon (^{12}C)	9.90	168	3-5*10^6	0.8-1.35
Carbon(^{12}C)	4.05	325	3-5*10^6	1.56-2.6
Gold (^{198}Au)	4.60	13,000	3*10^6	62.4
Helium (^{4}He)	1.62	76	5*10^6	0.6
Oxygen (^{16}O)	3.2 - 2.4	610	5*10^6	4.5 - 6.0
Xenon (^{132}Xe)	4.50	9,000	3*10^6	43.0
Uranium (^{238}U)	6.21	15,000	3*10^6	72.0

There were two possibilities to irradiate at the UNILAC facility: perpendicular and at low angle. For the perpendicular irradiation, the petri dishes were directly placed in the special samples holder (Figure 2.1) For the low angle irradiation the cells were plated on 24 mm x 24 mm glass coverslips, which were placed in a special adapter (Figure 2.1) allowing irradiation at an angle of 15°. The petri dish holder was filled with medium without additives and the cells were only for a few seconds during irradiation without medium. The irradiation process was performed by an automatic robotic arm, which pulled the samples out of the sample holder and held the petri dish or adapter in the beam.

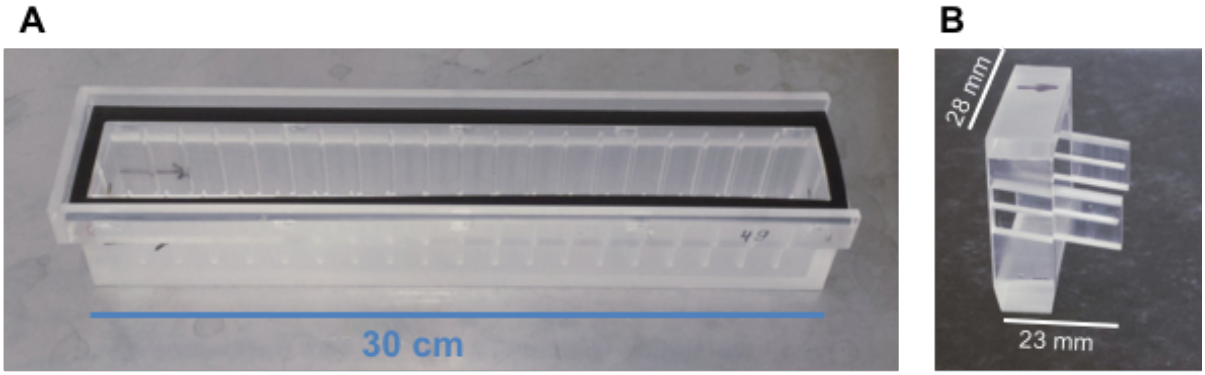

Figure 2.1: Equipment for low-angle irradiation at UNILAC. A: Sample holder. **B:** Adapter

2.7.3. Irradiation at the heavy ion synchrotron SIS

The synchrotron SIS at the GSI accelerator facility was an alternative possibility to irradiate the cells in a low angle. For the angular irradiation at SIS, the cells were seeded in petri dishes, which were placed atop each other and slightly tilted during irradiation. For clonogenic survival studies AG1522D cells were irradiated in 25 cm^2 flasks. During irradiation, the flasks were elevated for the few seconds of irradiation in vertical position. The beam was slowed down to appr. 24 MeV/u with LET of appr. 81 keV/µm on target with a range shifter. In Table 2.5 are listed the ion species used for SIS irradiation.

Table 2.5: The ion species used by irradiation at SIS

Ion species	Energy on target [MeV/u]	LET [keV/µm]	Fluence [particles/cm^2]	Dose [Gy]
Carbon (^{11}C)	100	27	$1.5\text{-}23*10^6$	0.2-3.0
Xenon (^{132}Xe)	600	1,000	$5*10^6$	8.0

2.8. Cell fixation and immunostaining

Fixation of the cells after cultivation and irradiation preserved the cells for further analyses. This process kills the cells but preserves the protein structure. In addition, the fixation process permeabilized the cells for immunostaining.

2.8.1. Fixation with Paraformaldehyde

For most antibodies used in this work, the appropriate fixation method was a fixation with paraformaldehyde (PFA). This fixation was always performed at room temperature. After cultivation by 37°C the cells were washed with $PBS^{-/-}$. Afterward the cells were incubated with 2 % PFA for 15 minutes and permeabilized with 0,5 % triton X-100 in $PBS^{-/-}$ for a maximum of 10 minutes. Subsequently, the cells were washed with PBS twice for 3 minutes and blocked with 0,4 % BSA solution in $PBS^{-/-}$ for 20 minutes at room temperature or for long storage at 4°C. The long storage in BSA solution was possible due to the addition of 0.02 % sodium azide.

2.8.2. Fixation with Trichloroacetic acid (TCA)

The fixation with trichloroacetic acid (TCA) was required for the immunofluorescence staining of Poly-ADP-ribose (Burkle, Chen et al. 1993). The cells were washed with PBS and treated with freshly prepared 10 % ice-cold TCA for 10 minutes. Afterwards the cells were washed

with rising ethanol concentration of 70 %, 90 % and 100 % at -20°C for 5 minutes each and left to evaporate. The cells were re-hydrated with PBS before antibody treatment

2.9. Immunofluorescence staining of fixed cells

For the analysis of the role and functions of proteins in the DNA repair process the target proteins must be made visible. For this purpose, the fixed sample was stained with antibodies coupled with a fluorescent dye. The BSA solution (blocking solution) was removed from the fixed cells and the primary antibody diluted in 0.4 % BSA in PBS was spread over the cell layer and covered with mylar foil to prevent the dehydrating of the samples (Table 2.6). The incubation time with primary antibody was 1 h at room temperature or overnight at 4°C. After incubation, the cells were washed in petri dish with PBS three times for 5 minutes. The incubation with secondary antibody followed the washing step (Table 2.7). The antibody was diluted in BSA solution as well. The incubation time for the secondary antibody was 45-60 minutes. Importantly, during the incubation with the secondary antibody the samples needed to be protected from light. Otherwise the fluorophore could be bleached by photons of the scattered light. Afterwards the cells were washed again twice with PBS and subsequently DNA was stained with 1µg/ml DAPI (4',6-Diamidin-2-phenylindol) solution in PBS for 20 minutes. Subsequently, the cells were rinsed once with PBS, once with water (millipore) and mounted in Vectashield Mounting Medium (Vector Laboratories, Canada). Finally, the cells were covered with coverslip and sealed with nail polish. The samples were stored at 4°C in the dark before microscopic analysis.

Table 2.6: List of primary antibodies for immunofluorescence staining.

Antigen	Antibody	Source of supply	Species	Concentration [mg/ml]	dilution
53BP1	53BP1 (ab36823)	Abcam	Rabbit polyclonal	1.0	1:500
BRCA1	BRCA1 ab-1	Oncogene	Mouse monoclonal	0.1	1:200
BRCA1	BRCA1 sc-642	Santa cruz	Rabbit polyclonal	0.2	1:50
CENP-F	CENP-F (Ab-5) NB500-101	Novus Biologicals	Rabbit polyclonal	2.5	1:750
CtIP	Ctip (A300-488A)	Bethyl Laboratories	Rabbit polyclonal	1.0	1:200

CtIP	CtIP (clone 14-1) (61141, 61142)	Active Motif	Mouse monoclonal	1.0	1:1,000
γH2AX	γH2AX (Ser139) clone JBW301 (05-636)	Millipore	Mouse monoclonal	1.0	1:500
Geminin	Geminin (1A8) H00051053-M01	Novus Biologicals	Mouse monoclonal	0.5	1:100
Ki67	Ki67 (ab6526)	Abcam	Mouse monoclonal	2.9	1:200
PAR	PAR (10H) (ALX-804-220)	Enzo Life Sciences	Mouse monoclonal	-	1:200
RIF1	RIF1 (LS-B7340)	Lifespan Biosciences	Goat polyclonal	0.5	1:400
RPA	RPA/p34 Clone 9H8 (R1280)	Sigma	Mouse monoclonal	2.2	1:1,000

Table 2.7: List of secondary antibodies for immunofluorescence staining.

Antigen	Antibody	Source of supply	Species	Concentration [mg/ml]	dilution
Mouse-IgG	Alexa Fluor 488 anti-mouse	Life Technologies	Goat	2	1:400
	Alexa Fluor 568 anti-mouse	Molecular Probes	Goat	2	1:400
	Atto 647N anti-mouse	Sigma	Goat	1	1:200
	Alexa Fluor 488 anti-mouse	Life Technologies	donkey	2	1:400
	Alexa Fluor 568 anti-mouse	Life Technologies	donkey	2	1:400
	Alexa Fluor 647 anti-mouse	Life Technologies	chicken	2	1:400
Rabbit-IgG	Alexa Fluor 488 anti-rabbit	Life Technologies	Goat	2	1:400

	Alexa fluor 568 anti-rabbit	Molecular Probes	Goat	2	1:400
	Alexa Fluor 488 anti-rabbit	Life Technologies	donkey	2	1:400
	Alexa fluor 568 anti-rabbit	Life Technologies	donkey	2	1:400
Goat IgG	Alexa Fluor 488 anti-goat	Molecular Probes (Invitrogen)	donkey	2	1:400
	Alexa fluor 647 anti-goat	Life Technologies	donkey	2	1:400

2.10. Microscopy

The immunofluorescence stained cells were analyzed and recorded with fluorescence microscope or with confocal Laser Scanning System Leica TCS SPE supplied with an inverse DMI4000 microscope (objective: HCX PL APO 63x 1.40-0.6 OIL) and solid-state lasers with excitation wavelengths of 405, 488, 532 and 635 nm. The images gained with the fluorescence microscope were analyzed with ImageJ software. The images gained with confocal scanning system were de-convoluted with Huygens essential software and subsequently analyzed with ImageJ software.

2.10.1. Overlapping analysis with ImageJ

The image processing software ImageJ was used to analyze intensity independent overlapping of two signals of interest. In this work, a double immunofluorescence staining of BRCA1-RIF1, BRCA1-RPA or RIF1-RPA was analyzed to determine the overlapping area of two signals of interest. A total area of a signal in projection of a signal channel was measured. The areas of two signals then were overlaid and the total overlapping area of two signals was measured. The measured overlapping area was normalized to the maximum of possible overlapping area, i.e. a smallest area of two signals, to achieve a range from 0 to 100 %.

2.11. Biochemical methods

2.11.1. Preparation of whole protein lysates from cells (Lämmli-Lysates)

The protein extraction with Lämmli buffer is suitable for the analysis and comparison of various proteins including nuclear located proteins. During the extract preparation, it is essential while to keep the cells continuously on ice. After washing the cells with $PBS^{-/-}$

solution, the fluid was completely removed and 100µl 2x Lämmli buffer was trickled on the surface of attached cells. Afterwards, the cells were easily removed from the petri dish surface with a cell scraper. The following transfer of cell lysates from the petri dish to reaction tubes was performed using a pipette with a cut tip. To shear the DNA, the solution was passed through a 25-gauge needle for at least 10 times or more. Thereafter the cell extracts were heated at 95°C for 10 minutes and centrifuged at 14,000 x g for 10 minutes. The water-soluble proteins remained in the supernatant. The debris in the sediment was discarded. The extract was kept at -20°C for long storage.

2.11.2. Determination of the protein concentration

The concertation of proteins was determined according to the Lowry protocol (Lowry, Rosebrough et al. 1951) with the DC™ Protein Assay Kit from Bio Rad. The reaction is based on the production of a copper-protein-complex, which is reduced through Folin-reagent. Thereby, the intensity of the blue color correlates with the protein concentration and was used for colorimetric analysis. The concertation can be determined with a standard curve which was always performed in parallel to samples. For the standard curve BSA solution with concentrations of 0.0, 0.2, 0.4, 0.8 and 1.0 mg/ml was used. For the procedure 5 µL of 1:3 to 1:5 diluted samples were used for the measurement according to the manufacture. The photometric measurement was performed with a ELISA-reader at 690 nm.

2.11.3. SDS-Poly-acrylamide-gel-electrophoresis (SDS-PAGE) and Western Transfer

SDS-PAGE is used for the protein separation according to their weight. The protein extracts were thawed on ice and mixed with 2x Lämmli loading buffer (5 % β-Mercaptoethanol) in proportion 2:1. The SDS in the loading buffer causes the denaturation of the proteins and their negative charge. As a result, they can migrate in an electric field according their molecular weight. The β-Mercaptoethanol cleaves the disulfide bridges. Moreover, SDS in the buffer counteracts the precipitation or the denaturized proteins. Subsequently, samples were heated at 95°C for 3 minutes and centrifuged at 14,000 x g for 2 minutes at 4°C. For SDS-PAGE were used commercially available gels with a concentration of acrylamide of 10 % or gradient gels with a concentration of acrylamide from 4 to 15 %. The latter were perfect for separation of proteins with large molecular weight difference. Together with the samples, a commercial protein marker was loaded on the gels to determine the protein weight after running of the SDS-PAGE. To separate the proteins in an electric field, the chamber with acrylamide gels was filled with running buffer and connected to the power supply. The current of 45 mA per gel was kept constant.

The protein transfer from gel to PVDF membrane for the protein immuno-analysis is known as a Western blot. For the protein transfer was performed a “sandwich” from acryl-amid gel,

PVDF-membrane, blotting papers and sponge. The PVDF membrane was pre-equilibrated with methanol and the blotting paper and sponge are soaked with cold blotting buffer. The transfer was performed in a transfer chamber where the gel was positioned on the side of the cathode and the membrane on the side the anode. For the transfer, the voltage of 300 V was constant. During the transfer, the blotting chamber was cooled against upcoming heat with ice.

2.12. Antibody staining and detection

The protein transfer from gel to a membrane allows the immunological detection and analysis of the target proteins. After the transfer, the membrane was incubated with blocking buffer at least 30 minutes to block unspecific binding of antibodies. The primary antibodies were diluted in blocking buffer and incubated at least 1 h at room temperature or overnight at 4°C. The primary antibodies that were used in Western analysis are listed in the Table 2.8 table 2.8. After incubation with primary antibody the membrane was washed with TBS-T 2-3 times for 5 minutes. Thereafter a secondary antibody, which is coupled with horseradish peroxidase (HRP) was diluted in blocking buffer as well and incubated for 1 h at room temperature. The dilution of the secondary antibodies for the Western analysis is listed in the Table 2.9. After incubation with a secondary antibody the membrane was washed again 4 times for 5 minutes with TBS-T and incubated with detection solution ECL Plus (Thermoscientific) protected from light. The reaction of luminol oxidation by HRP leads to a chemiluminescent signal that can be detected with a special camera. The devise used for this purpose was the FUSION FX7^{TM} (Peqlab). The exposure time varied for every single protein. With the assistance of the software FUSION the protein bands were quantified in linear range of the luminescent signal. For the determination of an expression level of a target protein the value of its intensity was normalized to the intensity of a housekeeping protein that was used as a loading control. The housekeeping proteins that were used in this work were β-actin, β-tubulin and vinculin.

Table 2.8: The primary antibodies for western analysis.

Antigen	Antibody	Source	Species	Concentration, mg/ml	dilution
53BP1	53BP1 (ab36823)	Abcam	Rabbit polyclonal	1.0	1:5,000
Actin	b-Aktin (ab34731)	Abcam	Rabbit polyclonal	1.0	1:1,000

BRCA1	BRCA1 (sc-642)	Santa cruz	Rabbit polyclonal	-	1:50
CtIP	CtIP (clone 14-1) (61141,61142)	Active Motif	Mouse monoclonal	1.0	1:2,000
DNA-PKcs	DNA-PKcs Ab-4 (Cocktail)	Lab Vision	Mouse monoclonal	0.2	1:5,000
pDNA-PKcs	pDNA-PKcs (phospho-S2056)	Abcam	Rabbit polyclonal	1.0	1:1,000
H3	H3 ChIP Grade (ab1791)	Abcam	Rabbit polyclonal	0.5	1:1,000
H3K27Me3	H3-Lys27-me3 (ab6002)	Abcam	Mouse monoclonal	1.0	1:200
H3K9Me3	H3-K9-Me3 (trimethyl-Lys9) Upstate 07-442	Upstate	Rabbit polyclonal	1.0	1:200
HUWE1	HUWE1 (ARF-BP1) (ab70161)	Abcam	Rabbit polyclonal	2.0	1:1,000
Ku80	Ku80 (ab1357)	Chemicon	Rabbit polyclonal	-	1:20,000
Ligase 4	Ligase IV (sc-11750)	Santa Cruz	Goat polyclonal	0.2	1:100
P27	P27 (sc-528)	Santa Cruz	Rabbit polyclonal	0.2	1:100
RIF1	RIF1 (A300-569A)	Bethyl (biomol)	Rabbit polyclonal	1.0	1:1,000
tubulin	Tubulin (T5168)	Sigma	Mouse monoclonal	6.7	1:8,000
UHRF1	UHRF1 (ICBP90) 612264	BD Bioscience	Mouse monoclonal	0.25	1:1,000
vinculin	Vinculin (ab18058)	Abcam	Mouse monoclonal	0.2	1:500

Table 2.9: The secondary antibodies for western analysis

Antigen	Antibody	Source	Species	Concentration, mg/ml	dilution
Mouse-IgG	Mouse-IgG HRP-conjugated	LI-COR	goat	-	1:10,000
Rabbit-IgG	Rabbit-IgG HRP-conjugated	LI-COR	goat	-	1:10,000

3. Materials

3.1. Cell lines

Cell line	Description
AG1522D	The human foreskin fibroblasts AG1522D were provided from Camden USA Coriell Cell Repositories. The cells were incubated in DMEM culture medium supplied with 15 % FCS. The in experiments used cells had CPD (cumulative population doublings) between 23 and 33. CPD were calculated each time before reseeding the cells: $$\mathrm{CPD(new)} = \mathrm{CPD(old)} + \frac{\ln \frac{\#\ \text{cells harvested}}{\#\ \text{cells seeded}}}{\ln 2}$$
U2OS	The U2OS cells were established in 1964 from moderately differentiated sarcoma of the tibia of 15-years-old female with osteogenic sarcoma. U2OS cells exhibit epithelial adherent morphology and have a doubling time of 28 h (Niforou, Anagnostopoulos et al. 2008). The cells are cultured in DMEM culture medium supplied with 10 % FCS.

3.2. Cell culture media and supplements

Solution	Company
Dulbecco's Minimal Essential Medium with 4,5 g/l Glucose (DMEM)	Biochrom
Fetal calf serum FCS	Biochrom
Phosphate buffered saline PBS	Biochrom
Glycerin	Sigma
DMSO	Roth
Trypsin/EDTA	PAN Biotech
Accutase	Sigma
OptiMEM	GIBCO

3.3. Chemicals

Chemical	Company
4‘,6-Diamidin-2-phenylindol (DAPI)	AppliChem
6x loading dye	Fermentas
30 % Acrylamid/Bisacrylamid (29:1)	Roth
Ammonium persulfate (APS)	Sigma
Bicine	Sigma
Bis-Tris	AppliChem
BSA	Roth
DNA-PKcs-inhibitor NU7026	Cayman Chemical
ECL Plus	GE Healthcare
EDTA	Sigma
Ethanol	AppliChem
Immersion oil (DIN58884)	Merck
Isopropyl alcohol	Roth
Löffler’s Methylene Blue solution	Roth
Methanol	Roth
Mounting Medium Vectashield	Vector Laboratories
INTERFERin	Polyplus
Paraformaldehyde	AppliChem
Potassium chloride	Merck
HiMarkTM Pre-Stained Protein Standard	Invitrogen
Page RulerTM Plus Prestained Protein Ladder	Thermo Fisher Scientific
PARP inhibitor PJ34	Cayman Chemical
SDS	Sigma
Skim milk powder	Great Value ®
Sodium acetate	AppliChem
Sodium azide	Sigma
Sodium chloride	AppliChem
TEMED	Merck
Tricine	AppliChem
Trichloroacetic acid	Merck
Tris HCl	Merck
Tris-Base	Roth

Triton x-100	AppliChem
Tween 20	Sigma-Aldrich

3.4. Buffers and solutions

Buffer	Composition
Blocking solution	5% skim milk powder in 1xTBST
Methylen blue	30% (v/v) löffler's methylen blue solution, 5 % (v/v) methanol, 0.009 % potassium hydroxide
$PBS^{-/-}$	137 mM sodium chloride, 7.9 mM disodium hydrogen phosphate, 2.7 mM potassium chloride, 1.5 mM potassium dihydrogen phosphate
Resolving gel	acrylamide mix, 0.4 M Tris-HCl (pH 8.8), 0.1 % (w/v) SDS, 0.1 % (w/v) ammonium persulfate, TEMED
SDS Lämmli buffer (2x concentrated)	100 mM Tris-HCl (pH 6.8), 2 % SDS, 20 % glycerine
SDS running buffer	25 mM Tris Base, 192 mM glycine, 0.1 % (w/v) SDS
SDS sample buffer (2x concentrated)	100 mM Tris-HCl (pH 6.8), 50 % (v/v) glycerine, 4 % (w/v) SDS, 0.2 % (w/v) bromophenol blue, 10 % β-mercaptoethanol
Stacking gel	acrylamide mix, 0.125 M Tris-HCl (pH 6.8), 0.1 % (w/v) SDS, 0.1 % (w/v) ammonium persulfate, TEMED
Transfer buffer	19.2 mM glycine, 25 mM Tris base, 20 % (v/v) methanol

3.5. Software

Software	Company
FUSION	PeqLab Biotechnologiy GmbH, Erlangen
GIMP 2.8.14	Adobe
ImageJ 1.48v	National Institutes of Health, USA
GraphPad PRISM	Statcon
Python	SciPy Library
Las AF TCS NT 1.6.587	Leica Microsystems Heidelberg GmbH

3.6. Technical equipment

Technical equipment	Company
Western blotting	Bio-Rad
Confocal Laser Scanning Microscope	Leica
Electrophoresis chamber	Bio-Rad
ELISA-Reader EL 808	BioTek
FUSION FX7^{TM}	PeqLab
X-ray tube IV320-13	Seifert
Z2 Coulter Counter	Beckmann Coulter

4. Results

The aim of this work was to get deeper insight into the regulation mechanism of DNA double strand break (DSB) resection after heavy ion irradiation. To investigate the regulation of DNA resection after heavy ion irradiation the recently described regulation after X-ray was chosen as the basis for further research (Escribano-Diaz, Orthwein et al. 2013). It was shown that RIF1 in a complex with 53BP1 (53BP1/RIF1) protects X-ray induced DNA DSBs from resection in G1 cells. In contrast, CtIP in complex with BRCA1 (CtIP/BRCA1) allows DNA resection when the cells enter the S-phase of the cell cycle. The detailed mechanism of mutual competition between these complexes had remained poorly understood. The results of this thesis are divided into two parts: the first part provides the results which are related to the mechanism of resection regulation of heavy ion-induced DSBs in G1 cells and the second part is related to characteristics of the cells in G0 phase which are responsible for the resection limitation.

4.1. RIF1 as a part of 53BP1/RIF1 complex does not alone prevent resection of DSB after heavy ion irradiation

4.1.1. RIF1 recruitment to the heavy ion-induced DSB is LET dependent in S/G2 cells

Several recently published studies have shown that RIF1 is involved in the regulation of DSBs resection after exposure to ionizing irradiation (Chapman JR 2013, Di Virgilio M 2013, Kumar R. 2014). Therefore, it was crucial to investigate the recruitment of RIF1 to heavy ion induced DSBs in dependency of the cell cycle and LET. The accumulation of RIF1 at complex DSB was analyzed in U2OS cells (human osteosarcoma cell line) (Figure 4.1 A) after irradiation with X-ray or various heavy ions. RIF1 accumulation at DSBs was analyzed via immunofluorescent staining. Interestingly, RIF1 as a part of the 53BP1/RIF1 complex, which works as a DNA end protector from the resection, was recruited to DSB after heavy ion irradiation not only in G1 cells, but also in S/G2 cells which are mostly resection positive at the analyzed LET of 15,000 keV/µm (Figure 4.1 B).

Empirical analysis revealed the recruitment of RIF1 to ion-induced DSBs in G1 cells. The following quantitative analysis of the positive RIF1 fraction after ionizing irradiation of different LET showed the quantitative differences related to the cell cycle. The fraction of RIF1 positive G1 cells always lay above the RIF1 positive fraction of S/G2 cells (Figure 4.1 B).

A

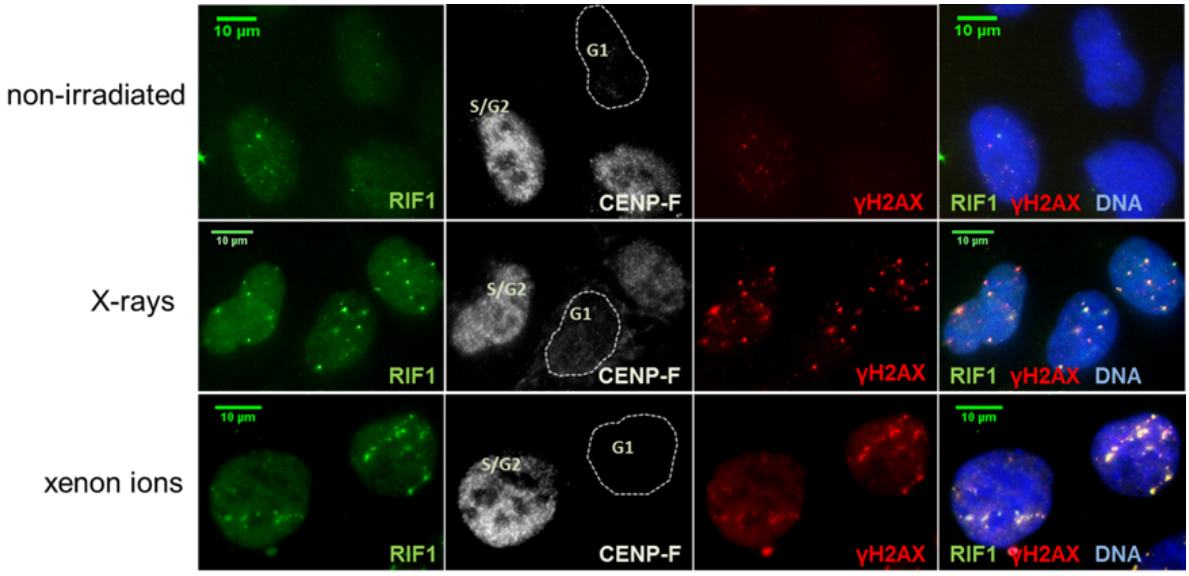

B

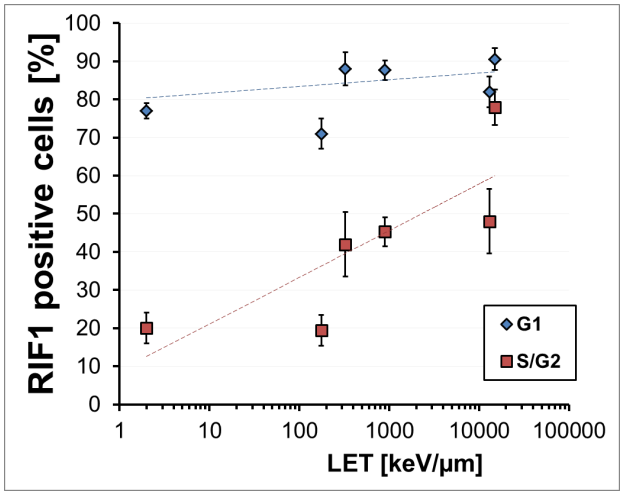

Figure 4.1: RIF1 is accumulated at DNA-DSBs after X-ray irradiation and after heavy ion irradiation A: U2OS cells 24 h after seeding were irradiated with X-rays (1 Gy), with xenon ions (LET 9,000 keV/µm; energy 4.5 MeV/u; fluence $3*10^6$ p/cm^2) or left without irradiation (control). 1 h post irradiation cells were fixed and immune-stained against RIF1 (green), CENP-F (white; cell cycle marker; S/G2 cells are CENP-F positive; G1 are CENP-F negative) and γH2AX (red; DSB marker). DNA was stained with DAPI (blue). Each panel shows one representative image of a non-irradiated (control), X-rays- and xenon ions irradiated sample, respectively. Merge shows overlapping of the DSB marker γH2AX with RIF1. RIF1 was recruited to ionizing irradiation induced DNA-DSBs in both G1- and S/G2 cells**. B:** Fraction of RIF1 positive cells upon irradiation with ionizing irradiation of different LET. Fraction of RIF1 positive cells after irradiation with different ions and X-rays (1 Gy). U2OS cells were irradiated with low LET X-rays (LET 2 keV/µm) and with high LET ions: carbon ions (LET 170 keV/µm or 325 keV/µm), xenon ions (LET 9,000 keV/µm); gold ions (LET 13,000 keV/µm) and uranium ions (LET 15,000 keV/µm). All ions were applied with fluence $3*10^6$ p/cm^2. The number of RIF1 positive cells (≥5 foci/cell) was counted in G1- and S/G2 cells. The number of RIF1 positive G1 cells was not changed with increasing LET. The number of RIF1 positive S/G2 cells increased with increasing LET. Error bars represent the binomial error.

The evaluation of RIF1 positive cells after irradiation with different heavy ions also showed that with increasing LET the number of RIF1 positive cells did not change, but remained at a high level of appr. 80 % in G1 phase cells. Yet, there was an increase in S/G2 cells from appr. 20 % up to 70 % within LET range from 2 keV/µm to 15,000 keV/µm (Figure 4.1). The number of RIF1 positive G1 cells did not change with increasing LET. The number of RIF1 positive S/G2 cells was exponentially increased as a function of LET with a slope of 4,97 (Figure 4.1).

Taken together, the fraction of RIF1 positive cells was much higher in G1 cells and lower in S/G_2 cells. The fraction of RIF1 positive in S/G2 phase was LET dependent.

4.1.2. RIF1 depletion does not influence the number of RPA positive cells after carbon ion irradiation

In order to study the function of RIF1 in the regulation of resection in ion-induced DSBs in G1 cells, depletion of RIF1, by RNAi (c. 2.3) was established in U2OS cells. The depletion of RIF1 was verified using Western analysis (Figure 4.2). The whole cell lysates from U2OS cells were prepared 48 h after transfection with RIF1 or BRCA1 siRNA.

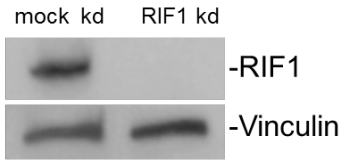

Figure 4.2: RIF1 depletion in U2OS cells. Western analysis was performed with RIF1 siRNA treated U2OS cells. Mock depleted cells (mock kd) were treated as RIF1 depleted (RIF1 kd) cells but without siRNA. Vinculin was used as a loading control.

In the following step, it was studied whether depletion of RIF1 had an influence on the fraction of RPA positive, i.e. resection positive cells in heavy ion irradiated G1 cells. The U2OS cells were treated with RIF1 siRNA or mock treated. For the mock treatment, the cells were treated with the transfection protocol, however, without siRNA. 48 hours later the samples were irradiated with carbon ions and fixed 1 h post irradiation. Immunofluorescence staining was performed against RPA (resection marker) and CENP-F (cell cycle maker). In each sample, at least 100 cells were counted (Figure 4.3).

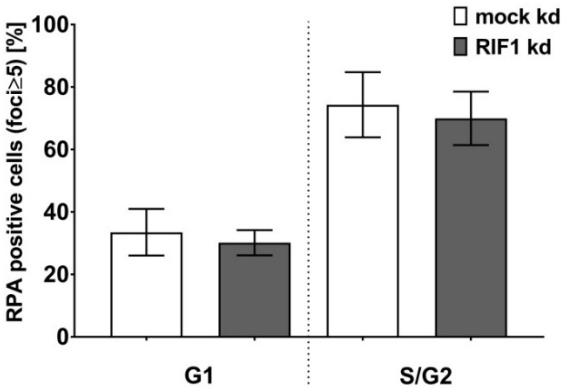

Figure 4.3: Depletion of RIF1 does not influence the fraction of resection positive cells. U2OS cells were mock depleted (mock kd) or depleted for RIF1 (RIF1 kd) by RNAi and irradiated angular with carbon ions (LET 325 keV/µm, 4.05 MeV/u, fluence $5x10^6$ p/cm^2). 1 h post-irradiation the samples were fixed and immun0-stained against RPA (resection marker) and CENP-F (cell cycle marker, S/G2 cells are positive, G1 cells are negative). RPA positive cells (foci/cell ≥ 5) were quantified in G1 cells or in S/G2 cells. The graph shows the mean value of RPA positive cells of three independent experiments (n=3); error bars represent ±SEM.

The evaluation of the three independent experiments showed no significant difference in the number of RPA positive cells after RIF1 in both G1 and S/G2 cells (Figure 4.3).

4.1.3. RPA foci formation at ion-induced DSBs was not impaired by RIF1 depletion

The analysis of the resection positive fraction in RIF1 depleted cells showed that RIF1 depletion did not result in the increased number of RPA positive cells upon carbon ion irradiation. However, further suggestion was that RIF1 depletion might have an impact on the number RPA foci per nucleus. Therefore, RPA foci were counted in carbon ion irradiated RIF1-depleted U2OS cells. Additionally, the RPA foci were also counted in non-irradiated and X-ray irradiated samples as a control. All irradiated samples were fixed 1 h post irradiation.

The number of RPA foci after X-ray irradiation was barely increased in both in G1 and S/G2 cells (Figure 4.4). The low value of RPA foci after X-ray irradiation indicated the low number of resected DSB sites per nucleus. This demonstrates that the photons of X-ray irradiation at relative low dose cannot provide complex DSBs.

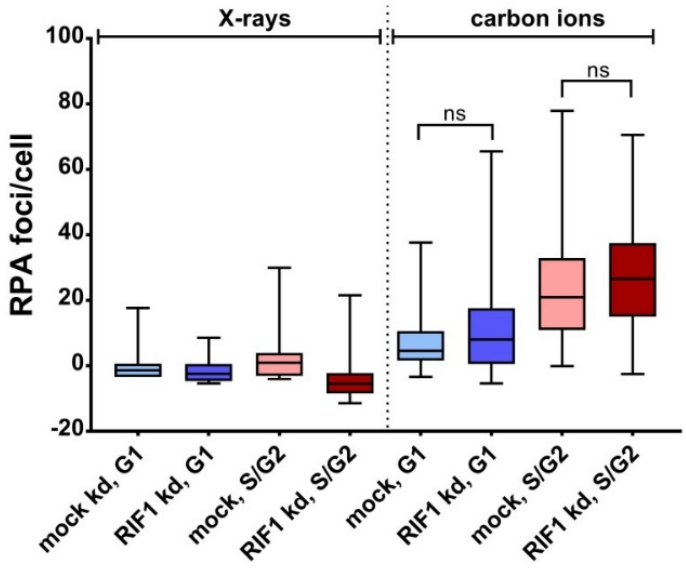

Figure 4.4: RIF1 depletion did not affect RPA foci generation after carbon ion irradiation. U2OS cells were mock depleted (mock), depleted for BRCA1 (BRCA1 kd) or depleted for RIF1 (RIF1 kd) by RNAi. 48 h after transfection U2OS cells were angular irradiated with carbon ions (LET 325 keV/µm; fluence $5*10^6$ p/cm^2; energy 4.05 MeV/u) or X-ray (2.6 Gy) or were left non-irradiated. One hour post-irradiated samples were fixed and by immune-fluorescence stained against RPA (resection marker) and CENP-F (cell cycle marker, S/G2 cells are positive, G1 cells are negative). RPA foci were counted in at least 50 cells per sample in three independent experiments (n=3); RPA foci counted in non-irradiated cells were subtracted; the box is extended from the 25th to 75th percentiles; whiskers represent minimum to maximum. To the data was applied the Mann–Whitney U test: ns indicate statistically not significant.

The number of RPA foci per nucleus after carbon ion irradiation was strongly increased compared to X-ray-irradiated cells (Figure 4.4). However, the statistical analysis revealed no significant increase of the RPA foci number per cell in RIF1 depleted cells compared to carbon ion irradiated mock depleted cells.

Taken together, RIF1-depletion alone did not show a statistical significant effect on the DSB resection after carbon ion irradiation in U2OS cells.

4.1.4. 53BP1 depletion increased the number of RPA positive cells in G1- and S/G2 phases

53BP1 as a binding partner and upstream regulator of RIF1 recruitment plays an important role in preventing resection in G1 cells (Bunting, Callen et al. 2010). 53BP1 in response to DNA damage binds chromatin at dimethylated histone 4 (H4) at lysine 20 (H4K20me2) and ubiquitylated histone 2A (H2A) at lysine 15 (Panier and Durocher 2013). Depletion of 53BP1 consequently permits DSB resection (Bothmer, Robbiani et al. 2010). To examine whether 53BP1 is involved in resection regulation of heavy ion-induced DSBs in G1 cells, U2OS cells were depleted for 53BP1 by siRNA and the fraction of RPA positive cells was determined 1 h post irradiation. The efficiency of 53BP1 depletion was tested in Western analysis (Figure 4.5

A). 48 h post transfection, the cells were irradiated with carbon ions and fixed 1 h after irradiation. Immunofluorescence staining was performed against RPA (resection marker) and CENP-F (cell cycle marker).

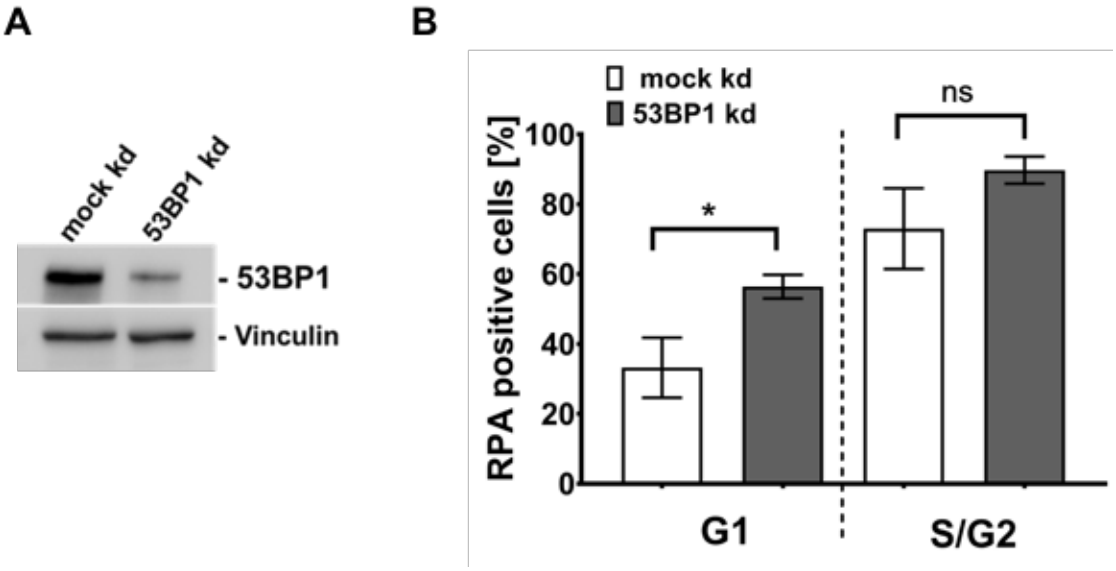

Figure 4.5: 53BP1 depletion increases the fraction of resection positive cells after carbon ion irradiation. U2OS cells were mock depleted (mock kd) or depleted for 53BP1 (53BP1 kd) by RNAi. **A:** Verification of 53BP1 depletion in Western analysis. The cells were irradiated angular with carbon ions (LET 325 keV/µm; 4.05 MeV/u; fluence 5 x 10^6 p/cm^2). 1 h post-irradiation, the samples were fixed and stained against RPA (resection marker) and CENP-F (cell cycle marker). RPA positive cells (foci/cell ≥ 5) were quantified in G1 (CENP-F negative cells) or in S/G2 phase (CENP-F positive cells). **B:** Graph shows mean value of RPA positive cells of two independent experiments (n=2); error bars show standard deviation. To the data was applied t-test. (*) represents P<0.05; ns indicates statistically not significant.

The mean value of RPA positive cell fraction was increased by 61,4 % in 53BP1 depleted G1 cells and by 20 % in 53BP1 depleted S/G2 cells compared to mock depleted cells (Figure 4.5 B). This result suggests that 53BP1 plays an important role in the prevention of the DSB resection in G1 cells after heavy ion irradiation.

4.1.5. RIF1 recruitment to the ion-induced DSBs is 53BP1 independent

Several publications have shown that the recruitment of RIF1 (as a part of ATM pathway and downstream partner of 53BP1) to the ionizing radiation induced DSBs is 53BP1 dependent (Silverman 2004, Chapman 2013, Escribano-Diaz, Orthwein et al. 2013). Yet, this work showed that RIF1 recruitment to the ion-induced DSBs was increased in S/G2 cells with increased LET. Concomitant, RIF1 depletion did not affect the resection at ion-induced DSBs in both G1- and S/G2 cells (Figure 4.3 and Figure 4.4). In contrast, 53BP1 depletion increased the fraction of resection positive cells post carbon ion irradiation (Figure 4.5 B). Moreover, the fraction of resection positive cells is increased with increasing LET (Averbeck, Ringel et al. 2014). Altogether these results suggest that RIF1 might operate 53BP1-

independent at ion-induced DSBs. To prove this idea of 53BP1-independent RIF1 recruitment to DSBs the cells were depleted by 53BP1 siRNA and irradiated with carbon ions (Figure 4.6 A).

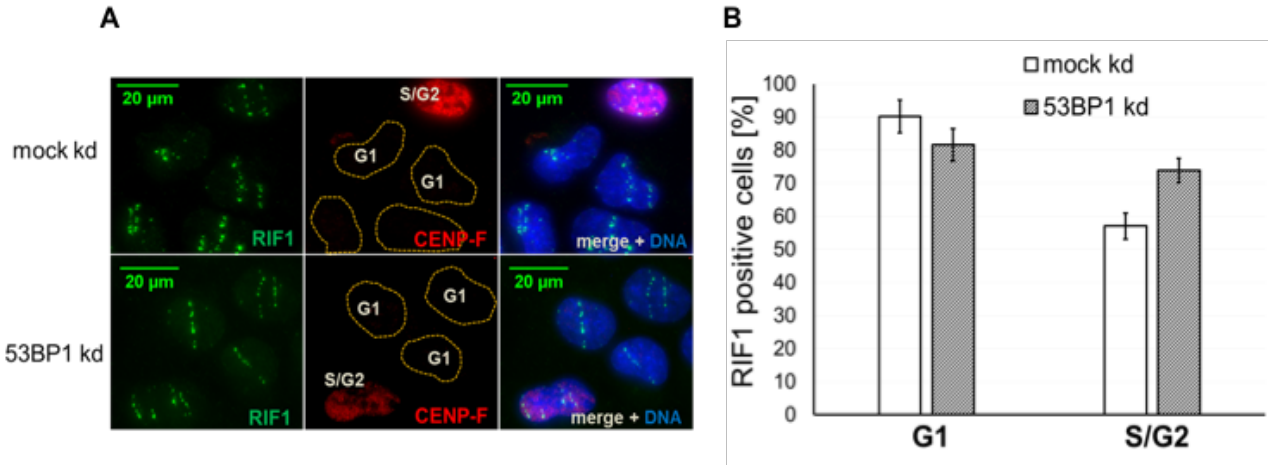

Figure 4.6: RIF1 recruitment after carbon ion irradiation was 53BP1 independent. U2OS cells were mock depleted (mock kd) or depleted for 53BP1 (53BP1 kd) by RNAi (the sample is depicted in Figure 4.5). **A:** Representative images of the cells irradiated angular with carbon ions (LET 325 keV/µm; 4.05 MeV/u; fluence 5 x 10^6 p/cm^2), fixed and stained 1 h post-irradiation against RIF1 and CENP-F (cell cycle marker). RIF1 positive cells were quantified in G1 (CENP-F negative cells) or in S/G2 phase (CENP-F positive cells). **B:** Graph shows mean value of RIF1 positive cells in G1 and S/G2 phases. Error bars show binomial error.

The 53BP1-depletion showed only 11 % decrease of the RIF1 positive G1 cell fraction compared to mock depleted G1 cells (Figure 4.6 B). Unexpectedly, there was 29,8 % increase of the RIF1 positive S/G2 cell fraction in 53BP1 depleted cells compared to mock depleted S/G2 cells (Figure 4.6 B). This result suggests that RIF1 might be recruited to the ion-induced DSBs by a 53BP1-independent pathway in both G1- and S/G2 cells.

4.1.6. BRCA1 depletion increased RIF1 foci formation at ion-induced DSBs

Some publications revealed that RIF1 in complex with 53BP1 opposes BRCA1 at ionizing radiation induced DSBs (Escribano-Diaz, Orthwein et al. 2013, Feng, Fong et al. 2013). Presuming that RIF1 as a partner of 53BP1 could participate in antagonism between 53BP1 and BRCA1 at ion-induced DSBs, the formation of RIF1 foci in BRCA1 depleted cells post carbon ion irradiation was analyzed. The BRCA1-depleted cells were irradiated with carbon ions or with X-rays of equivalent dose and the fixed cells were immunofluorescence stained against RIF1. The RIF1 foci number was increased from 31.9±1.4 to 43.2±1.2 foci/cell in BRCA1-depleted S/G2 cells compared to mock depleted cells after X-ray irradiation which corresponds with an increase of 35,4 % (Figure 4.7). In contrast, the RIF1 foci formation was not impaired by the BRCA1 depletion in G1 cells after X-ray irradiation.

Nevertheless, the number of RIF1 foci/cell was increased in G1 cells after carbon ion irradiation from 12.8±0.7 in mock depleted cells to 17.0±0.8 foci/cell in BRCA1 depleted cells that corresponds with an increase of 32,8 % (Figure 4.7). Moreover, the RIF1 foci formation was increased even stronger in BRCA1 depleted S/G2 cells after carbon ion irradiation from 9.2±0.9 in mock depleted cells to 23.2±1.1 in BRCA1 depleted cells, which corresponds with an increase of 152,2 %.

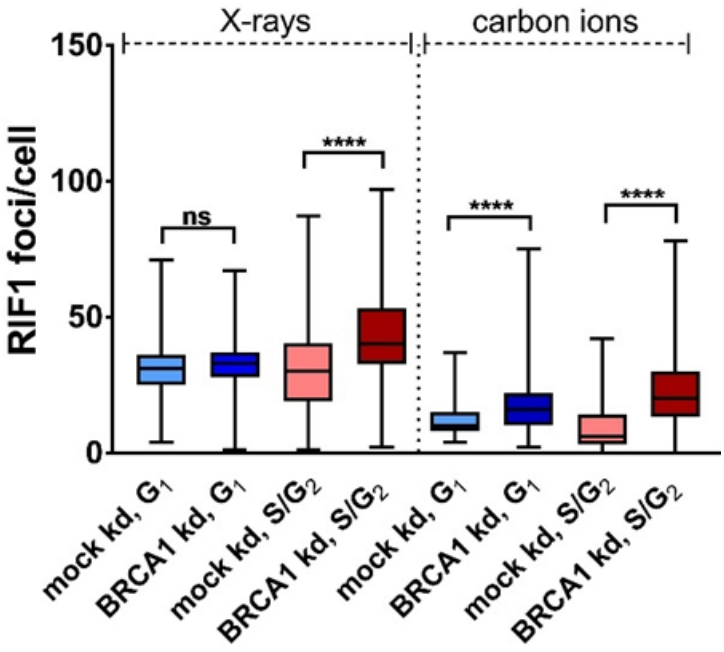

Figure 4.7: The number of RIF1 foci was increased in BRCA1 depleted G1 cells after carbon ion irradiation. U2OS cells were mock depleted (mock kd) or depleted for BRCA1 (BRCA1 kd) by RNAi. 48 h after transfection U2OS cells were angular irradiated with carbon ions (LET 325 keV/µm; fluence $5*10^6$ p/cm^2; energy 4.05 MeV/u) or X-rays (2.6 Gy) or were left non-irradiated. One hour post irradiation, samples were fixed and immune-stained against RIF1 and CENP-F (cell cycle marker, S/G2 cells are CENP-F positive, G1 cells are negative, G1 are CENP-F negative). RIF1 foci were counted in at least 50 cells per sample in three independent experiments (n=3); the average number of RIF1 foci in non-irradiated samples was subtracted from the number in irradiated cells; the box is extended from the 25th to 75th percentiles; whiskers represent minimum to maximum. To the data was applied the Mann–Whitney U test. (****) indicates P<0.0001; ns represents statistically not significant.

These results indicate that BRCA1 might antagonized RIF1 at ion-induced DSBs to facilitate DNA resection at ion-induced DSBs.

4.2. BRCA1 as a part of CtIP/BRCA1 complex promotes resection at ion-induced DSBs

BRCA1 emerged as a key regulator of the homology dependent DNA repair pathway and therefore contributes to the genomic stability (Moynahan, Chiu et al. 1999). Furthermore, the 53BP1 replacement by BRCA1 at DSB sites leads to a shift of the repair pathway choice in S/G2 cells to the homology dependent repair (Chapman, Sossick et al. 2012). This role of

BRCA1 was shown in context with the cells cycle (Shrivastav, De Haro et al. 2008). However, the mechanism of resection regulation after heavy ion irradiation and the role of interaction between BRCA1 and 53BP1/RIF1 complex remains poorly understood. The BRCA1-recruitment to the complex DSBs may play a crucial role in the repair pathway choice.

4.2.1. BRCA1 recruitment to ion-induced DSBs is cell cycle dependent

BRCA1, as an antagonistic factor of RIF1, promotes resection after sparsely ionizing irradiation in S/G2 cells (Escribano-Diaz, Orthwein et al. 2013). Since it is known that the number of resection positive cells increases with increasing LET (Averbeck, Ringel et al. 2014) it was expected that also the fraction of BRCA1-positive cells might be increased with increasing LET. To examine this notion, the cells were irradiated with heavy ions of different LET and analyzed by immunofluorescence staining against BRCA1 1 h post irradiation. BRCA1 was recruited to heavy ion- and X-ray induced DSBs in both G1 and S/G2 cells (Figure 4.8 A). Interestingly, the BRCA1 background foci were visible in non-irradiated S/G2 cells suggesting an additional, ionizing radiation-independent, function of BRCA1 in S/G2 cells. Moreover, the accumulation of BRCA1 foci was more pronounced in S/G2 cells after X-ray irradiation than in G1 cells (Figure 4.8 A). The BRCA1 foci in irradiated cells were associated with γH2AX foci indicating that BRCA1 was recruited to the DSB sites. The evaluation of the BRCA1 positive cell fraction after heavy ion irradiation with different LETs resulted in a stable fraction of BRCA1 positive cells in G1 phase between 20 and 30 % (Figure 4.8 B).

Taken together, the recruitment of BRCA1 to ion-induced DSB was LET independent. The fraction of BRCA1 positive cells was high in S/G2, but low in G1 cells.

A

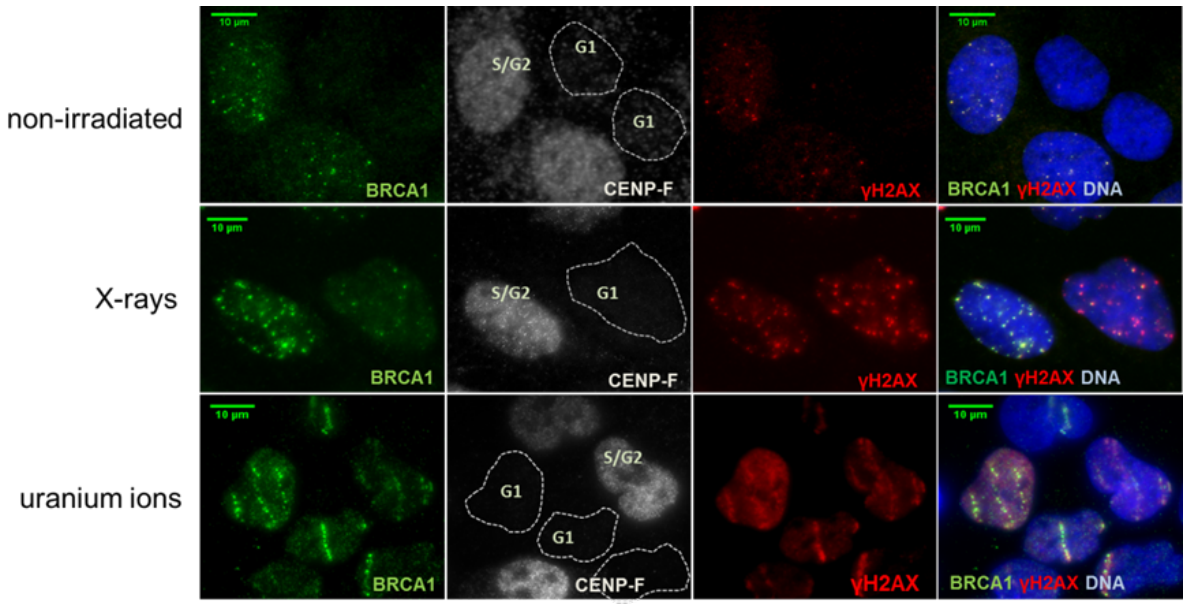

B

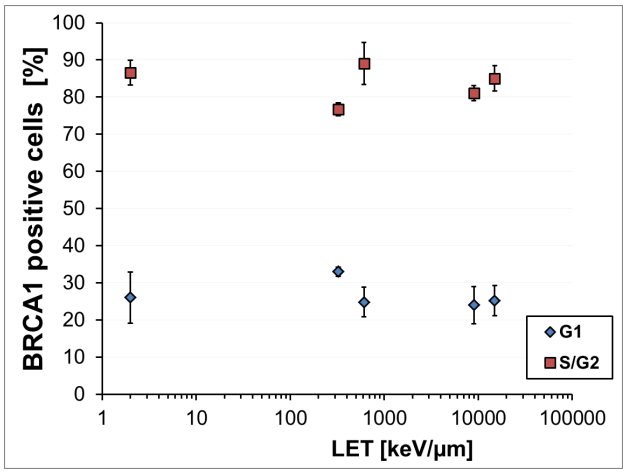

Figure 4.8: BRCA1 recruitment to ion-induced DSBs is LET independent. A: U2OS cells 24 h after seeding were irradiated angular with uranium ions (LET 15,000 keV/µm; 6.21 MeV/u; fluence $3*10^6$ p/cm^2) or with X-rays (1 Gy). 1 hour post irradiation cells were fixed and immunofluorescence stained against BRCA1 (green), CENP-F (white; cell cycle marker, S/G2 cells are CENP-F positive; G1 cells are CENP-F negative) and γH2AX (red; DSB marker). DNA was stained with DAPI (blue). BRCA1 was recruited to ionizing irradiation induced DNA-DSBs in G1- and S/G2 cells. The BRCA1 signal co-localized with the γH2X signal in the merged image. **B:** Fraction of BRCA1 positive cells after irradiation with different ions or X-rays (1 Gy). U2OS cells were irradiated with low LET X-rays (LET 2 keV/µm) or with high LET ions: carbon ions LET 170 keV/µm or 325 keV/µm; oxygen ion LET 610 keV/µm; xenon ion LET 9,000 keV/µm and uranium ion LET 15,000 keV/µm. All ions were applied with fluence $3*10^6$ p/cm^2. The cells were stained as described in A. The number of BRCA1 positive cells (with ion tracks) was counted in G1- and S/G2 cells. Error bars represent the binomial error.

4.2.2. BRCA1 depletion did not influence the number of RPA positive cells after carbon ion irradiation

BRCA1 was reported in several publications to promote DNA resection by an interaction with resection protein CtIP and by antagonistic interaction with an anti-resection factor 53BP1 and its effector RIF1 (Panier and Boulton 2014, Jiang and Greenberg 2015).

To examine the role of BRCA1 in the resection regulation after heavy ion irradiation BRCA1 depletion by RNAi was established (Figure 4.9 A). The successfully BRCA1 depleted U2OS cells were irradiated with carbon ions and stained by immunofluorescence against RPA (resection marker) (Figure 4.9 B). The evaluation of resection positive cells with resection marker RPA in BRCA1 depleted cells after irradiation showed that number of resection positive cells was not significantly altered either in G1- or in S/G2 phase compared to mock depleted irradiated cells.

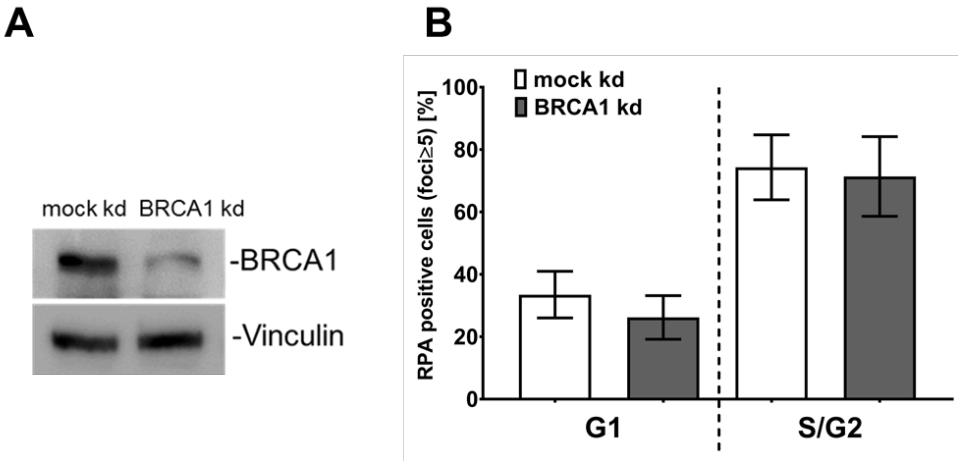

Figure 4.9: BRCA1 depletion does not influence the fraction of resection positive cells. A: Western analysis of BRCA1 depleted cells. U2OS cells were treated with BRCA1 siRNA or mock treated. Mock depleted cells (mock kd) were treated as BRCA1 depleted (BRCA1 kd) cells but without siRNA. Vinculin was used as a loading control. **B:** BRCA1 depleted or mock depleted U2OS cells were irradiated angular with carbon ions (LET 325 keV/µm, 4.05 MeV/u, fluence $5x10^6$ p/cm^2). 1 h post-irradiation the samples were fixed and immunofluorescence stained against RPA (resection marker) and CENP-F (cell cycle marker, S/G2 cells are positive, G1 cells are negative). RPA positive cells (foci/cell ≥ 5) were quantified in G1 cells or in S/G2 cells. The graph shows the mean value of RPA positive cells of three independent experiments (n=3); error bars represent ±SEM.

Altogether, the number of resection positive cells was not impaired in BRCA1 depleted cells either in G1- or in S/G2 cells.

4.2.3. HUWE1 depletion increased BRCA1 positive cells in G1 phase, but did not increase the number of RPA positive cells

The BRCA1 positive cell fraction in G1 phase after heavy ion irradiation was between 20 - 30 % and LET independent (Figure 4.8 B). Based on these results, it could be assumed that the BRCA1 protein level might be regulated in cell cycle dependent manner. This notion can be supported with earlier studies that the BRCA1 protein level is decreased in G1 phase compared to BRCA1 level in S/G2 cells (Chen, Farmer et al. 1996, Gudas, Li et al. 1996). An increase of BRCA1 protein level could positively influence the number of resected cells in G1 phase. The BRCA1 protein level is controlled by HUWE1, a ubiquitin ligase E3, which binds its N-terminus degron domain to promote BRCA1 degradation (Wang, Lu et al. 2014). Consequently, the HUWE1 depletion (Figure 4.10) could influence the BRCA1 foci formation and subsequently, the accumulation of resection positive cells after heavy ion irradiation in G1 cells.

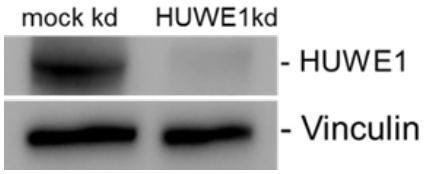

Figure 4.10: HUWE1 depletion in U2OS cells. Western analysis was performed with HUWE1 siRNA treated U2OS cells. Mock depleted cells (mock kd) were treated as HUWE1 depleted (HUWE1 kd) cells but without siRNA. The cells lysates were performed 72 h after transfection. Vinculin was used as a loading control.

The HUWE1 depleted or mock depleted U2OS cells were irradiated with oxygen ion and fixed 1 h post irradiation. The fraction of BRCA1 positive cells was strongly increased in HUWE1 depleted G1 cells compared to mock depleted cells (Figure 4.11 A). However, the increase of BRCA1 protein level was not mirrored in the fraction of resection positive cells after oxygen ion irradiation (Figure 4.11 B). Consistently, the HUWE1 depleted S/G2 cells showed slight increase of BRCA1 positive cells. However, the analysis of the resection positive cells in HUWE1 depleted cells did not reveal a difference between HUWE1 depleted and mock depleted S/G2 cells after oxygen ion irradiation (Figure 4.11 B).

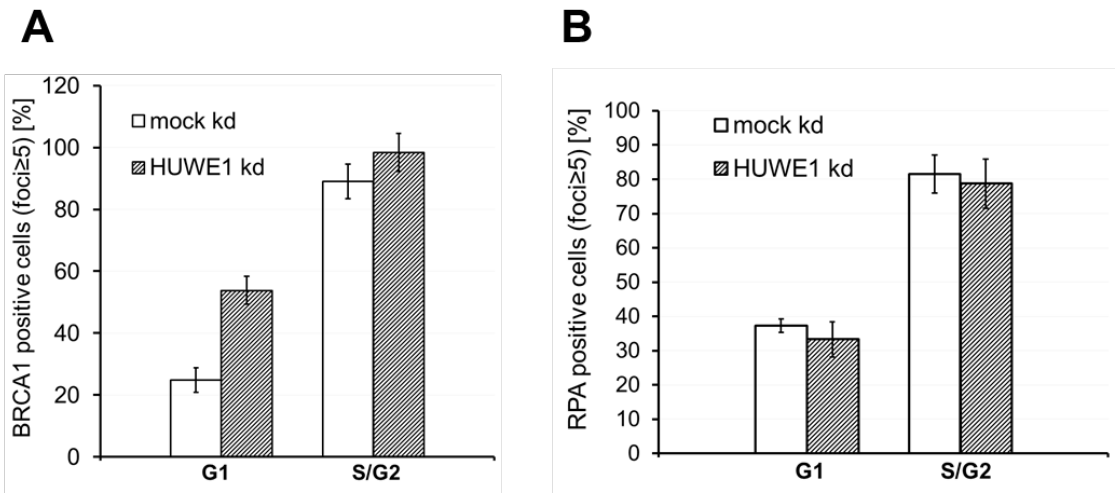

Figure 4.11: HUWE1 depletion increases the fraction of BRCA1 positive G1 cells after oxygen ion irradiation. U2OS cells were mock depleted or depleted for HUWE1 (HUWE1 kd) by RNAi. The cells were irradiated with oxygen ions (LET 650 keV/µm; energy 3.2-2.4 MeV/u; fluence $3*10^6$ p/cm^2). 1 h post-irradiation the cells were fixed and immuno-stained against BRCA1 or RPA (resection marker) and CENP-F (cell cycle marker S/G2 cells are CENP-F positive, G1 cells are CENP-F negative) **A:** Fraction of BRCA1 positive cells in HUWE1 depleted cells. **B:** Fraction of resection positive (RPA) cells in HUWE1 depleted cells. The cell with at least 5 BRCA1- or RPA foci was considered as positive. At least 100 cells were counted per each condition. Error bars represent binomial error.

Taken together, neither the BRCA1 depletion nor the increase of BRCA1 protein level through HUWE1 depletion affected the fraction of resection positive G1- and S/G2 cells.

4.2.4. BRCA1 depletion decreased RPA foci formation at ion-induced DSBs

The results in section 2.2 suggest that BRCA1 depletion does not have an effect on the resection at ion-induced DSBs. Nevertheless, some publications argue that BRCA1 may have an important role in the regulation of DNA resection, particularly in the promoting of resection initiation as well as in regulating the resected length of the DNA (Feng, Fong et al. 2013, Cruz-Garcia, Lopez-Saavedra et al. 2014, Densham, Garvin et al. 2016, Biehs, Steinlage et al. 2017). Therefore, further analysis was proposed in which the RPA foci formation at ion-induced DSBs in BRCA1- versus mock depleted cells was evaluated. Additionally, to assess the role of DSB complexity in the resection regulation the cells were irradiated with equivalent dose of X-ray and treated identically as the carbon ion irradiated cells. As expected, low LET radiation hardly induces DSB resection in G1 cells (Figure 4.12). Moreover, the number of RPA foci in S/G2 cells was much lower in X-ray irradiated cells (1.45±0.44 foci/cell) than in carbon ion irradiated cells (24.33±1.67 foci/cell). Interestingly, BRCA1 depletion impaired RPA foci formation in both G1- and S/G2 cells after carbon ion irradiation (Figure 4.12). In G1 cells RPA foci/cell were decreased from 7.66±0.94 foci/cell to 4.17±0.56 foci/cell (45,6 %) and in S/G2 cells RPA foci/cell were decreased from 24.33±1.67

foci/cell to 10.05±0.97 foci/cell (58,9 %). This result confirms the assumption that BRCA1 is involved in the positive regulation of DSB resection. Furthermore, this result suggests that BRCA1 may be an important player in the resection regulation at ion induced DSBs in G1 cells.

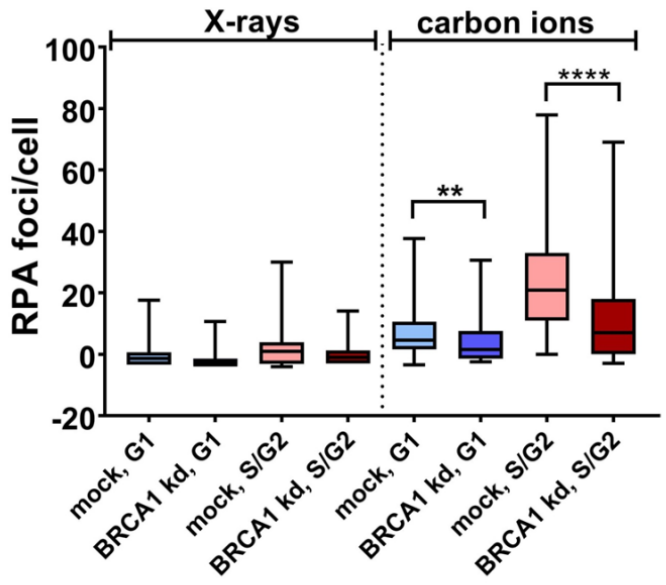

Figure 4.12: BRCA1 depletion affects RPA foci generation after carbon ion irradiation. U2OS cells were mock depleted (mock), depleted for BRCA1 (BRCA1 kd) by RNAi. 48 h after transfection U2OS cells were angular irradiated with carbon ions (LET 325 keV/µm; fluence $5*10^6$ p/cm^2; energy 4.05 MeV/u) or X-ray (2.6 Gy) or were left non-irradiated. One hour post-irradiated samples were fixed and by immunofluorescence stained against RPA (resection marker) and CENP-F (cell cycle marker, S/G2 cells are positive, G1 cells are negative). RPA foci were counted in at least 50 cells per sample in three independent experiments (n=3); RPA foci counted in non-irradiated cells were subtracted; the box is extended from the 25th to 75th percentiles; whiskers represent minimum to maximum. To the data was applied the Mann–Whitney U test: (**) indicates P<0.01 and (****) indicates P<0.0001.

Taken together, BRCA1 depletion significantly reduces RPA foci formation at ion-induced DSB in both G1- and S/G2 cells. However, BRCA1 depletion did not completely eliminate the RPA foci formation after carbon ion irradiation.

4.2.5. RIF1 depletion increased BRCA1 foci formation at ion-induced DSBs

Since the BRCA1 depletion compromised the RPA foci formation after carbon ion irradiation the investigation whether RIF1 depletion can reinforce BRCA1 accumulation at ion-induced DSBs might help to understand the mechanism of resection at complex DSBs in G1 cells. To test the contribution of RIF1 to the inhibition of BRCA1 at ion-induced DSBs, the cells were depleted by RIF1 RNAi. The 48 h post transfection cells were irradiated with carbon ions or

equivalent dose of X-ray or remained non-irradiated. One hour after irradiation the cells were fixed and immunofluorescence stained against BRCA1 and CENP-F (cells cycle marker).
The evaluation of BRCA1 foci formation in RIF1 depleted cells supports the above assumed competition of BRCA1 and RIF1 at ion induced DSBs in G1 cells. The number of BRCA1 foci was significantly increased by appr. 25.4 % after X-ray irradiation only in RIF1 depleted S/G2 cells, from 29.5±1.7 in mock depleted cells up to 37±1.6 foci per cell in RIF1 depleted cells (Figure 4.13).

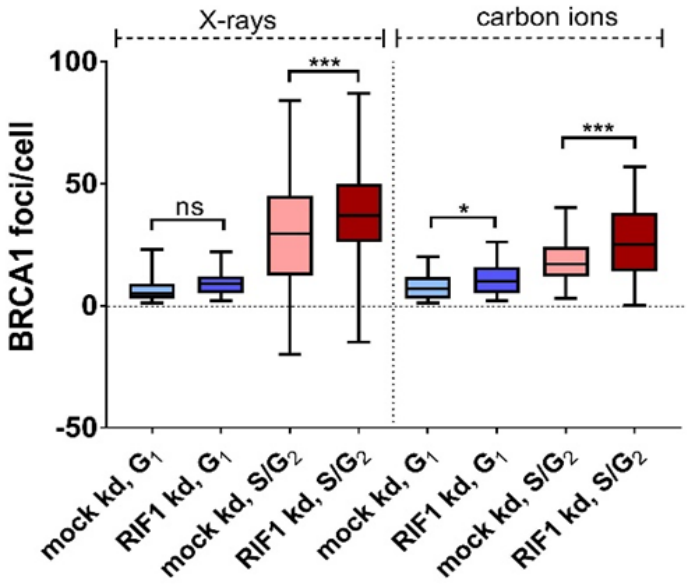

Figure 4.13: The number of BRCA1 foci was increased in RIF1 depleted U2OS cells after X-ray and carbon ion irradiation. U2OS cells were mock depleted (mock kd) or depleted for RIF1 (RIF1 kd) by RNAi. 48 h after transfection U2OS cells were irradiated angular with carbon ion (LET 325 keV/µm; fluence $5*10^6$ p/cm^2; energy 4.05 MeV/u) or X-ray (2.6 Gy) or were left non-irradiated. 1 h post irradiation the cells were fixed and stained by immunofluorescence against BRCA1 and CENP-F (cell cycle marker, S/G2 cells are CENP-F positive; G1 cells are CENP-F negative). The BRCA1 foci were counted in at least 50 cells per sample in three independent experiments (n=3); the average number of BRCA1 foci in non-irradiated samples was subtracted from the foci number in irradiated cells; the box is extended from the 25th to 75th percentiles; whiskers represent minimum to maximum. To the data was applied the Mann–Whitney U test (*) indicates P<0.05 and (***) indicates P<0.001; ns indicates statistically not significant.

The number of BRCA1 foci was increased even more in RIF1 depleted S/G2 cells after carbon ion irradiation – appr. 47 % - from 17±0.9 foci per cell in mock depleted S/G2 cells up to 25±1.5 foci per cell in RIF1 depleted S/G2 cells (Figure 4.13). In contrast to X-ray irradiated RIF1 depleted G1 cells, those irradiated with carbon ions showed a clear increase number of BRCA1 foci. The increase was appr. 42.8 % from 7±0.9 foci per cell in mock depleted up to 10±1.2 foci per cell in RIF1 depleted G1 cells (Figure 4.13). This result also suggests that BRCA1 and RIF1 are antagonists at ion-induced DSBs in G1 cells. Thus,

RIF1's recruitment to ion-induced complex DSBs seems not to be 53BP1 dependent (c. 4.1.5) it is, however, BRCA1 dependent.

Taken together, RIF1 depletion increases the BRCA1 foci formation in S/G2 cells after X-ray- and carbon ion irradiation. Moreover, the number of BRCA1 foci was increased in RIF1 depleted G1 cells after carbon ion irradiation but not after X-ray irradiation.

4.2.6. RIF1 and BRCA1 foci formation at ion-induced DSB was stable up to three hours in G1 cells

The experiments revealed that RIF1 (Figure 4.1 B) and BRCA1 (Figure 4.8 B) are recruited to ion-induced DSBs in both G1 and S/G2 cells. The depletion experiments, however, presumed that BRCA1 and RIF1 might be recruited to DSBs in a mutually exclusive manner (Figure 4.7 and Figure 4.13). These observations led to the working hypothesis that BRCA1 might actively replace RIF1, as a protector of DNA ends from resection, at DSB in G1 cells. If that is true, the number of RIF1 foci per ion track should decrease with time after irradiation whereas BRCA1 foci should increase. To test this hypothesis, the recruitment of BRCA1 and RIF1 to ion-induced DSBs was analyzed at three time points after irradiation. The earliest time point was 0.25 h post irradiation to observe whether both factors, BRCA1 and RIF1, were already recruited to the DSBs. The next chosen time point was 1 h post irradiation, which is the earliest time point to see DSB resection. The last time point was 3 h post irradiation, at which is expected an increase in number of resected cells after heavy ion irradiation (Averbeck, Ringel et al. 2014). The number of RIF1 and BRCA1 foci per ion track in dependence of the cell cycle was evaluated in U2OS cells angular irradiated with carbon ions. In G1 cells the number of RIF1 foci per track was higher than the number of BRCA1 foci per track. In S/G2 cells, however, it was the opposite result. At all three time points after irradiation the number of BRCA1 and RIF1 foci remained at the same level in G1 cells (Figure 4.14). A slight decrease of the foci number per ion track of both BRCA1 and RIF1 was observed in S/G2 cells which might be due to DSB repair. The observed foci number at the chosen time points after irradiation did not indicate that RIF1 is replaced by BRCA1 at DSB sites.

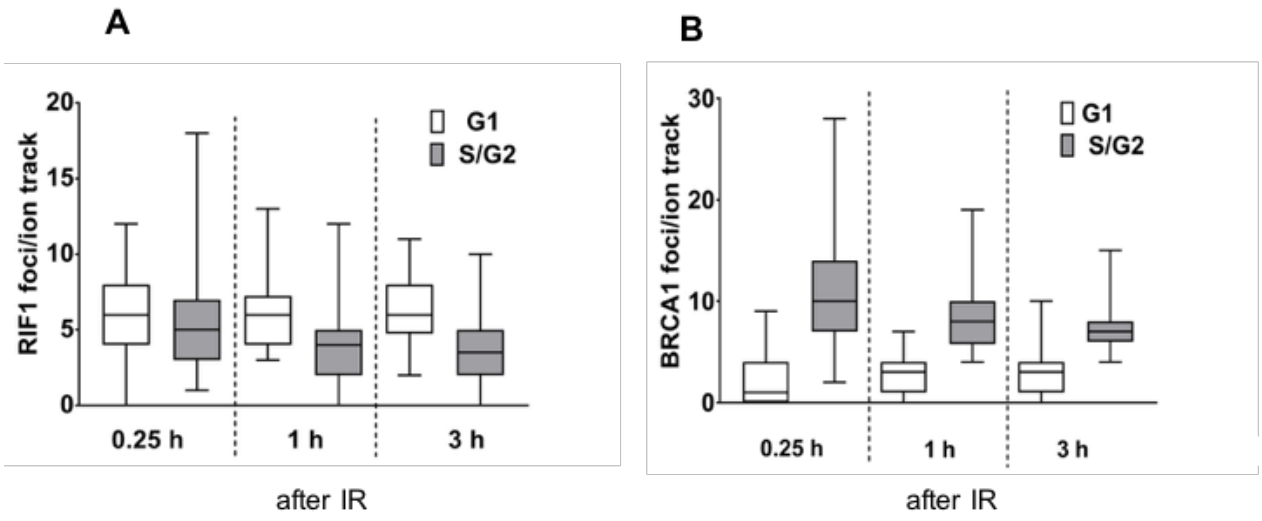

Figure 4.14: RIF1 and BRCA1 foci per ion track after carbon ion irradiation. 24 h after seeding U2OS cells were irradiated angular with carbon ion (LET 325 keV/µm; fluence $5*10^6$ p/cm^2; energy 4.05 MeV/u). Subsequently, the cells were fixed 0.25 h, 1 h and 3 h after irradiation. Double immunofluorescence staining was performed against RIF1 **(A)** or BRCA1 **(B)** and against CENP-F (cell cycle marker, S/G2 cells are CENP-F positive; G1 cells are CENP-F negative). The BRCA1 and RIF1 foci number per ion track were counted in at least 50 cells per time point and cell cycle phase; the box is extended from the 25th to 75th percentiles; whiskers represent minimum to maximum.

Taken together, consistent with the predominant number of RIF1 positive cells in G1 phase after heavy ion irradiation the number of RIF1 foci per ion track was higher in G1 cells compared to S/G2 cells. Furthermore, the number of BRCA1 foci per ion track was in S/G2 cells higher than in G1 cells.

4.2.7. Co-localization of BRCA1 and RIF1 at ion-induced DSBs

The foci dynamic at carbon ion induced DSB showed that BRCA1 do not seem to replace RIF1 at DSB sites (Figure 4.14 A and B). Nevertheless, the fact that G1- and S/G2 cells bear both BRCA1 and RIF1 foci led to the question whether BRCA1 and RIF1 operate at the same DSB to regulate the resection process. Therefore, a double immunofluorescence staining against BRCA1 and RIF1 in uranium ion irradiated U2OS cells was performed. The number of RIF1 positive cells was high enough not only in G1 cells but also in S/G2 cells as the result of very high LET of uranium ions, therefore, these samples were chosen (Figure 4.1 B). Yet, the fraction of BRCA1 positive cells was limited in G1 cells (Figure 4.8 B), hence, for this analysis only BRCA1 positive cells were considered. Interestingly, most of the BRCA1 and RIF1 signal did not co-localize in both G1- and S/G2 cells (Figure 4.15 A and B) indicating independent recruitment to the DSB sites. A detailed analysis of the images with intensity profiles revealed that the overlapping of RIF1 and BRCA1 signals in G1 was more expanded than in S/G2 cells.

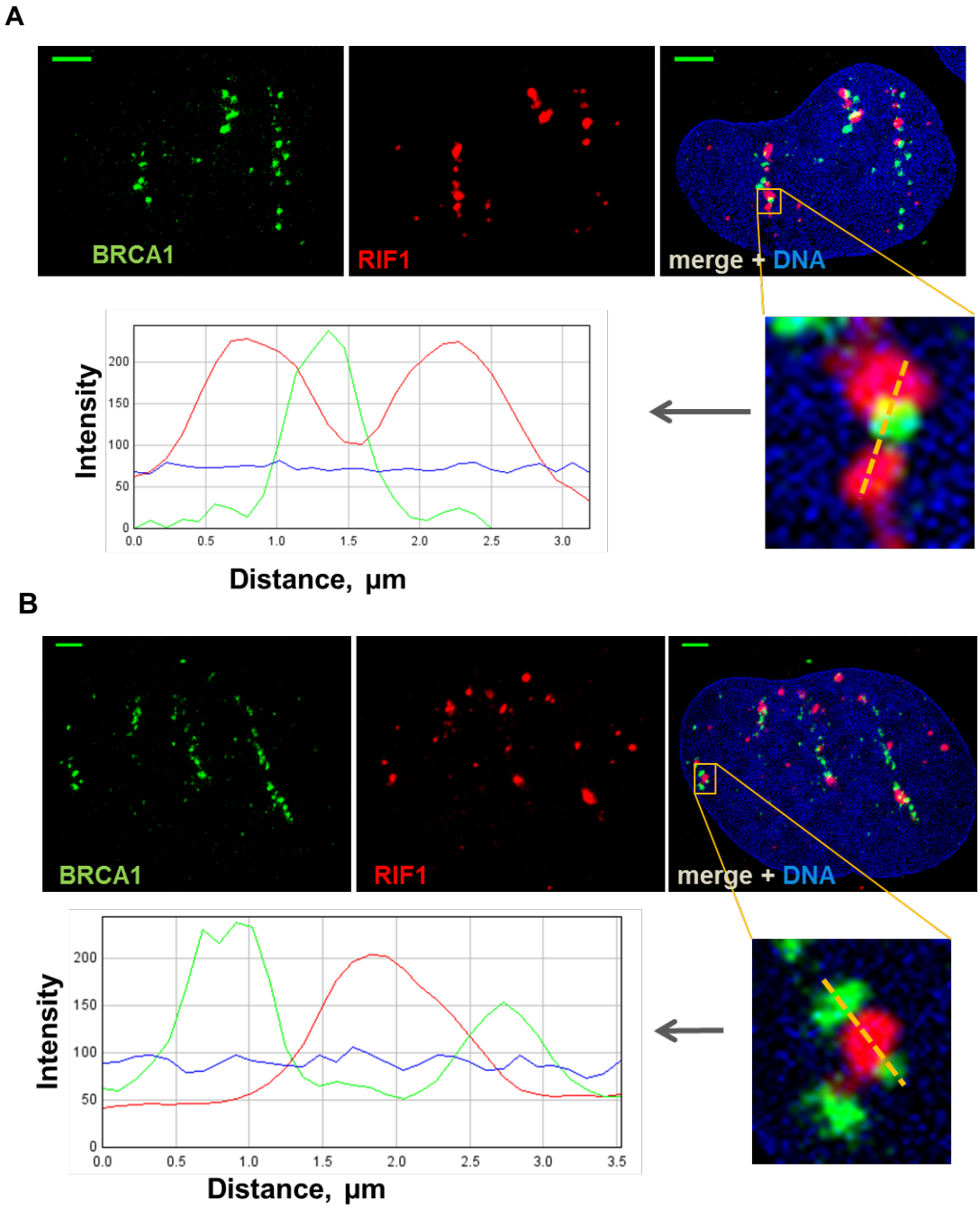

Figure 4.15: Co-localization analysis of BRCA1 and RIF1 after uranium ion irradiation. U2OS cells were irradiated angular with uranium ions (LET 15,000 keV/µm; fluence $3*10^6$ p/cm^2). 1 hour post irradiation cells were fixed and stained against BRCA1 and RIF1 as well as CENP-F (cell cycle marker, S/G2 cells are CENP-F positive; G1 cells are CENP-F negative). DNA was stained with DAPI (blue). The intensity profile was measured along dashed yellow line. **A**: CENP-F negative cell (G1). **B:** CENP-F positive cell (S/G2). The images were de-convolved using "Deconvolution Wizard" of Huygens essentials software. Intensity profiles of ion tracks were measured by Image J software. Scale bar 5 µm.

In brief, both BRCA1 and RIF1 were operating in the same nucleus, but in general not at the same DSB site.

4.2.8. Extent of BRCA1 and RIF1 co-localization at ion-induced DSBs is cell cycle dependent

Since in G1 cells the ion-induced BRCA1 and RIF1 signals in the same nucleus were partially co-localized, it was suggested that the extent of their overlapping in G1 versus S/G2 phase within first three hours after irradiation might elucidate the functional interaction between them. A different degree of BRCA1-RIF1 overlapping signals in G1- versus S/G2 cells might indicate a dual role of BRCA1-RIF1 interaction in dependency on the cell cycle progression and/or the complexity of DSBs. Therefore, the overlapping area analysis was performed with carbon ion- as well as with X-ray of equivalent dose irradiated cells. The cells were fixed at three different time points: 0.25 h, 1 h and 3 h post irradiation and immunofluorescence double-stained against BRCA1 (green) and RIF1 (red).

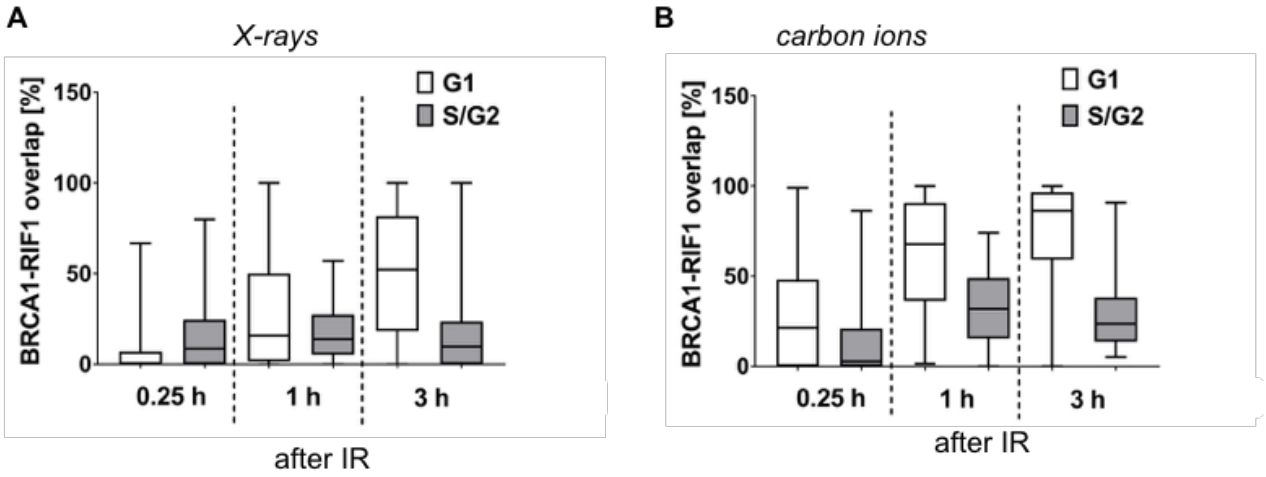

Figure 4.16: BRCA1-RIF1 overlapping after X-ray or carbon ion irradiation. U2OS cells were irradiated with **(A)** X-rays (2.6 Gy) or with **(B)** carbon ions (LET 325 keV/µm; energy 4.05 MeV/u; fluence $5*10^6$ p/cm^2). The cells were fixed 0.25 h, 1 h and 3 h after irradiation. Immunofluorescence staining was performed against RIF1, BRCA1 and against CENP-F (cell cycle marker, S/G2 cells are CENP-F positive; G1 cells are CENP-F negative). The area simultaneously positive for BRCA1 and RIF1 per nucleus was measured with Image J software. The total BRCA1- or RIF1 signal area per nucleus was used for standardization (explanation in text). At least 40 cells per time point were analyzed in a single experiment; n = 1; the box is extended from the 25th to 75th percentiles; whiskers represent minimum to maximum.

The relative BRCA1-RIF1 overlapping areas, i.e. the area of a nucleus positive for both BRCA1 and RIF1 signal was measured by Image J software and normalized to a total BRCA1 or RIF1 signal area, namely the smallest signal area was chosen for normalization. That implies that if the area of total RIF1 signal in a nucleus is smaller than BRCA1 signal total area, the RIF1 signal area represents 100 %. If the opposite is the case, then the BRCA1 signal area represents 100 %.

The BRCA1-RIF1 overlapping area in G1 cells after X-ray irradiation was increased over time after irradiation from the overlapping from less than 10 % at 0.25 h up to 50 % at 3 h time point (Figure 4.16 A), whereas in S/G2 cells BRCA1 and RIF1 signals were barely overlapped. Interestingly, the carbon ion irradiation provided a larger BRCA1-RIF1 overlap in comparison to X-ray irradiation (Figure 4.16 B). Moreover, the BRCA1-RIF1 overlapping areas increase at a later time point, the increase was from 30 % at 0.25 h up to 70 % at 3 h in G1 cells and from 1 % at 0.25 h up to 30 % at 1 h (and 23 % at 3 h) in S/G2 cells. Nevertheless, the BRCA1-RIF1 overlapping area in G1 cells was about twofold higher than in S/G2 cells after carbon ion irradiation.

Taken together, the difference in extent of BRCA1-RIF1 signal overlap - depending on radiation quality and the cell cycle - suggests a distinct role for BRCA1-RIF1 interaction in G1 cells after heavy ion irradiation.

4.2.9. Co-localization BRCA1 and RIF1 with resection marker RPA

From the higher extent of BRCA1-RIF1 overlap in G1 cells compared to S/G2 cells arose the question as to how are BRCA1- or RIF1 signals related to the RPA signal in G1 versus S/G2 cells after heavy ion irradiation? Might the extended BRCA1-RIF1 overlap in G1 cells give a hint for the mechanism of the resection regulation after heavy ion irradiation? To pursue these questions the carbon ion irradiated cells were double immunofluorescence stained against RPA and RIF1 or against RPA and BRCA1 1 h post irradiation - the earliest time point to see DNA resection by immunofluorescence staining (Averbeck, Ringel et al. 2014). The RIF1 and RPA signals hardly showed an overlap (Figure 4.17) indicating that RIF1 is not involved in the resection process. In contrast, the BRCA1 and RPA signals showed larger overlapping areas in S/G2 cells (Figure 4.17) suggesting that BRCA1 might be involved in resection machinery in S/G2. However, the BRCA1-RPA overlapping areas in G1 cells were significantly smaller than in S/G2 cells suggesting that BRCA1 might play a minor role in the resection regulation machinery in G1 cells.

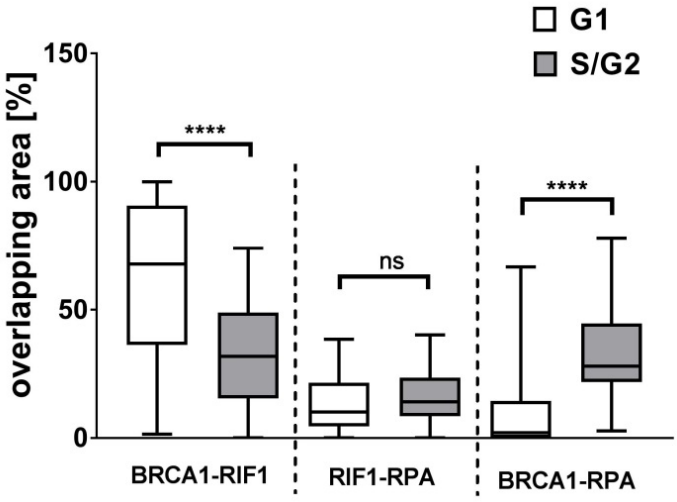

Figure 4.17: Analysis of BRCA1, RPA and RIF1 overlapping after carbon ion irradiation. U2OS cells were irradiated with carbon ions (LET 325 keV/µm; fluence $5*10^6$ p/cm^2; energy 4.05 MeV/u). 1 h post-irradiation the cells were fixed and immunofluorescence stained against RIF1 and RPA or BRCA1 and RPA as well as against CENP-F (cell cycle marker, S/G2 cells are CENP-F positive; G1 cells are CENP-F negative). To better comparison, the data of BRCA1 and RIF1 immuno-staining at 1 h time point was taken from Figure 4.16. The area simultaneously positive for RIF1 and RPA, or RIF1 and BRCA1, or RPA and BRCA1 per nucleus was measured with ImageJ software. The total RPA signal area per nucleus was used for standardization. At least 40 cells were analyzed in the RIF1-BRCA1 sample and at least 25 cells were analyzed in the RPA-RIF1 and RPA-BRCA1 samples in a single experiment. The box is extended from the 25th to 75th percentiles; whiskers represent minimum to maximum. The t-test was applied to the BRCA1-RIF1 and RIF1-RPA data sets. The Mann–Whitney U test was applied to the BRCA1-RPA data. (****) indicates P<0.0001. ns indicates statistically not significant.

The overlapping approach performed here support the notion that BRCA1 might play a dual role at the DSB sites dependent on cells cycle progression (Wei, Lan et al. 2008, Jiang, Plo et al. 2013)

4.3. UHRF1 is a regulation partner of CtIP/BRCA1 complex

BRCA1 and RIF1 foci remained longer at DSBs along the ion track in G1 cells compared to S/G2 cells. Since BRCA1 depletion decreased RPA- and increased RIF1 foci of ion-induced DSBs also in G1 cells, it was hypothesized that BRCA1 removes RIF1 together with 53BP1 from ion-induced DSBs, most probably in case of c-NHEJ failure. Up until now the mechanism is not fully understood. Recently reported E3 ubiquitin ligase UHRF1 might be the interacting factor between RIF1 and BRCA1 at ion-induced DSBs (Zhang, Liu et al. 2016).

4.3.1. UHRF1 depletion decreased the number of RPA positive cells

UHRF1 as a multi-domain protein, which is originally known as a key epigenetic regulator by bridging DNA methylation and chromatin modification related to DNA replication (Bostick, Kim et al. 2007), was reported to be positively correlated with cellular proliferation (Fujimori, Matsuda et al. 1998) . Its sequence, among other domains, possesses PHD and RING motifs with E3 ubiquitin ligase activity. The lack of UHRF1 RING domain sensitizes cells to treatment with DNA damaging agents (Citterio, Papait et al. 2004, Jenkins, Markovtsov et al. 2005). Moreover, the E3-ubiquitin-ligase activity of UHRF1 was shown to ubiquitinate RIF1 and remove it from DSBs (Zhang, Liu et al. 2016). Hence, UHRF1 might play an important role in the resection regulation at heavy ion induced DSBs. The ubiquitination of RIF1 effectuates its release from 53BP1 and dissociation from DSBs. However, the remained 53BP1 still can protect DSBs from resection. Another study revealed that BRCA1, which also contains RING domain with E3-ubiquitin-ligase activity, is needed to ubiquitinate 53BP1 at DSB to release it from the break and prevent 53BP1 from phosphorylation by ATM (Feng, Li et al. 2015). This work initiated the examination of the UHRF1 role in the resection regulation at ion-induced DSBs. For this purpose, an UHRF1-depletion in U2OS cells by RNAi was established (Figure 4.18).

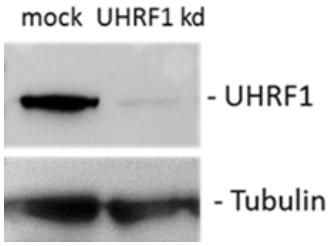

Figure 4.18: Western analysis of UHRF1 depleted U2OS cells. The cells were treated with UHRF1 RNAi (UHRF1 kd) or mock treated (without siRNA) and cultivated 48 h post transfection. The cell extract of UHRF1 siRNA treated and mock treated U2OS was analyzed in Western blot. Tubulin was used as a loading control.

UHRF1- or mock depleted cells were irradiated with carbon ions. One hour post irradiation cells were immunofluorescence stained against RPA or RIF1 and analyzed by microscopy. The RPA- and RIF1 positive cells were counted in both G1 and S/G2 cells. UHRF1 depletion decreased the fraction of RPA positive G1 cells appr. 46.8 % as well as the fraction of RPA positive S/G2 cells appr. 38.5 % compared to mock depleted cells respectively (Figure 4.19 A). The fraction of RIF1 positive cells was slightly affected by UHRF1 depletion and with carbon ion irradiated cells. The number of RIF1 positive cells was decreased appr. 8.9 % in G1 cells, whereas in S/G2 cells the number of RIF1 positive cells was increased appr. 12.7 % (Figure 4.19 B).

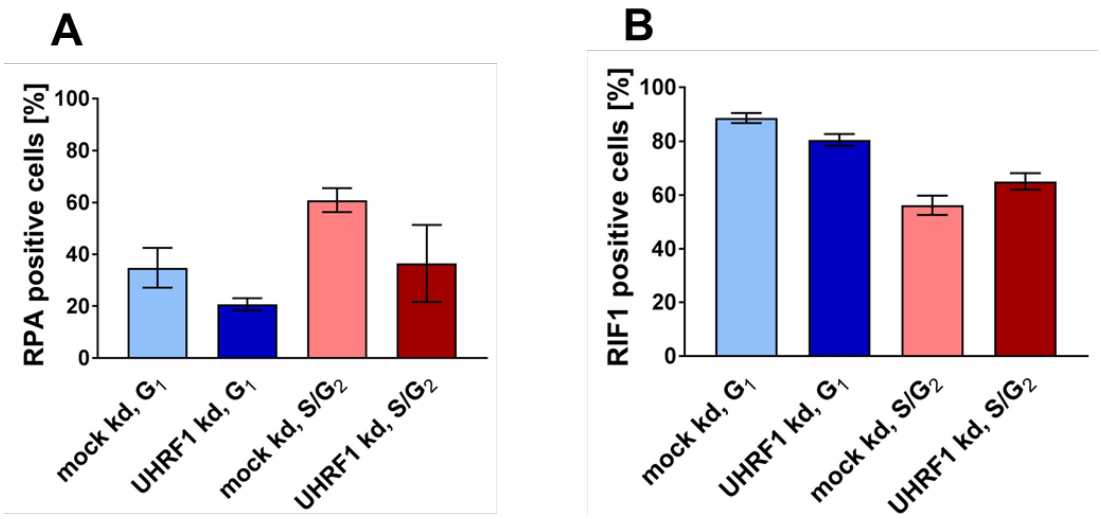

Figure 4.19: UHRF1 depletion may modulate the number of RPA and RIF1 positive cells after carbon ion irradiation. U2OS cells were mock depleted (mock kd) or depleted for UHRF1 (UHRF1 kd) by RNAi. 48 h after siRNA transfection the cells were irradiated angular with carbon ions (LET 325 keV/µm; fluence $5*10^6$ p/cm^2; energy 4.05 MeV/u). 1 h post irradiation the samples were fixed and immuno-stained against RPA (resection marker) **(A)** or against RIF1 (**B**) and CENP-F (cell cycle marker, S/G2 cells are CENP-F positive, G1 cells are negative, G1 are CENP-F negative). At least 200 cells were analyzed per sample; error bars indicate ±SEM of two biological replicates (n = 1).

Taken together, the number of RPA positive cells was strongly compromised in UHRF1 depleted G1- and S/G2 cells compared to mock depleted cells after carbon ion irradiation indicating an involvement of UHRF1 in the regulation of the resection at complex DSBs. The weak effect of the UHRF1 depletion on the fraction of RIF1 positive cells suggests that UHRF1 might promote the resection through impairment of other factors like 53BP1.

4.3.2. UHRF1 depletion decreased RPA foci number in S/G2 cells after carbon ion irradiation

For the further investigation of the effect of UHRF1 depletion on resection regulation of carbon ion- induced DSBs the number of RPA- and RIF1 foci in UHRF1 depleted U2OS cells was evaluated. The UHRF1 depletion did not influence the number of RPA foci in both G1 and S/G2 after X-ray irradiation (Figure 4.20 A). The number of RPA foci/nucleus after carbon ion irradiation was decreased from 21±1.7 foci/cell in mock depleted S/G2 cells to 13±2.4 foci/cell in UHRF1 depleted cells which corresponds with a decrease of 38.1 %. In contrast, the number of RPA foci/nucleus after carbon ion irradiation was not changed in G1 cells.

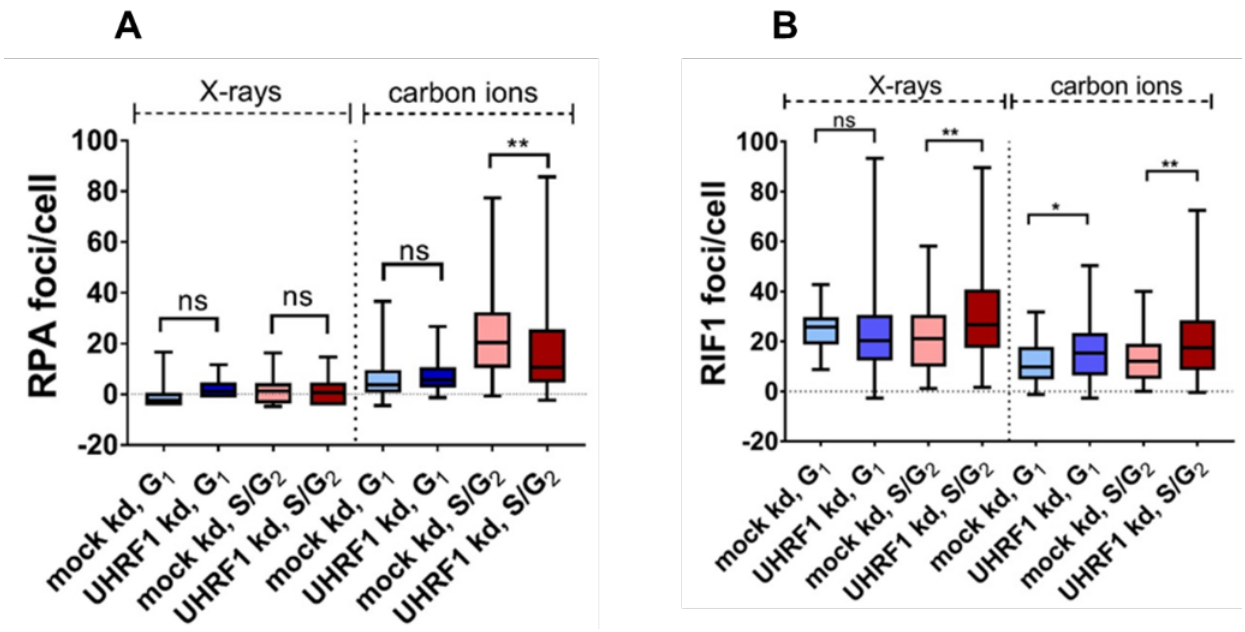

Figure 4.20: UHRF1 depletion modulates the number of RPA and RIF1 foci in carbon ion irradiated U2OS cells. The cells were mock depleted (mock) or depleted for UHRF1 (UHRF1 kd) by RNAi. 48 h after transfection the cells were angular irradiated with X-ray (2.6 Gy) or carbon ion (LET 325 keV/µm; fluence $5*10^6$ p/cm^2; energy 4.05 MeV/u). 1 h post irradiation the samples were fixed and immune-stained against RPA (resection marker) **(A)**, against RIF1 **(B)** and CENP-F (cell cycle marker, S/G2 cells are CENP-F positive, G1 cells are CENP-F negative). RPA or RIF1 foci were counted in at least 50 cells per sample (n = 1). The average number of RPA- and RIF1 foci in non-irradiated samples was subtracted from the data of irradiated cells. The box is extended from the 25th to 75th percentiles; whiskers represent minimum to maximum. To the data was applied the Mann–Whitney U test. (*) indicates P<0.05; (**) indicates P<0.01; ns represents statistically not significant.

Furthermore, the number of RIF1 foci/nucleus was affected by UHRF1 depletion after X-ray irradiation in S/G2 cells and after carbon ion irradiation in both G1- and S/G2 cells. The number of RIF1 foci/cell was increased in UHRF1 depleted S/G2 cells appr. 42,8 % compared to mock depleted S/G2 cells after X-ray irradiation as well as appr. 52.9 % after carbon ion irradiation (Figure 4.20 B). The number of RIF1 foci/cell was increased appr. 43.7 % in UHRF1 depleted G1 cells compared to mock depleted G1 cells after carbon ion irradiation; whereas there was no significant increase of RIF1 foci in G1 cells after X-ray irradiation indicating that UHRF1 might be involved in the resection regulation at complex DSBs in G1 cells by removing RIF1 at ion-induced DSBs.

Taken together, the UHRF1 depletion decreased the number of RPA foci/cell in S/G2 cells but not in G1 cells after carbon ion irradiation. Furthermore, the UHRF1 depletion increases the number of RIF1 foci/cell in both G1- and S/G2 cells after carbon ion irradiation.

4.3.3. UHRF1 depletion increased the number of 53BP1 positive cells in S/G2 phases

An increase of RIF1 foci/nucleus in UHRF1 depleted cells after carbon ion irradiation (Figure 4.20 B) together with the knowledge that 53BP1 recruits RIF1 to DSBs (Escribano-Diaz, Orthwein et al. 2013) suggests that UHRF1 may promote DNA resection by impairment of 53BP1 at DSBs. To investigate this idea UHRF1 depleted cells were irradiated with carbon- or xenon ions and stained 1 h post irradiation by immunofluorescence against 53BP1.

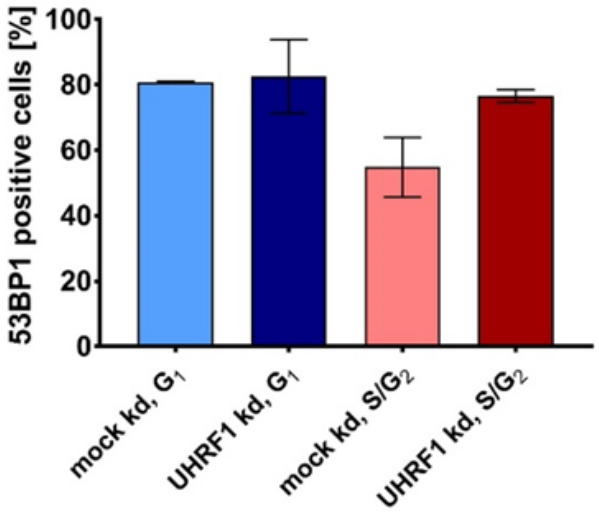

Figure 4.21: UHRF1 depletion increased the fraction of 53BP1 positive cells in the S/G2 population after heavy ion irradiation. U2OS cells were mock depleted (mock kd) or depleted for UHRF1 (UHRF1 kd) by RNAi. 48 h after siRNA transfection U2OS cells were irradiated angular with carbon ion (LET 325 keV/µm; fluence $5*10^6$ p/cm^2; energy 4.05 MeV/u) or xenon ion (LET 750 keV/µm; fluence $5*10^6$ p/cm^2; energy 600 MeV/u). One hour post-irradiated samples were fixed and stained by immunofluorescence against 53BP1 and geminin (cell cycle marker, S/G2 cells are geminin positive, G1 cells are geminin negative). At least 100 cells were counted per each sample; (n = 2); error bars represent standard deviation.

The fraction of 53BP1 positive cells was not impaired by UHRF1 depletion in G1 cells. By contrast, the fraction of 53BP1 cells was increased appr. 39.8 % in S/G2 compared to mock depleted S/G2 cells (Figure 4.21).

To summarize, UHRF1 depletion increased the fraction of 53BP1 positive S/G2 cells after heavy ion irradiation indicating that UHRF1 might antagonize 53BP1 at ion-induced DSBs in S/G2 cells.

4.4. DSB repair in G0 and G1-phase human fibroblasts after exposure to low- and high-LET irradiation

With increasing complexity of DNA damage resection of DSBs becomes increasingly important for DSB repair not only in S/G2 but also in G1 cells (Averbeck, Ringel et al. 2014). Therefore, the observation that human fibroblasts showed less resection positive cells upon heavy-ion irradiation with increasing time after seeding (compared 1-3-day old culture with 10-day old culture) was surprising (not published data). A similar observation was made by Yajima et al. (Yajima, Fujisawa et al. 2013) and is most likely connected to the fibroblasts' characteristic of contact inhibition. When they reach confluency, they withdraw from the cell cycle and undergo a quiescent state, G0 phase (Roycroft and Mayor 2016). To enable the investigation of the relation between G0 phase and DSB resection more closely, first goal was to establish an eligible technique to obtain a culture highly enriched in G0 cells. Subsequently, the capacity to resect, repair and survive complex DSBs was analyzed in this culture compared to G1 cells. Since it is known that most of the cells *in vivo* persist in non-cycling (G0) state (Pardee 1974), incorrectly repaired or unrepaired DSBs of G0 cells exposed to high LET irradiation represent a risk for the human. The increase of worldwide successful heavy particle therapy requires a more in depth understanding in this field. Therefore, to investigate more closely which DSB repair pathways the G0 cells use was important.

4.4.1. Establishment of the culture conditions for quiescent state of human fibroblasts

In order to obtain culture of human fibroblasts highly enriched in quiescent (G0) state two different cell-synchronization protocols were tested. The method, which is typically applied to synchronize the cells in G1 or G0 phase, is serum starvation. Thus, the protocol with serum deprivation described in Lemons et al. was tested in this work (Lemons, Feng et al. 2010). In this protocol, the cells are kept with 0.1 % FCS for 7 days. Alternative to this method, a protocol was used that is based on the contact inhibition characteristics of fibroblasts (Abercrombie 1970). As a control, a culture cultivated for 3 days in normal medium (with 15 % FCS), i.e. no serum deprivation was used ("proliferating culture"). The cell cycle phase was determined by immunofluorescence staining against Ki67 (proliferating marker) and CENP-F (cell cycle marker). The S/G2 cells were CENP-F-positive, G1 cells were CENP-F-negative and Ki67 positive, G0 cells were CENP-F- and Ki67 negative. The staining of the cell cycle distribution analysis is shown in Figure 4.22 A. The proliferating culture did not comprise G0 cells; the cells were all Ki67 positive, while the number of S/G2 cells was appr. 20 %. The first synchronization protocol with serum deprivation (c. 4.2.5.) showed less S/G2 cells compared to the proliferating control.

A

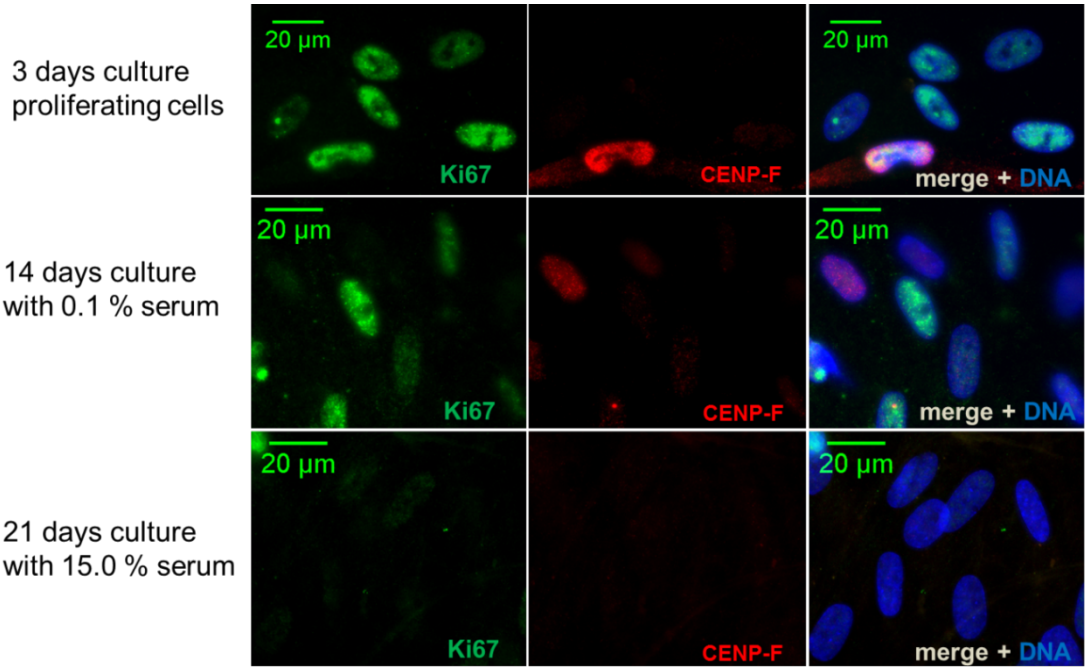

B

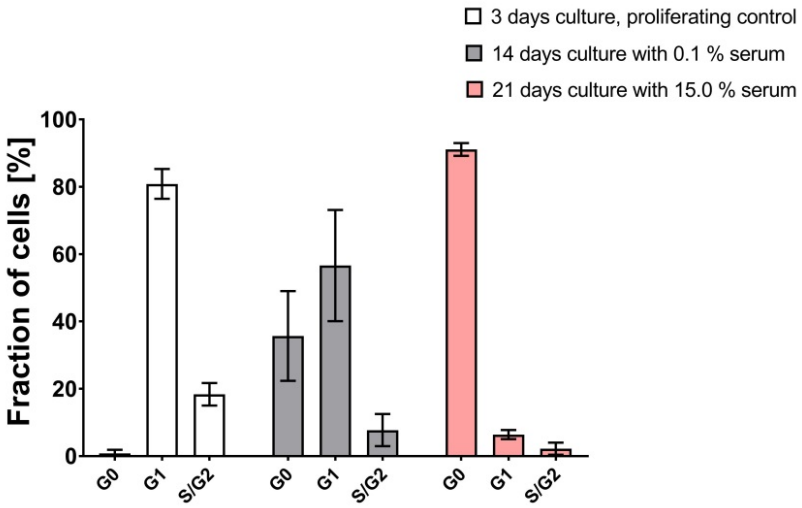

Figure 4.22: The transition of human fibroblasts AG1522D into the quiescent state. The human fibroblasts were cultivated for 14 days with serum deprivation in the last 7 days of cultivation (FCS concentration 0.1 %) or the cells were cultivated for 21 days for contact inhibition with a normal serum content (15 %) and once a week medium change. Proliferating cells were used as a control of the cell cycle distribution and were cultivated for 3 days with a normal serum content of 15 %. Immunofluorescence staining was performed against Ki67 (green), a proliferation marker, (G1/S/G2 cells are positive, G0 cells are negative) and CENP-F (red) cell cycle marker (S/G2 cells are positive; G1 cells are negative). DNA was stained with DAPI, thereby the M cells were excluded out of the counting. **A:** Representative images of the immunofluorescence staining of the cultures at the three different culture conditions. **B:** Cell cycle distribution of human fibroblasts cultured under the three different conditions. At least 100 cells per condition were analyzed in three independent experiments. Error bars represent ±standard deviation.

There was also an increase of G0 cells of appr. 30 %, however, appr. 60 % of the cells remained in G1 phase (Figure 4.22 B). This result was dissatisfactory as predominant number of the cells was still in G1 phase. Therefore, an alternative protocol was utilized, where the cells were incubated for 21 days before the subsequent experiment (Beucher, Deckbar et al. 2011). A very high fraction of appr. 90% of G0 cells was achieved with this protocol. Accordingly, the amount of the G1/S/G2 cell cycle phases was very low. There were appr. 6 % of G1- and appr. 2 % of S/G2 cells in the 21-day culture of human fibroblasts (Figure 4.22 B).

In addition, the plating efficiency (PE) under these culture conditions was 0.06; appr. 50 % below the PE of 0.15 of a G1 enriched culture. Therefore, a substantial fraction of these G0 cells is quiescent and not senescent or differentiated, hence, is able to re-enter the cell cycle. The latter is important for the performance of clonogenic survival assays.

Taken together, the protocol with the cells cultivated for 21 days in a normal medium supplemented with 15 % FCS was chosen for subsequent experiments as a culture enriched quiescent cells. Due to the low fraction of G0 cells, the 14-day protocol of cultivation and serum deprivation was no longer used.

4.4.2. Culture conditions to synchronize human fibroblasts in G1 phase

To pursue appropriate experiments with yielded quiescent fibroblasts it was essential to dispose a proper control cell population. For this purpose, a culture enriched with G1 cells was considered. The G1 cells display many similarities to G0 cells: they possess a non-doubled chromosome number and as they are post-mitotic cells, similar DNA damage response was expected (Yao 2014). Hence, another protocol where the cells were incubated for 10 days after plating with normal serum content (15 %) was developed. The cell cycle distribution was analyzed by immunofluorescence staining against Ki67 (proliferation marker) and against CENP-F (cell cycle marker) (Figure 4.23 A).

The number of G1 cells was determined by subtracting the number of CENP-F positive cells (S/G2 cells) from the number of Ki67 positive cells (proliferating cells). CENP-F marker indicates S- and G2 cells. The incubation of human fibroblasts by normal conditions (c. 4.4.1.) for 10 days showed that appr. 70 % of the cells were in G1 phase and the number of S/G2 cells was fewer than 5 % (Figure 4.23 B). Nevertheless, under these culture conditions up to 30 % G0 cells were obtained.

Moreover, the basic characteristic to distinguish between the cells synchronized in G1 and G0 phase can be verified through amount of p27 protein. P27 is a cell cycle regulator protein, which controls transition from G0 and early G1 to S phase by binding and inactivating cyclin-dependent kinases (CDKs), therefore, the maximum of the p27 protein amount is expected in non-proliferating G0 cells (Chu, Hengst et al. 2008).

A

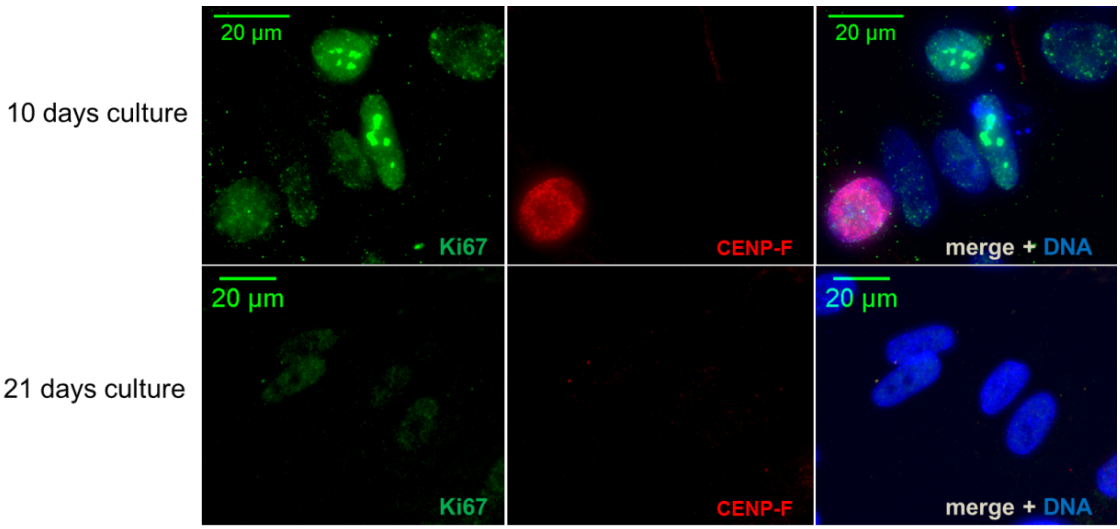

B

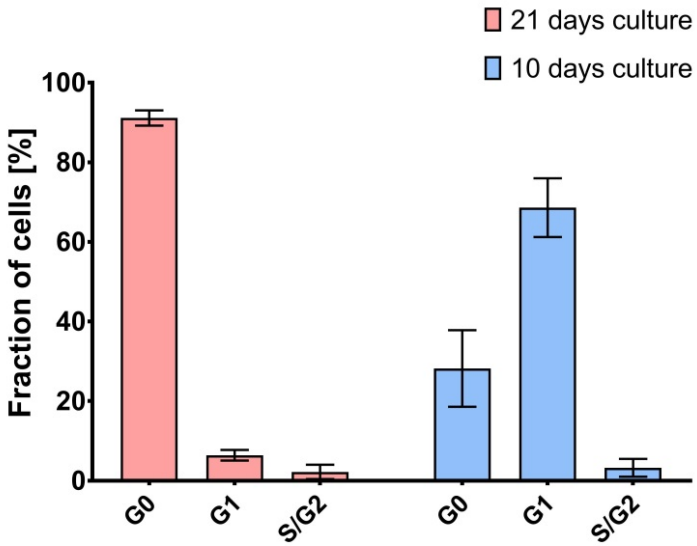

Figure 4.23: Synchronizing human fibroblasts AG1522D in G1 phase. The human fibroblasts were cultivated for 10 days or for 21 days with once a week medium change. Immunofluorescence staining was performed against Ki67 (green), a proliferation marker, (G1/S/G2 cells are positive, G0 cells are negative) and CENP-F (red) cell cycle marker (S/G2 cells are positive; G1 cells are negative). DNA was stained with DAPI. **A:** Representative images from the staining of the 10-day and 21-day cultures. **B:** At least 100 cells per condition were analyzed in three independent experiments. Error bars represent ±standard deviation.

The presence of p27 in protein extracts of a 10-day culture (G1) and 21-day culture (G0) was analyzed in a Western assay (Figure 4.24).

The protein extracts of both 10-day (G1) and 21-day culture (G0) was prepared and tested against p27 antibody. The band of p27 signal was most pronounced in G0 compared to G1 cells.

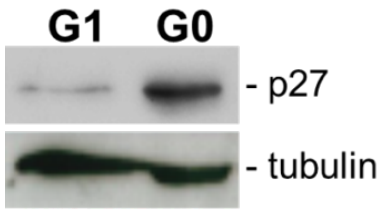

Figure 4.24: Inhibition of proliferation was indicated by increased presence of p27 in quiescent normal human fibroblasts. Western analysis was performed with extracts of AG1522D cultured for 10 days (G1) and 21 days (G0) with the antibody against p27 and the loading control tubulin. The p27 signal was much stronger in G0 than G1 cells indicating the non-proliferative state.

In summary, the culturing of human fibroblasts for 10 days rendered an effective protocol for enriching the cells in G1 phase.

4.4.3. Resection of xenon-ion induced DSBs is reduced in quiescent human fibroblasts

The initial supposition was that the decreased fraction of resection positive cells was related to the increased culturing time that results in increased fraction of G0 cells. A protocol which was based on the increasing of culturing time allows an enrichment in the culture of human fibroblast with over 90 % cells in G0 phase. As a control, regularly passaged culture of human fibroblasts (1-3-day culture) was used. The cells were irradiated with xenon ions and stained 1 h post irradiation against RPA (resection marker) and γH2AX (DSB marker) to identify the ion track (Figure 4.25 A). The fraction of RPA positive cells was determined in G1 cells (CENP-F negative in 3-day culture) and in G0 cells (Ki67 negative cells in 21-day culture). Additionally, the samples were stained against BRCA1 to analyze the role of BRCA1 at ion-induced resection in normal human fibroblasts. The quantification of resection positive cells after xenon ion irradiation showed that the resection positive cells were decreased in G0 phase appr. 29 % compared to G1 phase (Figure 4.25 B). The number of BRCA1 positive cells was decreased appr. 43 %.

A

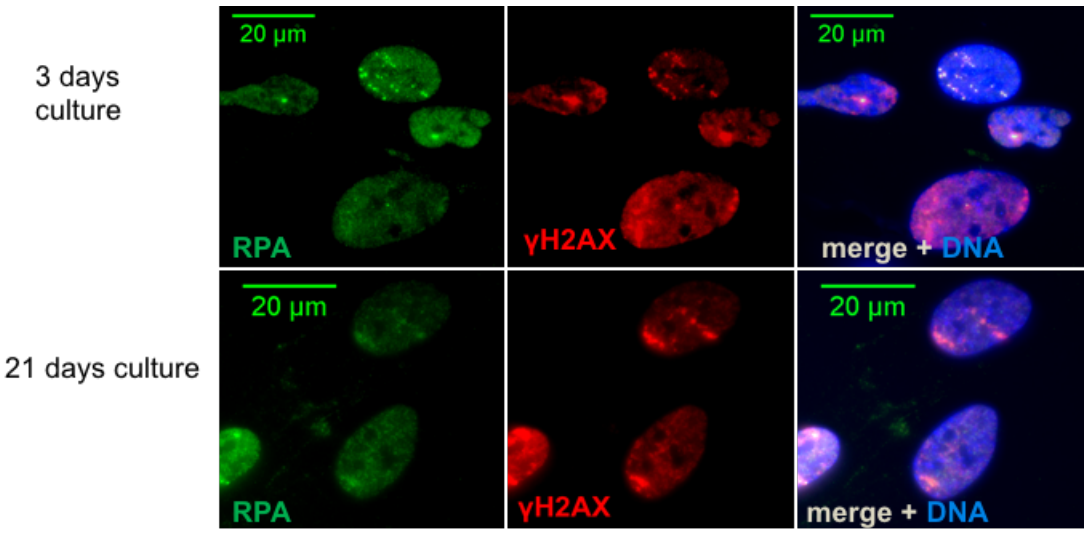

B

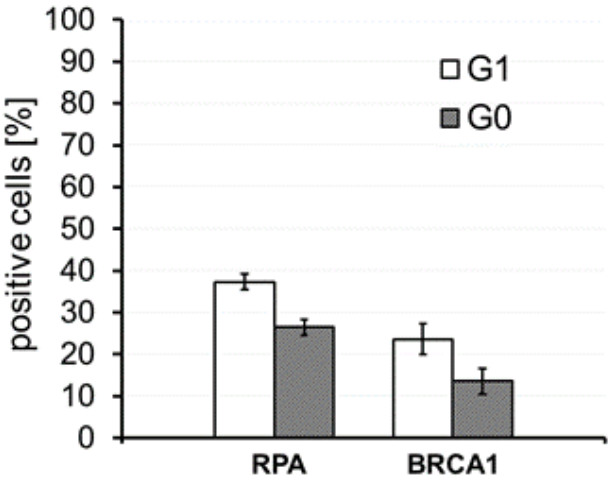

Figure 4.25: The fraction of RPA- and BRCA1 positive cells in G0 is lower than in G1 cells after xenon ion irradiation. A: Human fibroblasts were incubated for 10 days or 21 days and then irradiated angularly with xenon ions (LET 9,000 keV/µm; energy 4.5 MeV/u; fluence $3*10^6$ p/cm^2). The cells were fixed 1 h post-irradiation. The immunofluorescence staining was performed against RPA (resection marker) and γH2AX (DSB marker) **B:** Evaluation of quiescent (G0) and proliferating (G1) RPA- and BRCA1 positive cells (BRCA1 immunofluorescence image is not shown). The cells were additionally immunofluorescence stained against Ki67 (proliferation marker; G1/S/G2 cells are positive; G0 cells are negative) and CENP-F (cell cycle marker; S/G2 cells are positive; G1 cells are negative) to verify G0 and G1 cells, respectively (images not shown). n = 1; error bars represent binomial error.

To summarize, the comparison of the resection response at ion-induced DSBs in G1 versus G0 cells supported the assumption that quiescence results in restricted resection of complex DSBs.

4.4.4. Downregulation of resection-regulation factors in quiescent normal human fibroblasts.

Factors involved in the resection regulation of G0 cells are insufficient studied. G0 cells show less resection positive cells upon irradiation with xenon ions than the proliferating G1 cells. Hence, in the next step G0 and G1 cells were analyzed for the resection-regulation relevant factors in western assay: BRCA1 and CtIP, resection supporting factors, and RIF1, which together with 53BP1 antagonized resection (Chapman JR 2013, Escribano-Diaz, Orthwein et al. 2013).

The result of the Western analysis indicated that quiescence apparently prohibits the expression of positive resection regulation factors and RIF1 (Figure 4.26). CtIP signal was distinct decreased in G0 cells compared to G1 cells. Notable, the BRCA1 signal was not detectable in both G1- and G0 cells. These results were consistent with the decrease of the number of resection positive cells in quiescent fibroblasts at ion-induced DSBs compared to proliferating G1 cells (Figure 4.25 B)

Interestingly, the expression of RIF1, an interaction partner of 53BP1, was strongly compromised in G0 cells. Considering RIF1' supportive role in the replication process, a possible explanation could be that the replication in quiescent cells is strongly prohibited.

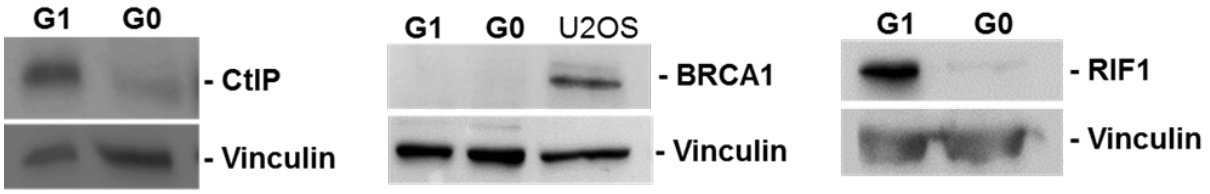

Figure 4.26: Expression of resection factors is prohibited in quiescent human fibroblasts. The whole cell extracts of human fibroblasts enriched in G0 (21-day culture) or in G1 phase (10-day culture) were used for the western analysis. The whole cell lysate of untreated U2OS cells was used as a positive control for BRCA1 signal. Vinculin signal was used as a loading control.

4.4.5. Classical NHEJ seems to be a main repair pathway in quiescent human fibroblasts after low LET irradiation

Resection influences the DSB repair pathway choice (Shibata, Conrad et al. 2011). Since G0 cells show less resection positive cells upon irradiation with heavy ions than G1 cells the question arose whether this impairs the repair capacity of G0 cells. To analyze the DNA-DSBs repair kinetics human fibroblasts were synchronized in G1 or in G0 state. Both cell populations were simultaneously irradiated with 0.5 Gy X-rays and fixed at different time points after irradiation (1 h, 4 h, 10 h, 24 h, 48 h or 72 h). Since X-ray irradiation AG1522D cells show the maximum γH2AX foci number, 1 h after irradiation was chosen as the first fixation time point (Herrlitz 2014). DSB repair kinetics was measured with a γH2AX assay (Lobrich, Shibata et al. 2010) where γH2AX serves as a DSB marker.

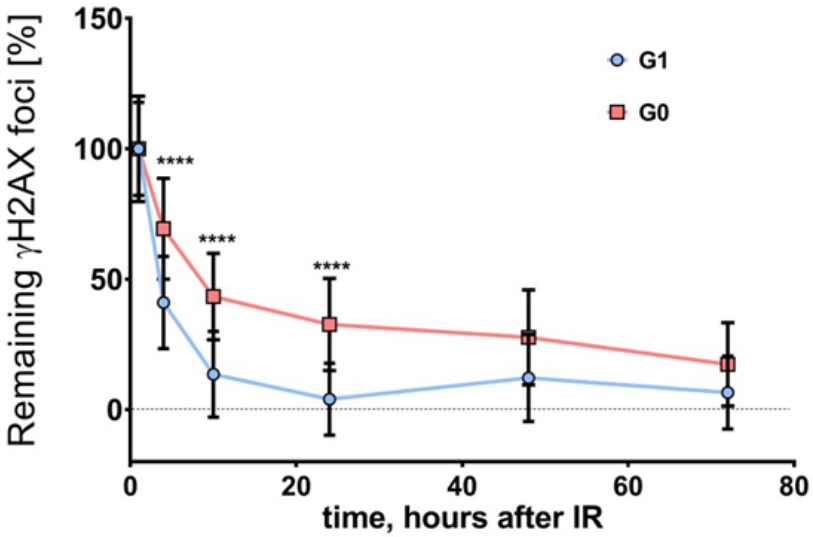

Figure 4.27: Human fibroblasts in quiescent (G0) state repair X-ray-induced DSB slower than fibroblasts in G1 phase. Human fibroblasts synchronized in G1 or G0 phase were X-ray irradiated (0.5 Gy) and fixed 1 h, 4 h, 10 h, 24 h, 48 h and 72 h after irradiation. All samples were immunofluorescence stained against γH2AX (DSB marker) and CENP-F (cell cycle marker; S/G2 cells are positive, G1 cells are negative) to exclude S/G2 cells from the analysis. At least 50 cells were counted per each time point. Data points were normalized to the mean value at t=1 h. The mean value of γH2AX foci in non-radiated samples was subtracted in each time point. To the data was applied the Mann–Whitney U test: (****) indicates P<0.0001. n = 2; error bars indicate ±standard deviation.

The number of remaining DSBs was counted at each fixation time point. The S and G2 cells were excluded from the analysis by CENP-F staining; S/G2 cells are CENP-F positive and G0 and G1 cells are CENP-F negative. Interestingly, the repair kinetics of quiescent normal human fibroblasts (G0) after X-ray irradiation was much slower than DSB repair kinetics of proliferating normal human fibroblasts in G1 phase (Figure 4.27).

The difference of the DSB repair kinetics in G1 versus G0 cells might be based on the utilization of different DSB-repair pathways. To understand and to be able to discriminate which pathway is used in G1 and G0 cells after X-ray irradiation, DSB repair kinetics were measured in the presence of the specific repair pathway inhibitors. The classical non-homologous end joining pathway (c-NHEJ) was inhibited through the addition of DNA-PKcs inhibitor (NU7026) (Willmore, de Caux et al. 2004). Whereas a PARP inhibitor (PJ34) was applied to inhibit PARP-dependent alternative NHEJ (alt-NHEJ) (Davar, Beumer et al. 2012). These two DSB repair pathways may possibly occur in G1 cells after ionizing irradiation (c. 4.4.4)

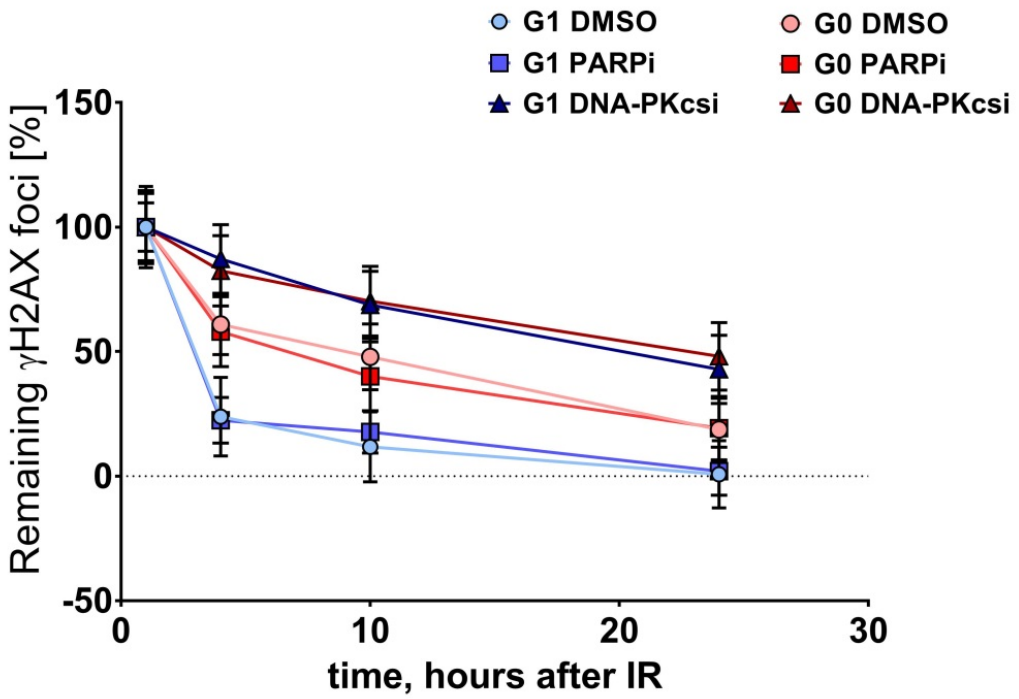

Figure 4.28: DNA-PKcs inhibition but not PARP inhibition or has a dramatically impact on the DSB- repair in G1 and G0 cells. Human fibroblasts AG1522D were synchronized in G1 or G0 phase. At least 1 h before irradiation the cells were incubated with 10 µM DNA-PKcs inhibitor (DNA-PKcsi; NU7026) or with 10 µM PARP inhibitor (PARPi; PJ34) or with DMSO (solvent control). The cells were irradiated with X-ray (0.5 Gy) and fixed 1 h, 4 h, 10 h or 24 h after irradiation. All samples were immunofluorescence stained against γH2AX (DSB marker) and CENP-F (cell cycle marker; S/G2 cells are positive, G1 cells are negative) to exclude S/G2 cells from the counting. The number of γH2AX foci was quantified in each sample. At least 50 cells were counted per each time point. Data points were normalized to the mean value at t=1 h. The mean value of the γH2AX foci number in non-radiated samples was subtracted in each time point; n = 2; error bars indicate ±standard deviation.

The synchronized G1 or G0 cells were incubated at least 1 h with 10 µM DNA-PKcs inhibitor (NU7026) or with 10 µM PARP inhibitor (PJ34). Then the cells were irradiated with 0.5 Gy X-rays and subsequently paraformaldehyde fixed at different time points (1 h, 4 h, 10 h or 24 h) after irradiation for a γH2AX foci assay. The number of γH2AX foci per nucleus was counted in 50 cells per condition. The measured repair kinetics reveals that the DSB repair was impaired G1 and G0 cells treated with DNA-PKcs inhibitor (NU7026), but not in G1 and G0 treated with PARP inhibitor (PJ34) (Figure 4.28). The functionality of the PARP inhibitor was tested positive (c. 4.5.1.). Of note, the DNA-PKcs inhibitor impairs the repair of G1 cells more severely than the repair of G0 cells; upon DNA-PKcs inhibition the repair kinetics of G1 and G0 cells.

Taken together, G0 cells showed slower DSB-repair kinetics compared to G1 cells. Nonetheless, both G0- and G1 cells seemed to use classical NHEJ as the main repair pathway.

4.4.5.1 Verification of the PARP inhibitor

A supply of PARP inhibitor did not have any effect on the repair kinetics either in G1 or in G0 cells. Therefore, an additional control of the inhibitor functionality was required to confirm this effect of PARP inhibitor. To verify the functionality of the PARP inhibitor an additional experiment with normal human fibroblasts was performed. The cells were treated for at least 1 h with 10 µM PARP inhibitor (PJ34). Subsequently, they were incubated with 5 mM hydrogen peroxide for 30 minutes. The hydrogen peroxide is strong oxidizing agent, which is unstable and decomposes very quickly in water and oxygen, thereby as a by-product the reactive oxygen species (ROS) are generated. The ROS are the DNA damaging agents and produce single strand breaks (SSBs) and nucleotide damage (c. 1.2). These DNA lesions are censored by PARP1 enzyme which forms the PAR chains near the DNA damage. Because of the even distribution of hydrogen peroxide in the medium, the equal distributed PAR-signal in the cell nucleus was anticipated. Afterwards, cells were fixed according to Buerkle's protocol (c. 2.8.2) (Burkle, Chen et al. 1993) and immunofluorescence stained against PAR (Poly-ADP-ribose) to pursue the PARP enzyme activity. In PARP inhibitor (PJ34) and with H_2O_2 treated cells the PARylation was strongly affected in comparison to DMSO (solvent control) treated cells (Figure 4.29). Hence, the PARP inhibitor PJ34 was functional at the applied concentration.

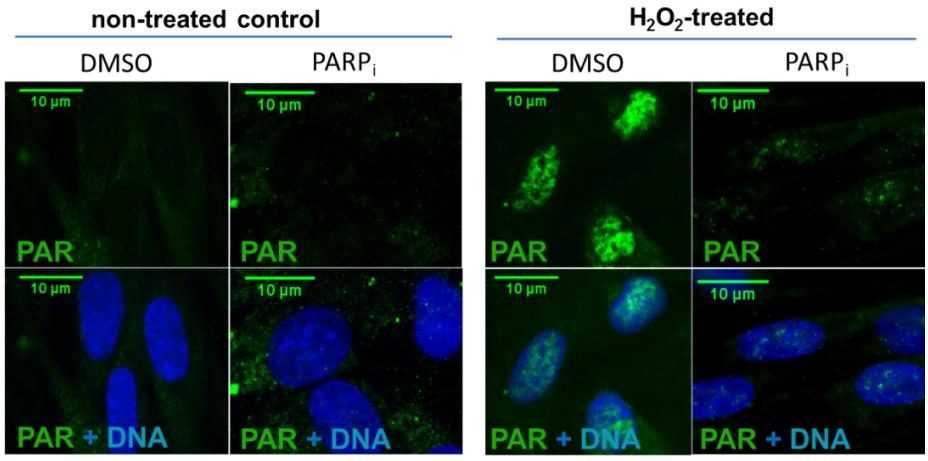

Figure 4.29: Verification of the PARP inhibitor (PJ34). Human fibroblasts (3 days culture) were incubated with 10 µM PARP inhibitor (PJ34) or DMSO (solvent control) for 1 h. Subsequently, the cells were incubated with H_2O_2 (5 mM) for 30 minutes or remained untreated (control). Treated cells were fixed (Buerkle' protocol) and stained by immunofluorescence against PAR. DNA was stained with DAPI (blue). PARylation was inhibited in PJ34 treated cells. The representative images show PARylation at the different conditions.

4.4.6. Human fibroblasts express classical NHEJ factors

Human fibroblasts hardly use resection dependent repair pathway due to the discovered lack of positive resection regulation factors such as BRCA1 and CtIP (c. 4.4.4 and 4.4.5). The predominant DSB repair pathway for human fibroblasts after X-ray irradiation used by G0- as

well as by G1 cells seems to be c-NHEJ. Yet, the latter repair faster than those in G0 phase. In order to explore whether the level of c-NHEJ factors such as Ku80, ligase IV and 53BP1 is responsible for the slower DSB repair kinetics in G0 cells compared to G1 cells, a Western analysis was performed. Ku80 and DNA ligase IV are proteins in c-NHEJ pathway (Mladenov, Magin et al. 2016). 53BP1 promotes c-NHEJ by protecting DSB-ends from resection (Panier and Boulton 2014, Zimmermann and de Lange 2014). Figure 4.30 shows Western analysis of the c-NHEJ factors. The quantitative analysis of the bands revealed an appr. 35 % decrease of Ku80 value in G0 cells compared to G1 cells. Moreover, the ligase IV value was also decreased in G0 cells appr. 26 % compared to G1 cells. Contrary to the decrease of ligase IV value, 53BP1 value was increased appr. 54 % in G0 cells compared to G1 cells.

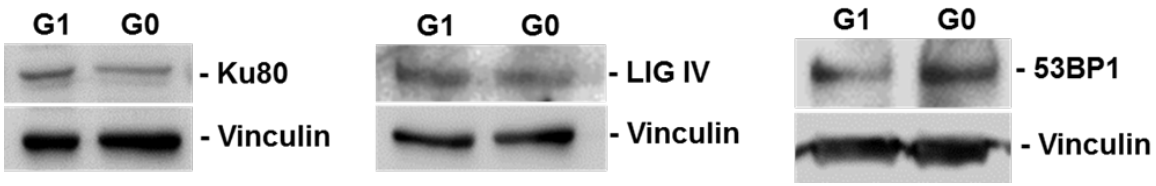

Figure 4.30: Expression of c-NHEJ factors in G0- versus G1 enriched human fibroblasts. The whole cell extracts of human fibroblasts enriched in G0- (21-day culture) or in G1 phase (10-day culture) were used for the western analysis. An equal protein amount of 20 μg per line was loaded to estimate the difference in protein expression. Vinculin signal was used as a loading control for quantitative evaluation.

Diminution of the protein expression of c-NHEJ factors in quiescent cells might be the cause of slower repair kinetics in quiescent cells. However, 53BP1 amount was increased in G0 cells suggesting stronger resection protection at DSBs compared to G1 cells.

4.4.7. Synchronized human fibroblasts showed stronger methylation pattern than non-synchronized cells

The concept that chromatin structure may influence the DSB repair kinetics was proposed by Rief and Löbrich and pursued by Krüger et al. (Rief and Lobrich 2002, Kruger, Rothkamm et al. 2004). The notion is based on the nature and movement dynamic of the heterochromatic regions. The higher order of chromatin compaction was shown to be regulated by posttranslational histone modifications including acetylation, phosphorylation and methylation (Jenuwein and Allis 2001, Nakayama, Rice et al. 2001). Furthermore, methylation pattern in particular at histone 3 (H3) and histone 4 (H4) was shown to regulate entry and maintenance of quiescent state (Hidalgo, Herrera-Merchan et al. 2012, Everts, Manning et al. 2013). To pursue the connection between chromatin structure and DSB repair kinetics was proposed in order to analyze the difference in the chromatin structure in G0- versus G1 cells. This was

done by analyzing the fraction of trimethylated histone 3 (H3) at amino acid lysine 9 (H3K9Me3) and lysine 27 (H3K27Me3) in G0- and G1 cells as well as in proliferating culture via Western analysis. Previously a tendency to higher chromatin compaction in quiescent (G0) cells compared to proliferating cells was also showed in the FLIM approach by Abdollahi (Abdollahi 2017).

Figure 4.31 shows the Western analysis of the whole cell protein extracts of human fibroblasts at three different conditions (c. 4.4.1 and 4.4.2). The cell culture enriched for G0 cells (21-day culture) revealed more pronounced band of methylation signal indicating higher chromatin compaction in direction to quiescence (Figure 4.31). The regularly passaged cell culture (3-day culture) was intended as a negative control confirming low or absence of the histone H3-methylated sites. Additionally, a modest signal was detectable in culture enriched with G1 cells indicating increase of histone 3 (H3) methylation compared to proliferating culture, but still lower than in quiescent cells.

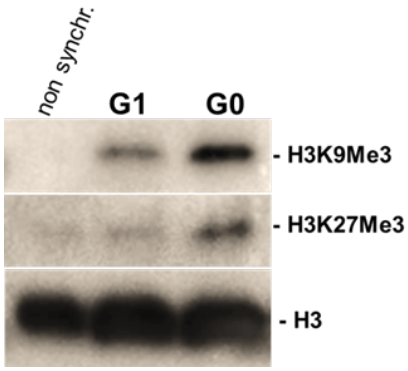

Figure 4.31: Quiescent human fibroblasts reveal a stronger histone methylation pattern than proliferating cells. The whole cell extracts of human fibroblasts of 21-day culture (cells enriched in G0), 10-day culture (cells enriched in G1) or 3-day culture were used for the analysis of histone 3 (H3) trimethylation at lysine 9 (H3K9Me3) or lysine 27 (H3K27Me3) by Western analysis. Histone 3 (H3) was used as a loading control.

This finding indicates that fibroblasts in the quiescent state G0 have a higher fraction of heterochromatin compared to G1 cells suggesting that the higher chromatin compaction might be a reason for their slow DSB repair kinetics.

4.4.8. c-NHEJ seems to be the main repair pathway of helium-ion induced DSBs in human fibroblasts

The results in section 4.5 suggest that human fibroblasts use c-NHEJ as a main repair pathway of X-ray induced DSBs. Whether this is also true for complex DSBs induced by heavy ions was tested in a next step. Cultures enriched for G0 or for G1 cells were treated with DNA-PKcs inhibitor (NU7026) or with DMSO (solvent control) for at least 1 h a priori irradiation.

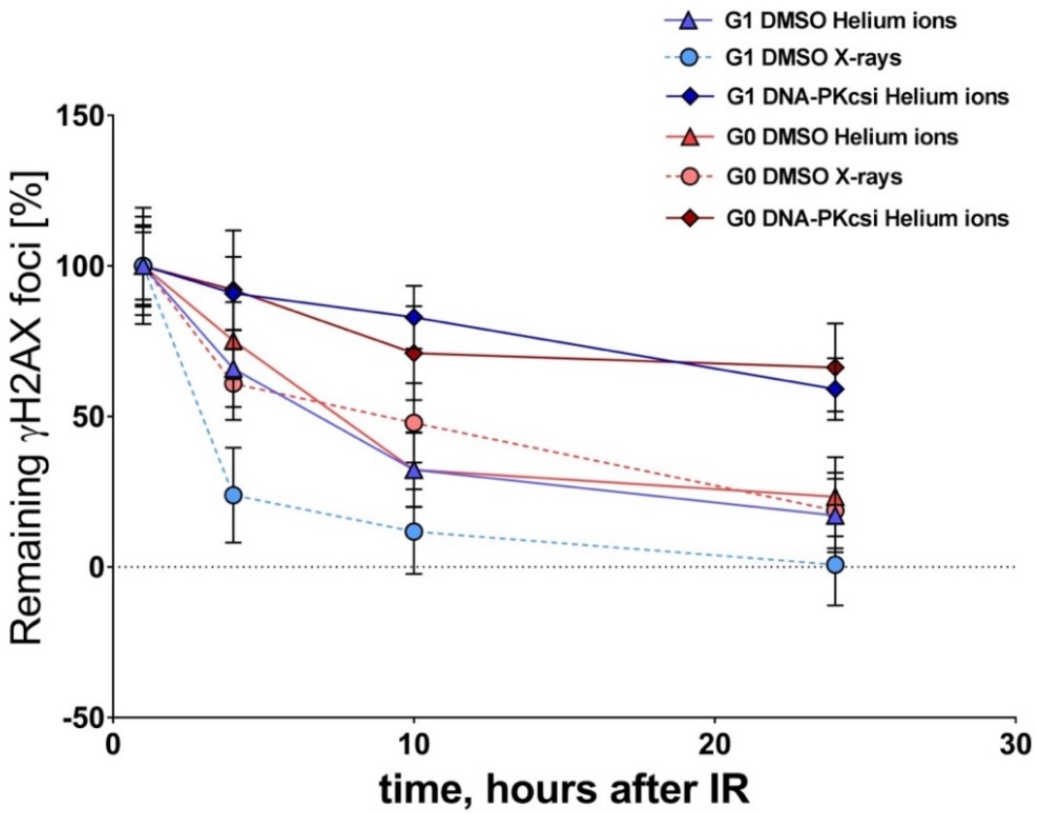

Figure 4.32: Human fibroblasts repair at the same speed in G1 and G0 state after helium ion irradiation. DNA-PKsc inhibitor has the same impact on G1 and G0 cells after helium ion irradiation. Human fibroblasts were synchronized in G1 or G0 phase. 1 h before irradiation the cells were incubated with DNA-PKcs inhibitor (NU7026) or with DMSO (solvent control). The cells were irradiated with helium ion (LET 76 keV/µm; energy 1.62 MeV/u; fluence $3.5*10^6$ p/cm^2) and fixed 1 h, 4 h, 10 h and 24 h after irradiation. All samples were immunofluorescence stained against γH2AX (DSB marker). Number of γH2AX foci was quantified in each sample, in at least 50 cells per each time point. Data points were normalized to the mean value at t= 1 h. Mean value of γH2AX foci in non-radiated samples was subtracted in each time point; n = 2; error bars indicate ±standard deviation. To better compare the data of the repair after X-ray irradiation was redrawn from Figure 4.28 (dashed line).

Subsequently the cells were irradiated with helium ions with a dose which is X-ray-equivalent dose of 0.5 Gy and fixed at corresponding time points after irradiation for immuno-fluorescence staining. The observed DSB repair kinetics was similar in G0 and G1 in DMSO treated cells (Figure 4.32). 24 h post-radiation the G1 cells had still 17 % ±12 % non-repaired DSBs, which was strikingly similar to the G0 cells with 23 % ±13 % non-repaired DSBs. Furthermore, the DNA-PKcs inhibitor treatment strongly compromised the DSB repair kinetics in both G0 and G1 cells indicating that DNA-PKcs-dependent NHEJ seemed to be a main repair pathway in human fibroblasts at ion-induced DSBs as well. The similar repair kinetics in G1 and G0 cells after helium ion irradiation suggests an identical repair capacity of complex DSBs in human fibroblasts in G1 and G0 phase.

Interestingly, the DSB repair kinetics after helium ion irradiation in G1 cells was notably slower than the repair kinetics after X-ray irradiation; it might be that the complexity of the DSBs influences the rejoining speed (Shibata, Conrad et al. 2011, Biehs, Steinlage et al. 2017). Strikingly similar was the DSB repair kinetics after X-ray- and after helium ion irradiation in G0 cells suggesting a similar repair capacity after low- and high LET irradiation in quiescent cells.

Taken together, these results suggest that human fibroblasts in G1 and G0 phase for the repair of complex DSBs use c-NHEJ as a main repair pathway. Moreover, the DSB repair kinetics was impaired by the complexity of DSBs in G1 cells, whereas the DSB complexity has no influence on the repair kinetics in G0 cells.

4.4.9. Survival of human fibroblasts in G1 and G0 phase after X-ray- and carbon ion irradiation mirrors their repair kinetics

The ability to repair DNA DSBs influences the survival of cell upon irradiation. Within repair, not only the ability to rejoin DSB ends but also the quality of the repair is important. The γH2AX-foci assay (c. 4.4.5 and 4.4.8) does not give any information about the repair quality. Since erroneous repair decreases cell viability, additional analysis of the clonogenic survival upon irradiation can indirectly give information about the repair quality. The survival data were planned to be compared with the obtained repair kinetics (c. 4.4.5). Hence, the treatment of the irradiated cells for the clonogenic survival assay was comparable to the treatment of the cells for the repair kinetics assay; after irradiation, the cells were left for 24 h in the incubator before they were detached, dissociated and seeded for the survival assay ("delayed plating"). In addition, the clonogenic survival assay was performed according the classical protocol (Munshi, Hobbs et al. 2005) by detaching, dissociating and seeding the cells immediately after irradiation ("immediate plating"). Having the survival data based on immediate and delayed plating allows the further study of the survival after potentially lethal damage (PLD) (Alpen 1998, Liu, Kawata et al. 2010, Maeda, Bell et al. 2014) in G1 versus G0 cells.

The survival was measured after X-ray- or after carbon ion irradiation. The cells were seeded 24 h after irradiation and subsequently cultivated for 14 days. Figure 4.33 A shows measurement points of survival colonies after X-ray irradiation. The single points indicate the percentage of survival of dividing capable cells from original seeded cell number. The survival after carbon ion cells were treated identical to the cells irradiated with X-rays (Figure 4.33 B).

The surviving fraction is plotted at a logarithmic scale and the dose as a function of survival is plotted on linear scale. The initial slope of the survival curve at low dose X-rays is linear and at higher dose the curve bends. The bending of the curve is typical for the survival after

X-rays. By contrast, the survival curve after heavy particle irradiation is linear and usually with very steep slope. The delayed plating survival curve of the culture enriched G0 cells after X-ray irradiation showed a slightly better survival curve than that of G0 cells seeded immediately after irradiation. In contrast, the delayed plated X-ray irradiated G1 cells showed a distinct improvement of survival compared to immediate plated G1 cells. Interestingly, the survival of delayed and immediate plated G0 is similar to immediate plated G1 cells after X-ray irradiation. The three curves: G0 immediate-, G0 delayed- and G1 immediate plating after X-ray irradiation have a similar initial slope indicating a similar survival at low dose and, hence, DSB repair capacity. The survival curve after carbon ion irradiation had, for heavy particles, characteristically linear shape without shoulder. In contrast to survival curves of quiescent fibroblasts after X-ray irradiation, the survival curve after carbon ion irradiation was improved in delayed plated G0 cells in comparison to immediate plated G0 cells. Moreover, the survival of delayed plated G1 cells, after carbon ion irradiation, was improved similar to G0 cells in comparison to immediate plated cells.

The survival curves after X-ray irradiation delayed plating G0- versus G1 cells showed a difference which mirrors their repair kinetics. Yet, the G0 cells 24 h post X-ray irradiation had appr. 20 – 30 % unrepaired DSBs, while the G1 cells showed mostly none of DSBs (Figure 4.27).

The survival curves after carbon ion irradiation in delayed plated G0 and G1 cells had the same slope indicating the similar DSB repair capacity. The immediate plating G1 cell survival curve revealed smaller slope than immediate plating G0 cell survival curve (Figure 4.33 B) suggesting together with repair curve after helium ion irradiation (Figure 4.32) that the DSB repair in G1 cells might be more accurate at an earlier time point after irradiation.

In general, clonogenic survival 24 h post-irradiation (“delayed plating”) showed improvement of survival compared to classical clonogenic survival assay with immediate plating, indicating that detaching, dissociating and seeding the cells immediately after irradiation contributed to the cell reproductive death. Moreover, the immediate plating of the human fibroblasts revealed that the survival of the G1 cells was not essentially better than the survival of the G0 cells after X-ray or carbon ion irradiation.

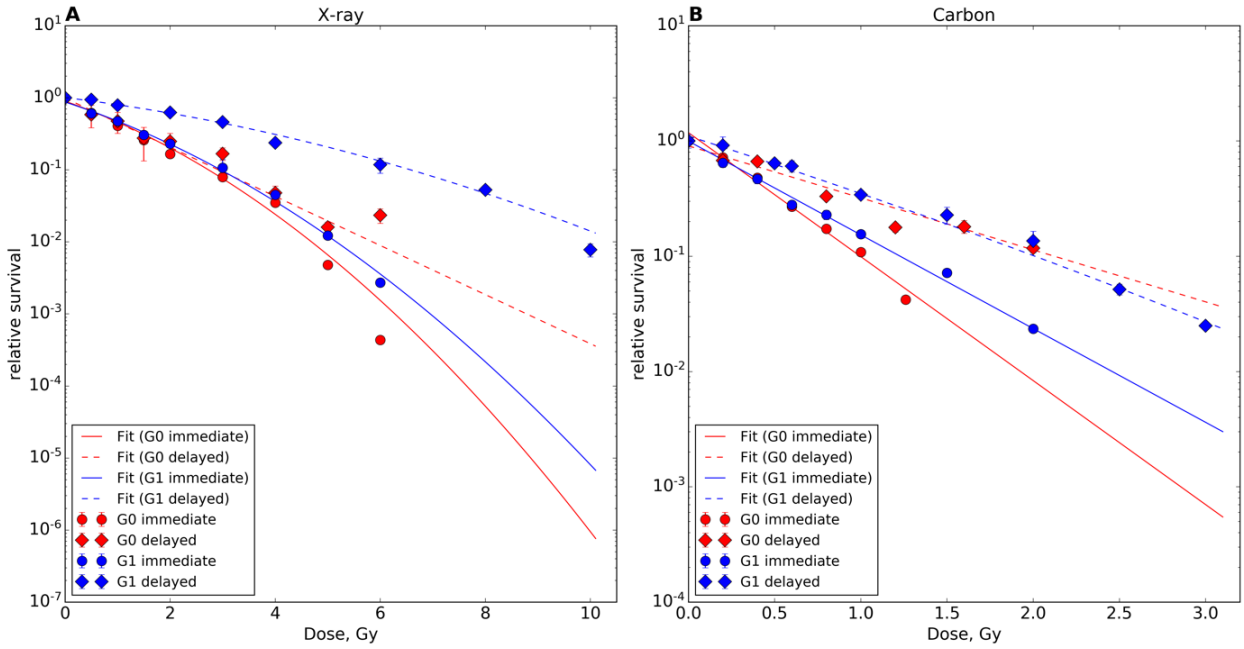

Figure 4.33: Clonogenic survival as a function of dose upon X-ray- or carbon ion irradiation A: Clonogenic survival of human fibroblasts after X-ray irradiation. The cultures enriched in G1 or G0 phase were X-ray irradiated with doses between 0.5 and 10 Gy (Table 2.3). The cells were treated the same way as in A. The measured data points were plotted using the matplotlib Library. The curves (lines) were fitted to the data points using the optimize.curve fit function from the Python library SciPy. **B:** Human fibroblasts were enriched in G1 or G0 phase. The cells were irradiated with carbon ions (with energy on target appr; 24 MeV/u and LET 81 keV/µm) with doses between 0.2 and 2.5 Gy (Table 2.3). The cells were re-plated as biological triplicates immediately after irradiation (immediate plating) or 24 h later (delayed plating). Subsequently, the samples were incubated for 14 days with one medium change at day 7. The grown colonies were then fixed, stained and counted. Error bars present ±SD of averaged triplicates. The measured data points were fitted: $S = S_0\, e^{-\alpha D - \beta D^2}$ (lines).

The comparison of delayed versus immediate plating showed better survival of delayed plated fibroblasts compared to immediately plated fibroblasts. Similar results were shown by Liu et al., where the human fibroblasts under delayed plating conditions had increased survival compared to immediately plated cells irradiated with an equal dose of X-rays or heavy ions (Liu, Kawata et al. 2013). Moreover, the increased survival upon delayed plating compared to immediate plating was LET dependent: with increasing LET the survival difference was decreasing in G1 cells (Figure 4.33). A far lower cell survival was observed in immediately plated X-ray irradiated cells than in delayed plated G1 cell. However, the difference in survival was relatively small in delayed and immediate plated G0 cells after X-ray irradiation, whereas after carbon ion irradiation it was increased in survival of delayed plated G0 cells similar to G1 cells.

In order to characterize the impact of the cell cycle phase – G0 and G1 - on the survival after irradiation, the ratio of the dose required to obtain 10 % survival (D_{10}) in G1 cells (D_{10}G1) and

D_{10} in G0 ($D_{10}G0$) was determined for X-ray and carbon ion irradiation (Table 4.1). The $D_{10}G1/D_{10}G0$ revealed that the survival of G1 cells upon delayed plating was two times better than in G0 cells after X-ray irradiation. However, the survival after carbon-ion irradiation was similar in G1 and G0 cells. In order to characterize the effect of delayed plating the survival recovery ratio (SRR) was determined. It represents the ratio of the dose required to obtain 10 % survival (D_{10}) after delayed plating ($D_{10}24h$) and D_{10} after immediate plating ($D_{10}0h$) (Table 4.1). Therefore, the LET dependent repair behavior was different in G1 and G0 cells: it was decreased with increased LET in G1 cells from SRR 2.33 after X-ray- to 1.78 after carbon ion irradiation. While the relative SRR value in G0 cells was increased from 1.20 after X-ray- to 1.85 after carbon ion irradiation (Table 4.1).

Table 4.1: $D_{10}G_1/D_{10}G_0$ ratio and survival recovery ratio (SRR).

	$D_{10}G1/D_{10}G0$		$D_{10}24h/D_{10}0h$ (SRR)	
	immediate	**delayed**	**G1**	**G0**
X-rays	1.06	2.05	2.33	1.20
Carbon ions	1.10	1.06	1.78	1.85

Taken together, the 24 h post irradiation survival curve of X-ray irradiated G0 and G1 cells mirrors their repair kinetics. The survival of delayed plated G1 cells was improved about twofold compared to immediate plated G1 cells, whereas the survival of delayed plated G0 cells was only slightly improved in comparison to immediate plated G0 cells. Therefore, the SRR of G1 cells after X-ray irradiation was better than after carbon ion irradiation. However, the SRR after carbon ion irradiation was equal in G1 and G0 cells.

Further characteristics which described the survival curves are α and β values derived from the fit of the curves (equation 4.1):

$$S = S_0 e^{-\alpha D - \beta D^2} \qquad (4.1)$$

S : survival;

S_0 : plating efficiency;

D : applied dose.

The α-value is a linear component which represents the initial slope of the survival curve and β-value is a quadratic component, which represents the bending of the curve. Survival curve after carbon ion irradiation had a linear shape without bending, hence, the β-value was zero. The α and β values are constants and are specific for cell type or tissue.

Table 4.2 demonstrates α-values after carbon ion irradiation as well as α and β values after X-ray irradiation. The α-value represents the initial slope of the survival curve and indicates the radio-sensitivity of the irradiated cells. The bigger the α-value, the steeper the curve, the more radio-sensitive the cell line. The α-values of the human fibroblasts survival curves were generally higher after carbon ion than after X-ray irradiation. Furthermore, the α-value of the G0 immediate seeded cells after carbon ion was higher than in the G1 immediate plating cells. However, delayed plating G1 and G0 curves showed almost the same α-value after carbon ion irradiation. After X-ray irradiation, the α-value was contrariwise: immediate plating G0 and G1 curves had a similar α-value, whereas delayed plating G0 curves showed higher α-value than G1 cells respectively.

Table 4.2: Survival curve parameters. Carbon irradiation α-values are derived from the linear fit. X-ray irradiation α- and β values derived from linear-quadratic fit.

	G1				G0			
	immediate		delayed		immediate		delayed	
	α [Gy^{-1}]	β [Gy^{-2}]	α [Gy^{-1}]	β [Gy^{-2}]	α [Gy^{-1}]	β [Gy^{-2}]	α [Gy^{-1}]	β [Gy^{-2}]
X-rays	0.683	0.034	0.205	0.016	0.713	0.079	0.327	0.000
Carbon ions	1.872	0.000	1.105	0.044	2.483	0.000	1.038	0.000

Given that survival curves upon X-ray irradiation have a shoulder, α/β ratio can be calculated. The α/β ratio reflects the repair capacity of a cell line (Iliakis 1980). The G1 cells showed higher α/β ratio compared to G0 cells (Table 4.3) suggesting a better repair capacity compared to G0 cells.

Table 4.3: α/β ratio after X-ray irradiation of the AG1522D survival curves.

	G1 immediate	G1 delayed	G0 immediate	G0 delayed
α/β	20.09	12.81	9.03	-

Additionally, the RBE (relative biological effectiveness) values were calculated at 10 % fraction of survival (Table 4.4). RBE is defined as (equation 4.2):

$$\mathrm{RBE} = \frac{\mathrm{D_{X-rays}}}{\mathrm{D_{carbon\ ions}}} \qquad (4.2)$$

The values were similar with immediate plating in both G1 and G0 cells at 10 % of survival fraction.

The RBE values in delayed plating G1 curves were higher than in delayed plating G0 curves indicating higher repair capacity of G1 cells compared to G0 cells reflecting the X-ray repair curves (Figure 4.27).

Table 4.4: RBE ($D_{X\text{-}ray}/D_{C\text{-}ion}$) values at D_{10} survival in the G1 and G0 human fibroblasts.

	G1 immediate	G1 delayed	G0 immediate	G0 delayed
RBE	2.29	3.00	2.73	1.59

In conclusion, delayed plating improves the clonogenic survival of the G1 and G0 cells after ionizing irradiation affirming earlier studies (Little 1969, Liu, Kawata et al. 2013). In this work, the improvement of clonogenic survival was stronger in G1 cells than G0 after X-ray irradiation confirming the repair kinetics after X-ray irradiation. Furthermore, the survival improvement was approximately equal in G1 and G0 cells after carbon ion irradiation which was, likewise, in agreement with the repair kinetics after helium ion irradiation.

5. Discussion

Heavy-ion radiation induces complex DNA damage (Lorat, Timm et al. 2016). The repair of heavy ion-induced DSBs based on the processing of break-ends is important not only in S/G2 cells but also in G1 cells (Averbeck, Ringel et al. 2014). The processing of DSB break-ends – DNA resection – was shown to be LET dependent in both G1- and S/G2 cells (Averbeck, Ringel et al. 2014). The higher LET of the ion the more complex DNA damage occurs and therefore more cells are resected (Figure 1.14). To quantify resection positive cells, ssDNA was visualized by immunofluorescence staining against RPA (replication protein A). RPA binds the ssDNA immediately to protect it from degradation by nucleases and to stabilize it (Bochkarev, Pfuetzner et al. 1997).

The studies that focused on the machinery of the resection regulation are mostly concentrated on S/G2 cells where DNA resection predominantly occurs (Chapman JR 2013, Escribano-Diaz, Orthwein et al. 2013). Nevertheless, the regulation of heavy ion-induced DNA resection in G1 cells remains poorly explored. It was shown that the resected DNA ends in G1 cells are repaired by error prone alternative NHEJ (Wang, Wu et al. 2006, Barton, Naumann et al. 2014) or by the sub-pathway of classical NHEJ (Biehs, Steinlage et al. 2017). These two possibilities to repair DSBs in G1 cells are error prone and thus might result in mutations, chromosomal aberrations and cell death. Therefore, it is very important to understand the regulation mechanism of DNA resection and the factors that are involved in this regulation in G1 cells. Escribano-Diaz et al. proposed a regulatory circuit operating in cell cycle dependent manner at DSB sites. It is comprised of two complexes, 53BP1/RIF1 and CtIP/BRCA1, which play a crucial role in the repair-pathway choice. (Escribano-Diaz, Orthwein et al. 2013). The studies to elucidate the role of these regulatory factors were performed with low LET radiation which induces mostly simple, fast reparable DSBs. Further investigations are needed to understand the role of resection regulation factors at ion-induced DSBs. Therefore, it was essential to study the function of these regulatory factors at complex DSB in G1 cells. RIF1 was recently shown to be an interacting factor of 53BP1 in the protection of DSB ends from resection. Furthermore, recent publications showed that RIF1 contributes to the suppression of resection in S/G2 cells (Chapman JR 2013, Di Virgilio M 2013, Escribano-Diaz, Orthwein et al. 2013, Zimmermann, Lottersberger et al. 2013). The protection of DSB ends from resection is of high relevance in G1 cells, because they do not possess a sister chromatid as a homologous template to utilize the faithful repair pathway - homologous recombination (HR). As a consequence, G1 cells are predestined to repair resected DSBs with error prone repair pathways, such as alt-NHEJ (Iliakis, Murmann et al. 2015) or resection dependent c-NHEJ (Biehs, Steinlage et al. 2017). Therefore, the main interest was focused on whether RIF1 is a key factor to support 53BP1 in resection

prevention of ion-induced DSBs. Additionally, several studies showed that BRCA1, as a tumor suppression factor, interacts with 53BP1 to remove it from DSBs and allows resection (Bouwman, Aly et al. 2010, Bunting, Callen et al. 2010, Chapman, Sossick et al. 2012, Kakarougkas, Ismail et al. 2013). However, the exact mechanism is still unclear. Whether this regulation is also available at ion-induced DSBs in G1 cells remains to be discovered. A hypothesis that BRCA1 might initiate resection of ion-induced DSBs in G1 was one of the main questions of this thesis.

5.1. RIF1

The investigation of the role of RIF1 in this work showed that its active recruitment to complex DSBs was LET independent in G1 cells, but LET dependent in S/G2 cells (Figure 4.1). Since it was shown in several studies (Chapman JR 2013, Di Virgilio M 2013, Escribano-Diaz, Orthwein et al. 2013, Zimmermann, Lottersberger et al. 2013) that RIF1 plays a DSB protective role against resection, it was expected that fraction of RIF1 positive cells decreases with increasing of DSB complexity which correlates with the number of RPA positive cells. The outcome was opposite. The fraction of RIF1 positive G1 cells remained at high level of appr. 80 – 90 % independent of the LET but was increasing with increasing LET in S/G2 cells from appr. 20 % (LET 2 keV/μm) up to appr. 80 % (LET 15,000 keV/μm). The increasing of RIF1 positive S/G2 cells with increased LET as well as high portion of RIF1 positive G1 cells after heavy ion irradiation suggest an essential role of RIF1 at complex DSBs. RIF1 acts downstream of 53BP1 to operate at DNA damage induced during replication in S-phase (Buonomo, Wu et al. 2009). This involvement of RIF1 in DNA repair of S cells might contribute to the increase of RIF1 positive S/G2 cells.

To investigate the role of RIF1 in resection of high LET radiation-induced DSBs, RIF1 depleted U2OS cells were used. The results of this subset of experiments suggest a modest role of RIF1 in the resection protection of complex DSBs. RIF1 deficient cells showed hardly an increase either in the fraction of resection positive G1 cells or in the number of RPA foci per nucleus compared to RIF1 proficient cells. These results run contrary to the data of several publications which claim that RIF1 has a resection protective role at DSB sites (Di Virgilio M 2013, Escribano-Diaz, Orthwein et al. 2013). However, other authors showed that RIF1 depletion cannot fully rescue the formation of Rad51 foci (Rad51 recruitment to DSBs relies on resection), HR defect and hyper-radio-sensitivity in BRCA1 deficient cells like 53BP1 deficient cells do (Feng, Fong et al. 2013). These results suggest that either 53BP1 might have another binding partner to protect DSBs from resection or RIF1 could possess an additional function in HR pathway. The first assumption is supported by the knowledge that 53BP1 has another binding partner, PTIP, which was shown to protect DNA ends from resection (Callen, Di Virgilio et al. 2013). The second notion is that RIF1 might support

resection of complex DSBs rest upon recent studies that shown RIF1 as a binding partner of BLM helicase which is involved in DNA resection at the initial stages of HR (Xu, Muniandy et al. 2010, Nimonkar, Genschel et al. 2011, Li, Poon et al. 2017).

The depletion of 53BP1 (as a main protector of DSB ends predominantly in G1 cells) significantly increased the number of RPA positive cells in G1 phase by appr. 61.4 % (Figure 4.5 B) indicating that 53BP1 is a main protector of DSBs from resection. The number of RPA positive cells in 53BP1 depleted S/G2 cells - compared to mock depleted cells - was slightly increased, appr. 23 %. This result was consistent with other studies reporting the resection protection function of 53BP1 (Chapman 2013, Escribano-Diaz, Orthwein et al. 2013, Zimmermann, Lottersberger et al. 2013).

However, RIF1 foci formation of ion-induced DSBs was not affected in 53BP1 depleted cells (Figure 4.6) contradicting the findings by Escribano-Diaz et al. that RIF1 required phosphorylated by ATM 53BP1 to be recruited to DSBs (Escribano-Diaz, Orthwein et al. 2013). Nevertheless, the 53BP1-independent RIF1 recruitment to chromatin was also shown by Feng and coworkers (Feng, Fong et al. 2013). The 53BP1-independent RIF1 recruitment to complex DSBs opens the door to speculation as to whether RIF1 might play a protective- and stabilizing role for damaged DNA independent on repair pathway. It was shown that mammalian RIF1 possess a DNA binding domain located in its C-terminus (Xu, Muniandy et al. 2010). Moreover, the possible involvement of RIF1 in HR pathway through binding of BLM helicase suggests an additional, 53BP1 independent role of RIF1 at ion-induced DSBs (Li, Poon et al. 2017).

Nevertheless, the RIF1 foci formation at DSBs were increased in BRCA1 depleted cells after low LET irradiation in S/G2 phase and after high LET irradiation as well as in BRCA1 depleted G1 cells (Figure 4.7). Upon X-ray irradiation, the number of RIF1 foci per nucleus in S/G2 cells was increased by 35,4 %. Furthermore, an induction of complex DSBs by carbon ion irradiation revealed an increase in RIF1 foci formation of 32.8 % in BRCA1 depleted G1 cells and by 152.2 % by BRCA1 depleted S/G2 cells compared to mock depleted cell, respectively. This result suggests that BRCA1 and RIF1 are antagonists at complex DSBs not only in S/G2 cells but also in G1 cells. It was shown that BRCA1 is phosphorylated in a cell cycle dependent manner and this phosphorylation contributes to the timing of DNA resection (Parameswaran 2014). The results after X-ray irradiation confirm this statement; BRCA1 depletion increased the number of RIF1 foci only in S/G2- but not in G1 cells. In contrast, there was an increase of the number of RIF1 foci after heavy ion irradiation in BRCA1 depleted G1 cells suggesting that BRCA1 might be phosphorylated in G1 after heavy ion irradiation. Recently discovered phosphorylation of BRCA1 by PLK1, which is also available in G1 cells, may play an important role in this regulation (Chabalier-Taste, Brichese et al. 2016).

5.2. BRCA1

BRCA1 foci formation at ion induced DSBs was strongly cell cycle dependent but concomitantly LET independent. The fraction of BRCA1 positive cells in G1 phase, appr. 20 – 30 %, was much lower than in S/G2 phase, appr. 80 – 90 % (Figure 4.8 B). This difference of the cell cycle dependent BRCA1 foci distribution lead to the question whether the small fraction of BRCA1 positive G1 cells upon irradiation is due to a low BRCA1 amount in G1 cells or due to the tightly regulated BRCA1 foci formation in G1 cells. From published studies, it is not clear whether or not the BRCA1 amount in G1 cells is limited. Chen et al. showed that the BRCA1 protein level is low in G1 cells (Chen, Farmer et al. 1996), whereas others showed no difference in the BRCA1 protein level during the cell cycle progression (Escribano-Diaz, Orthwein et al. 2013, Jiang, Plo et al. 2013). However, Wang et al. identified HUWE1 as a regulator of the BRCA1 protein level through its N-terminus degron domain (Wang, Lu et al. 2014). In this thesis was shown that HUWE1 depletion increased the fraction of BRCA1 positive cells in G1 phase twofold suggesting that the fraction of BRCA1 positive cells might be due to a protein level limitation (Figure 4.11 A). Nevertheless, neither an increase of the BRCA1 protein level through HUWE1 depletion nor decreasing BRCA1 protein amount through BRCA1 depletion contributed to the alteration of the fraction of resection positive cells upon heavy ion irradiation. These results suggest that not the BRCA1's concentration, but its post-translational modification, like phosphorylation, might play a crucial role in its resection regulation function.

The evaluation of RPA foci numbers in BRCA1 depleted cells upon carbon ion irradiation revealed a significant decrease of RPA foci compared to BRCA1 proficient cells in both G1- and S/G2 cells (Figure 4.12). This effect was "invisible" by the analysis of the fraction of RPA positive cells and can be explained as followed: by the counting of the fraction of RPA positive S/G2 cells, the cells with at least 5 RPA foci were considered as positive. However, the foci number per cell in S/G2 population was decreased from 24.33±1.67 foci/cell in mock depleted cells to 10.05±0.97 foci/cell in BRCA1 depleted cells. The number of RPA foci in BRCA1 depleted S/G2 cells was still over the threshold of 5 foci/cell and, therefore, could not be detected. In the case of G1 cells (that generally display much less RPA foci than S/G2 cells) the predominant portion of G1 cells showed < 5 RPA foci per cell. Moreover, the effect of BRCA1 depletion was less prominent in G1- than in S/G2 cells. Hence, the chosen threshold to be considered as an "RPA positive cell" was not sensitive enough to observe differences and, therefore, the evaluation on the foci per nucleus level represents a more powerful tool to elucidate the mechanistic role of BRCA1 in resection regulation at complex DSBs.

Recruitment of both BRCA1 and RIF1 to ion-induced DSBs was cell cycle dependent: RIF1 was recruited preferentially in G1 cells, whereas BRCA1 was recruited predominantly in

S/G2 cells (Figure 4.1Fig B and Figure 4.8 B). Likewise, the analysis of the BRCA and RIF1 foci distribution along ion tracks within the first 3 h after irradiation showed generally that the ion tracks in G1 cells have more RIF1 foci and only few BRCA1 foci, whereas it was the opposite in S/G2 cells (Figure 4.14). Furthermore, the BRCA1 and RIF1 foci numbers in G1 cells were unchanged within 3 h after irradiation, while in S/G2 cells their number was decreasing over time (Figure 4.14). The decrease of BRCA1 and RIF1 foci in S/G2 cells may be based on DSB repair or regulation processes that occur differently in G1 cells.

The analysis of BRCA1/RIF1 double immunostaining showed that BRCA1 and RIF1 do not co-localize at ion-induced DSBs which is in accordance with the previous results which showed an antagonistic relationship between BRCA1 and RIF1. Nevertheless, the a more detailed analysis of single nuclei was needed to gain the information about possible overlapping of RIF1 and BRCA1 signals over time separately in G1- and S/G2 cells (Figure 4.16 A and B). Whether the overlapping pattern was cell cycle dependent is discussed next.

5.3. Overlapping BRCA1 and RIF1 at ion-induced DSBs

At the earliest time point - 0.25 h after irradiation both RIF1 (Figure 4.14 A) and BRCA1 (Figure 4.14_B) were already recruited to carbon ion-induced DSBs. At this time point, most of the BRCA1 and RIF1 signals did not overlap suggesting their antagonistic role at DSBs. However, at later time points, 1 h and 3 h after irradiation some of the nuclei showed partially overlapping patterns which were more pronounce in G1 cells (Figure 4.16). The BRCA1/RIF1 overlapping area after carbon ion irradiation was more pronounced than after X-ray irradiation suggesting that the BRCA1/RIF1 overlapping areas were influenced by the complexity of the DNA damage. Furthermore, the overlapping areas increased with time after X-ray- and after carbon ion irradiation. This increase might be related to the mobility of damaged chromatin. A more speculative assumption to explain the observed increase of BRCA1/RIF1 overlapping area might be different recruitment kinetics of BRCA1 and RIF1 to DSBs in G1- versus S/G2 cells.

Moreover, the increased overlapping areas of BRCA1 and RIF1 in G1 cells compared to S/G2 cells might indicate a different function of BRCA1 depending on the cell cycle. The RPA and BRCA1 overlapping analysis supports this idea where the RPA and BRCA1 overlapping areas in G1 cells were significantly smaller than in S/G2 cells (Figure 4.17). In contrast, overlapping areas of RPA and RIF1 were small in both G1 and S/G2 cells suggesting RIF1 as anti-resection factor in both G1- and S/G2 cells. This presumption is in line with studies that showed BRCA1's interaction with Ku80 operating within c-NHEJ only in G1 cells (Wei, Lan et al. 2008, Jiang, Plo et al. 2013).

5.4. UHRF1 as a potential key factor in the BRCA1-RIF1 antagonism

The mechanism of the interaction of BRCA1 and RIF1 at complex DSBs remains not completely understood. A putative intermediator for the antagonistic function of BRCA1 and RIF1 in the DNA repair pathway choice was shown to be UHRF1 (Ubiquitin like, with PHD and RING domains 1), an E3 ubiquitin ligase that was shown to be recruited to DSBs by BRCA1 (Zhang, Liu et al. 2016). This protein contains several functional domains such as TUDOR, UBL, PHD, SRA and RING (Tauber and Fischle 2015). The TUDOR, PHD and SRA domains were reported to be important in epigenetic regulation (Hashimoto, Horton et al. 2008, Wang, Shen et al. 2011, Cheng, Yang et al. 2013). The relatively poor studied RING domain of UHRF1 is important for its E3 ligase activity. This function of UHRF1 was shown to be important for K63-linked poly-ubiquitination of RIF1 at DSBs to remove it from the break site and requires UHRF1's phosphorylation at S674 by CDK2/cyclin A (Zhang, Liu et al. 2016). These kinases operate in S/G2 cells and are not available in G1 cells.

This work demonstrated that UHRF1 depletion decreased the number of RPA positive cells compared to mock depleted cells after carbon ion irradiation. The fraction of RPA positive cells in UHRF1-depleted cells was about 46.8 % lower in G1- and about 38.5 % lower in S/G2 cells compared to UHRF1 proficient cells (Figure 4.19 A). A decrease of the fraction of RPA positive cells in UHRF1 depleted cells is in accordance with findings by Zhang et al. that HR is strongly compromised in UHRF1 deficient cells (Zhang, Liu et al. 2016). Furthermore, UHRF1 depletion increased the number of RIF1 positive S/G2 cells compared to mock depleted S/G2 cells which is in accordance with UHRF1's function of ubiquitinating RIF1 so that it can be removed from the break site (Zhang, Liu et al. 2016). However, there was no increase in the fraction of RIF1 positive cells in G1 phase after carbon ion irradiation (Figure 4.19). Yet, considering the large fraction of RIF1 positive cells in G1 phase an increase would be hardly visible. The analysis of the RIF1 foci formation in UHRF1 depleted versus mock depleted cells revealed an increase in the RIF1 foci number in S/G2 cells about 52.9 % as well as in G1 cells about 43.7 % after carbon ion irradiation (Figure 4.20 B). This result confirms the UHRF1's involvement in removing RIF1 from DSBs as well as suggests the UHRF1 is required for this action in G1 cells. How and whether the UHRF1 is phosphorylated at S674 to be active in G1 cells remains to be discovered. In contrast, after X-ray irradiation the number of RIF1 foci per cell was increased only in UHRF1 depleted S/G2 cells about 42.8 %, but not in UHRF1 depleted G1 cells. These results suggest that UHRF1 might be involved in the BRCA1-RIF1 interplay in G1 cells after high LET irradiation and therefore in the resection modulation of complex DSBs in G1 cells.

However, the studies with RIF1 depleted cells showed that RIF1 had no directly detectable influence either on the fraction of resection positive cells or on the number of RPA foci per cell after heavy ion irradiation (Figure 4.3 and Figure 4.4), whereas UHRF1 depletion led to

significantly compromised resection (Figure 4.19 A). Therefore, it is conceivable that UHRF1 might influence resection through other factors, for instance through 53BP1. The 53BP1 depletion alone leads to unlimited resection of DNA DSBs (Figure 4.5 B) (Daley JM 2014). In this work, the UHRF1 depletion showed an increase of the fraction of 53BP1 positive cells in S/G2 cells compared to mock depleted cells after heavy ion irradiation (Figure 4.21), indicating an impairment of 53BP1 recruitment to DSBs in S/G2 cells. Considering a high portion of 53BP1 positive cells in mock depleted G1 cells an increase of the faction of 53BP1 positive G1 cells after UHRF1 depletion could not be proven. How UHRF1 exactly impairs the 53BP1 recruitment to DSBs still remains to be investigated.

Another possibility of impairment of the DSB end processing by UHRF1 depletion could be a direct interaction between UHRF1 and resection relevant nucleases (Tian, Paramasivam et al. 2015). Moreover, it was shown that the toxic influence of UHRF1's activity in cell cycle progression is in line with overexpressed in malignant tumors (Wang, Yang et al. 2012, Mudbhary, Hoshida et al. 2014). Indeed, UHRF1 was shown as an essential factor for the progression from G1 to S phase (Arima, Hirota et al. 2004, Jeanblanc, Mousli et al. 2005, Jenkins, Markovtsov et al. 2005) suggesting that the UHRF1 depletion might reduce the number of cells in late G1 phase which are supposed to be resection positive (Yajima, Fujisawa et al. 2013). Furthermore, UHRF1's correlation with cancer progression and in this thesis presented data suggests that UHRF1 might promote toxic repair in G1 cells by stimulating DNA resection. Therefore, it is of interest to check whether UHRF1 is involved in alternative NHEJ repair pathway in G1 cells (Ceccaldi, Rondinelli et al. 2016). Additionally, an interaction of UHRF1 with BRCA1 introduced by Zhang et al. might support BRCA1's promotion of resection at complex DSBs (Zhang, Liu et al. 2016).

Based on the results of this work a hypothesized mechanism of the resection regulation in G1 cells at heavy ion-induced DSBs is shown in Figure 5.1. The DSB ends are protected from resection after X-ray irradiation by 53BP1/RIF1 complex and therefore these DSBs are repaired quickly with a resection-independent pathway. The complexity of DSBs induced by heavy ion irradiation requires resection dependent repair pathway suggesting that BRCA1 and subsequently UHRF1 are recruited to DSBs to counteract 53BP1/RIF1 complex. Whether BRCA1 and/or UHRF1 counteract 53BP1-independent RIF1 at ion induced DSBs remains to be elucidated.

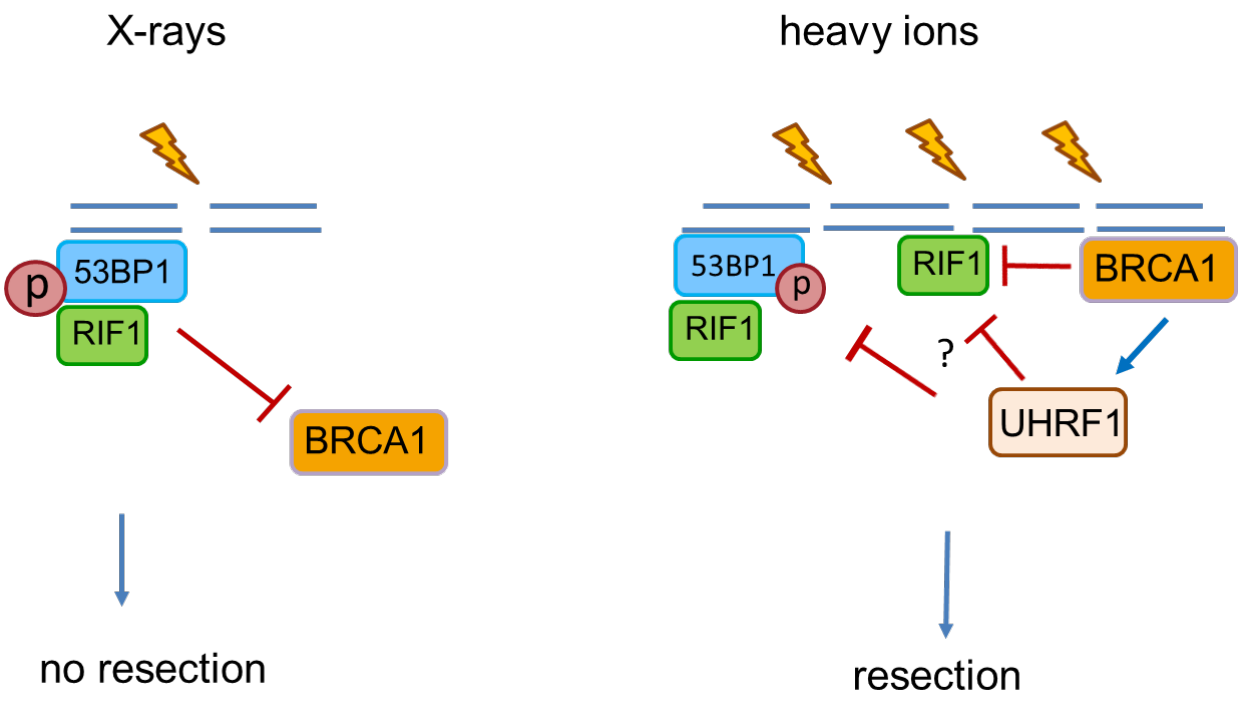

Figure 5.1: Model illustrating a hypothesized mechanism of the resection regulation after heavy ion irradiation in G1 cells compared to the resection regulation after X-ray irradiation.

In conclusion, this work was an effort to understand the sophisticated mechanism of the resection regulation in G1 cells of heavy ion induced DSBs. Presumably, the relevance of the BRCA1/RIF1-counteraction at DSBs increases with the damage complexity in G1 cells. It still remains to be discovered which factors modulate the BRCA1's recruitment and function at complex DSBs in G1 cells. There appears to be a diversity of possible functions of BRCA1 as well as RIF1 at ion-induced DSBs in G1 versus S/G2 cells, for instance, post-translational modification of BRCA1, like phosphorylation, which might play a crucial role in this regulation, requires further investigations. Additionally, it was shown that phosphorylation of 53BP1 (which is required for RIF1 recruitment to DSBs) is strongly reduced in S/G2 cells (Feng 2015), although the number of RIF1 positive S/G2 cells increases with increasing LET (Figure 4.1), therefore, the function of 53BP1-independent RIF1 recruitment to the ion-induced DSBs in G1 as well as S/G2 cells (Figure 4.6) needs further examinations.

5.5. Resection is reduced in quiescent cells after high LET irradiation

The DSB repair pathway choice is strongly cell cycle regulated (Shrivastav, De Haro et al. 2008). Within this regulation the interplay between the complexes 53BP1/RIF1 and CtIP/BRCA1 plays an important role (Escribano-Diaz, Orthwein et al. 2013).The antagonistic function of BRCA1 and 53BP1 was described in several studies (Chapman, Sossick et al. 2012, Croke, Neumann et al. 2013). Nonetheless, the role of these complexes for the resection regulation in quiescent cells remains unexplored. This work demonstrated that the

predominant part of these resection regulation factors was not detectable in western analysis (Figure 4.26 and Figure 4.30). A very low amount of CtIP and the absence of BRCA1 indicated the difficulty for quiescent cells to initiate end resection of ion-induced DSBs. This result is in accordance with the finding that the fraction of resection positive cells was 29 % decreased in the G0 cell population compared to G1 cell after xenon ion irradiation (Figure 4.25). Interestingly, the resection antagonist RIF1 could also not be detected within a Western analysis of G0 cells indicating a very low level or the lack of this protein in non-cycling cells. Given that the quiescent cells showed a severely reduced level of the resection promotors CtIP and BRCA1 it was assumed that these cells do not require the antagonistic function of the 53BP1/RIF1 complex. Since the quiescent cells do not enter S-phase the translation of RIF1 as an important replication factor is not required (Xu, Muniandy et al. 2010, Yamazaki, Ishii et al. 2012, Kumar R. 2014). The higher amount of CtIP in G1- compared to G0 cells was consistent with greater number of resection positive cells in G1. Yet, the resection of DSB might be a source for error prone repair in G1 cells (Averbeck, Topsch et al. 2016). The aim of this part of work was to investigate the role of quiescent state in the resection regulation compared to proliferating state after low- and high LET irradiation.

5.6. DSB repair kinetics and survival of human fibroblasts in G1- and G0 phase after low- and high LET irradiation

The biochemical characteristics as well as DSB repair-kinetics after X-ray irradiation of human fibroblasts in G1- and G0 phase showed essential differences between these two cell cycle states. In addition, quiescent cells showed a decreased fraction of resection positive cells after heavy ion irradiation, they also revealed slower repair kinetics of X-ray induced DSBs than G1 cells (Figure 4.27). The 24 h post irradiation G0 cells comprised still 20 - 30 % unrepaired DSBs detected by γH2AX staining (Lobrich, Shibata et al. 2010), whereas DSBs in G1 cells were almost all repaired.

It was hypothesized that the G0 and G1 cells may utilize different DSB repair pathways which were examined by using DNA repair pathway inhibitors: DNA-PKcs inhibitor in order to inhibit classical NHEJ and PARP inhibitor to inhibit alternative NHEJ. The severe repair impairment of X-ray induced DSBs by the DNA-PKcs inhibitor indicated that the main repair pathway of G1 as well as G0 cells is classical NHEJ to repair this type of damage (Figure 4.28). Interestingly, upon irradiation with the same dose of helium ions there was no difference in the repair kinetics of G1 and G0 cells (Figure 4.32).

It is well known that the DSBs are repaired with biphasic rejoining kinetics – fast and slow kinetics (Riballo, Kuhne et al. 2004, Lobrich and Jeggo 2005) - and this biphasic kinetics is due to the chromatin structure and the complexity of DSBs. Simple DSBs are repaired faster than more complex DSBs (Li, Reynolds et al. 2014) and the heterochromatin located DSBs

require more time for their repair (Downs, Nussenzweig et al. 2007, Goodarzi and Jeggo 2012). In this thesis presented data, G1 cells repaired X-ray-induced DSBs faster than helium ion-induced DSBs which are more complex than X-ray-induced DSBs (Figure 4.32).

Since the repair kinetics after low- but not after high LET irradiation was different in quiescent and proliferating human fibroblasts the question arose whether there is a difference in the quality of repair in G1 versus G0 fibroblasts. To evaluate the repair fidelity of X-ray- or heavy ion irradiated G1 and G0 cells clonogenic survival assay was performed. The clonogenic survival mirrors the accuracy of the DSB repair. If the cells repair the DSBs faithfully they are capable of mitotic proliferation and to colony generation. In the performed assay the cells were not seeded until 24 h after irradiation (delayed plating). This 24 h gap between irradiation and seeding of the cells was chosen to create the same repair condition as for the γH2AX foci assays (Figure 4.27). Additionally, the G1 and G0 cells were seeded immediately after irradiation in accordance with the classical clonogenic survival assay (Elkind 1967). The survival of delayed plated cells mirrored the difference of the repair kinetics in G1 and G0 cells after low- and high LET irradiation. The difference in survival between G0 and G1 cells was greater after X-ray- than after carbon ion irradiation (Figure 4.33). In contrast, immediately plated G1 and G0 cells showed almost no difference in their survival after X-ray- and carbon ion irradiation. This could be due to the cells undergoing the same cell cycle condition after detaching, dissociating and re-seeding them.

A far lower survival was observed in delayed plated G0 cells compared to delayed plated G1 cells upon X-ray irradiation suggests that the majority of simple DSBs in quiescent cells remains unrepaired. A similar idea was argued by Ambrosio et al. which showed a persistent accumulation of DSBs in G0 cells. Furthermore, these accumulated DSBs are repaired only after re-entering the cells into cell cycle (Ambrosio 2015). Additionally, Ambrosio et al. showed that a persistent accumulation of γH2AX and DSB repair factors at DSBs suggests a repair defect in G0 cells which is not dependent on the expression level of the DSB repair factors (Ambrosio 2015). Since the clonogenic survival mirrors the fidelity of DNA repair, the similar survival in delayed and immediate plated post X-ray irradiated G0 cells indicates that the G0 cells might accumulate the DNA damage several days after irradiation without repair.

However, the survival was increased in delayed plated G0 cells compared to immediately plated G0 after carbon ion irradiation. Moreover, this increase was similar with survival increase in delayed plated G1 cells compared to immediately plated G1 cells suggesting a different, LET-dependent behavior on G0 and G1 cells. The survival was decreased with increased LET in G1 cells from SRR 2.33 after X-ray- to 1.78 after carbon ion irradiation (Table 4.1). While the relative SRR value in G0 cells was increased from 1.20 after X-ray- to 1.85 after carbon ion irradiation. The severity of DSBs might dictate the acuteness of their repair in quiescent cells whereas simple DSBs, the majority of DSBs induced by X-ray, may

partially remain unrepaired if cells are exposed to an additional stress like detaching and re-seeding after irradiation.

The cell killing of high LET radiation was stronger compared to the cell killing of low LET irradiation. This effect can be expressed as relative biological effectiveness (RBE), i.e. the ratio of dose of the survival after X-rays (reference radiation) by the survival after heavy particles radiation (test radiation required for equal biological effect) (Hall 2012). It was shown that the RBE peaks are between an LET of 100 and 200 keV/µm (Weyrather, Ritter et al. 1999). In this work, human fibroblasts were irradiated with carbon ions of an LET of 81 keV/µm. Hence, at this LET the RBE is expected to be high, which allows the detection of differences between G1- and G0 cells. The point for the RBE calculation was selected at 10 % survival where survival fell exponentially. Furthermore, the measurement points of all performed survival curves covered this range. The RBE values of immediately plated G1 and G0 cells were nearly similar, 2.3 and 2.7 respectively, but delayed plated G1 cells showed a higher RBE, 3.0, than delayed plated G0 cells, 1.6. The higher RBE value in delayed plated G1- compared to delayed plated G0 cells presumes higher repair capacity of G1- than G0 cells upon X-ray irradiation. While the nearly similar RBE value of immediate plated G1 and G0 cells indicates that the cells undergo the similar conditions by detaching and re-seeding directly upon irradiation which force them to undergo the cell cycle. Weyrather et al. showed that the relatively small RBE value is caused by the DSB repair defect (Weyrather, Ritter et al. 1999). The lower repair capacity of G0 cells mirrored in RBE together with slower repair kinetics after X-ray irradiation (Figure 4.27) suggest a repair detriment which might be caused by more compactly structured chromatin or limited availability of repair proteins compared to G1 cells.

Further parameters that describe the survival curves are α and β values. The α-value indicates the sensitivity of the cell line, the higher the α value the more sensitive are the cells to the radiation exposure. The α value in G0 delayed plated cells after X-ray irradiation was 0.327, thus, higher than 0.205 in delayed plated G1 cells indicating better survival of G1- than G0 cells at very low radiation dose (Table 4.2). However, the α values of immediately plated G1 and G0 cells were similar after X-ray irradiation, 0.683 and 0.713, respectively, indicating the adjusted repair conditions of these two cell cultures, namely the both are forced to re-enter into the cell cycle.

Nevertheless, the β values of the X-ray survival curves were different in G1 and G0 cells at both plating conditions (Table 4.2). In average, the β value were twofold higher in G0 than in G1 cells in immediate plated cells suggesting a higher sensitivity of G0 cells at higher radiation dose compared to G1 cells. Moreover, the β value was higher of immediate plated G1 compared to delay plated G1 cells which might be related to the additional stress of the cell detaching and re-seeding for clonogenic survival assay (Table 4.2).

Additionally, the α/β ratio indicates the dose where the contribution to the cell killing of linear component is equal to the contribution of the quadratic component (Hall 2012):

$$\alpha D = \beta D^2$$

$$\frac{\alpha}{\beta} = D$$

The α/β ratio might indicate the proliferation activity of the cell culture. From empirical data, the high α/β ratio in range 10 to 20 suggests fast proliferating tissue, while the low α/β ratio from about 0.5 to about 7 indicates slow- or non-proliferating tissue (Alpen 1998). In line with this, the G1 cell culture contained 70-80 % of proliferating cells showed high α/β ratios of 20.1 and 12.8 in immediate and delayed plating, respectively (Figure 4.23). Whereas the α/β ratios in immediate plated G0 cells were 9.0. Since the survival curve of delayed plated G0 cells after X-ray irradiation has a linear fit, the α/β ratio could not be calculated.

In conclusion, this work was the first to compare the biological effect of low- and high LET in quiescent versus enriched in G1 phase human fibroblasts. The results of this work provide some insights into the non-tumor cell line response to low- and high LET irradiation. The molecular origin of the difference in DNA damage response of G0 and G1 cells might be based on the differences of chromatin structure and the repair protein availability. Moreover, the different metabolic activity of G1 and G0 cells might play a role in the DNA damage response. Further experiments will be required to elucidate the molecular mechanism underlying the regulation of repair efficiency in quiescent cells which will be significant data for the tumor therapy.

5.7. Outlook

The analysis of the resection regulation at ion-induced DSB in G1 phase of the cell cycle, which was performed in this work, gave indications on how this regulation is organized in G1 and G0 cells. The resection regulation is driven by the interaction of two important complexes: CtIP/BRCA1 and 53BP1/RIF1. Particular attention was concentrated on the interaction between RIF1 and BRCA1 at ion-induced DSBs. It was found that the BRCA1 interaction partner UHRF1 is involved in the resection regulation of complex ion-induced DSBs; the UHRF1 depletion compromises resection of ion-induced DSBs in G1 cells. UHRF1 supposes to function downstream of BRCA1 mediating the RIF1 removal from DSBs (Zhang, Liu et al. 2016). Since it was shown that RIF1 depletion does not influence DNA resection of ion-induced DSBs and it also does not restore HR deficiency in BRCA1 deficient cells (Escribano-Diaz, Orthwein et al. 2013, Feng, Fong et al. 2013, Zimmermann, Lottersberger et al. 2013), it is speculated that UHRF1 might promote resection through compromising of 53BP1 recruitment or phosphorylation at ion-induced DSBs. Therefore, further investigations should be directed towards the influence of UHRF1 on 53BP1

recruitment and phosphorylation at ion-induced DSBs. Moreover, another interacting partner of 53BP1 PTIP might play a compensative role in RIF1 depleted cells in the prevention of DSB end resection (Callen, Di Virgilio et al. 2013).

The effects of BRCA1- or RIF1 depletion did not reveal a strong impairment on DNA resection after heavy ion irradiation suggesting that the applied technique to measure DNA resection by immunofluorescence stained RPA foci with a relatively low resolution, which was used in this thesis, could not give definitive information in regard to length or speed of the resected DNA track. A new technique was developed by Cruz-Garcia et al., which allows a measurement of resection length and speed of a single molecule after exposure to ionizing irradiation or radiomimetic drugs, could provide a more accurate elucidation of resection regulation of ion-induced DSBs in G1 cells (Cruz-Garcia, Lopez-Saavedra et al. 2014).

However, the very small effects of BRCA1- or RIF1 deficiency on DNA resection suggest an existence of further regulatory factors in G1 cells. Several publications showed that Ku80 as a protector of DNA ends from resection play a regulatory role in the suppression of homology directed repair (Fattah, Lee et al. 2010, Shao, Davis et al. 2012, Tomimatsu, Mukherjee et al. 2012, Chang, Watanabe et al. 2015).

In this work, it was shown that RIF1 is recruited to ion-induced DSBs in 53BP1 deficient cells (Figure 4.6). The 53BP1-idependet role of RIF1 might be attributed to its direct interaction with DNA through its DNA-binding site (Xu, Muniandy et al. 2010). Furthermore, Xu et al. showed that RIF1 can bind BLM helicase with its conservative N-terminus (Xu, Muniandy et al. 2010). However, despite the role of BLM helicase in HR, BLM helicase was shown to prevent alt-NHEJ and excessive resection by CtIP/Mre11 in G1 through its interaction with 53BP1 (Grabarz, Guirouilh-Barbat et al. 2013). Therefore, investigation of the interaction of 53BP1, RIF1 and BLM helicase at ion-induced DSB is important to understand their role in resection prevention in G1 cells.

A perfect model to study the limitations of DSB end resection is the quiescent human fibroblasts. This thesis demonstrates that DSB resection in quiescent human fibroblasts is distinctly decreased compared to proliferating cells. This decrease was in line with reduction of some resection regulatory factors. Therefore, further resection factors, besides restricted expression of BRCA1 and CtIP proteins, should be examined in quiescent cells. The analysis of the repair kinetics and survival of quiescent human fibroblasts after low LET irradiation suggests the G0 cells accumulates unrepaired DSBs for a long time. The comparable repair kinetics and survival of proliferating versus quiescent human fibroblasts after high LET irradiation showed quite similar behavior of these cells, suggesting that LET plays an important role in the DNA damage response of G0 cells. Therefore, it is of high importance to elucidate the impact of LET and/or low dose versus high dose effects on the repair capacity of quiescent cells attributing to their chromatin structure. Indications that quiescent cells have

an altered chromatin structure compared to proliferating cells were given in this work and in other studies (Evertts, Manning et al. 2013). Furthermore, the altered chromatin structure in quiescent cells might contribute to understanding on a molecular level the reduction of the cells' clonogenic potential called delayed reproductive death (Bettega, Calzolari et al. 2005, Hamada, Funayama et al. 2006). Altogether, these findings provide an important information for the exposure to heavy particle radiation, which is crucial for the long-term space flights as well as for the heavy ion based tumor therapy.

6. Bibliography

Abdollahi, E. (2017). Establishment of fluorescence lifetime imaging microscopy to monitor radiation-induced DNA decondensation Dissertation, TU Darmstadt.

Abercrombie, M. (1970). "Contact inhibition in tissue culture." In Vitro 6(2): 128-142.

Alberts, B., Johnson, A., Lewis, J., Raff, M., Roberts, K., and Walter, P. (2002). Molecular Biology of the Cell.

Alpen, E. L. (1998). Radiation biophysics. San Diego, Academic press.

Ambrosio S, D. P. G., Napolitano G, Amente S, Dellino GI, Faretta M, Pelicci PG, Lania L, Majello B (2015). "Cell cycle-dependent resolution of DNA double-strand breaks." Oncotarget. 7(4): 4949-4960.

Ames, B. N. (1989). "Mutagenesis and carcinogenesis: endogenous and exogenous factors." Environ Mol Mutagen 14 Suppl 16: 66-77.

Aparicio, T., Baer, R. and Gautier, J. (2014). "DNA double-strand break repair pathway choice and cancer." DNA Repair (Amst) 19: 169-175.

Arima, Y., Hirota, T., Bronner, C., Mousli, M., Fujiwara, T., Niwa, S., Ishikawa, H. and Saya, H. (2004). "Down-regulation of nuclear protein ICBP90 by p53/p21Cip1/WAF1-dependent DNA-damage checkpoint signals contributes to cell cycle arrest at G1/S transition." Genes Cells 9(2): 131-142.

Audebert, M., Salles, B. and Calsou, P. (2004). "Involvement of poly(ADP-ribose) polymerase-1 and XRCC1/DNA ligase III in an alternative route for DNA double-strand breaks rejoining." J Biol Chem 279(53): 55117-55126.

Averbeck, N. B., Ringel, O., Herrlitz, M., Jakob, B., Durante, M. and Taucher-Scholz, G. (2014). "DNA end resection is needed for the repair of complex lesions in G1-phase human cells." Cell Cycle 13(16): 2509-2516.

Averbeck, N. B., Topsch, J., Scholz, M., Kraft-Weyrather, W., Durante, M. and Taucher-Scholz, G. (2016). "Efficient Rejoining of DNA Double-Strand Breaks despite Increased Cell-Killing Effectiveness following Spread-Out Bragg Peak Carbon-Ion Irradiation." Front Oncol 6: 28.

Bahassi, E. M., Ovesen, J. L., Riesenberg, A. L., Bernstein, W. Z., Hasty, P. E. and Stambrook, P. J. (2008). "The checkpoint kinases Chk1 and Chk2 regulate the functional associations between hBRCA2 and Rad51 in response to DNA damage." Oncogene 27(28): 3977-3985.

Bakr, A., Kocher, S., Volquardsen, J., Reimer, R., Borgmann, K., Dikomey, E., Rothkamm, K. and Mansour, W. Y. (2016). "Functional crosstalk between DNA damage response proteins 53BP1 and BRCA1 regulates double strand break repair choice." Radiother Oncol 119(2): 276-281.

Barton, O., Naumann, S. C., Diemer-Biehs, R., Kunzel, J., Steinlage, M., Conrad, S., Makharashvili, N., Wang, J., Feng, L., Lopez, B. S., Paull, T. T., Chen, J., Jeggo, P. A. and Lobrich, M. (2014). "Polo-like kinase 3 regulates CtIP during DNA double-strand break repair in G1." J Cell Biol 206(7): 877-894.

Betermier, M., Bertrand, P. and Lopez, B. S. (2014). "Is non-homologous end-joining really an inherently error-prone process?" PLoS Genet 10(1): e1004086.

Bethe, H. (1930). "Zur Theorie des Durchgangs schneller Korpuskularstrahlen durch Materie." Annalen der Physik 397: 325–400.

Bettega, D., Calzolari, P., Doneda, L., Durante, M. and Tallone, L. (2005). "Early and delayed reproductive death in human cells exposed to high energy iron ion beams." Adv Space Res 35(2): 280-285.

Beucher, A., Birraux, J., Tchouandong, L., Barton, O., Shibata, A., Conrad, S., Goodarzi, A. A., Krempler, A., Jeggo, P. A. and Lobrich, M. (2009). "ATM and Artemis promote homologous recombination of radiation-induced DNA double-strand breaks in G2." EMBO J 28(21): 3413-3427.

Beucher, A., Deckbar, D., Schumann, E., Krempler, A., Frankenberg-Schwager, M. and Lobrich, M. (2011). "Elevated radiation-induced gammaH2AX foci in G2 phase heterozygous BRCA2 fibroblasts." Radiother Oncol 101(1): 46-50.

Biehs, R., Steinlage, M., Barton, O., Juhasz, S., Kunzel, J., Spies, J., Shibata, A., Jeggo, P. A. and Lobrich, M. (2017). "DNA Double-Strand Break Resection Occurs during Non-homologous End Joining in G1 but Is Distinct from Resection during Homologous Recombination." Mol Cell 65(4): 671-684 e675.

Bloch, F. (1933). "Zur Bremsung rasch bewegter Teilchen beim Durchgang durch Materie." Annalen der Physik 408.

Bochkarev, A., Pfuetzner, R. A., Edwards, A. M. and Frappier, L. (1997). "Structure of the single-stranded-DNA-binding domain of replication protein A bound to DNA." Nature 385(6612): 176-181.

Bostick, M., Kim, J. K., Esteve, P. O., Clark, A., Pradhan, S. and Jacobsen, S. E. (2007). "UHRF1 plays a role in maintaining DNA methylation in mammalian cells." Science 317(5845): 1760-1764.

Bouwman, P., Aly, A., Escandell, J. M., Pieterse, M., Bartkova, J., van der Gulden, H., Hiddingh, S., Thanasoula, M., Kulkarni, A., Yang, Q., Haffty, B. G., Tommiska, J., Blomqvist, C., Drapkin, R., Adams, D. J., Nevanlinna, H., Bartek, J., Tarsounas, M., Ganesan, S. and Jonkers, J. (2010). "53BP1 loss rescues BRCA1 deficiency and is associated with triple-negative and BRCA-mutated breast cancers." Nat Struct Mol Biol 17(6): 688-695.

Bruun, D., Folias, A., Akkari, Y., Cox, Y., Olson, S. and Moses, R. (2003). "siRNA depletion of BRCA1, but not BRCA2, causes increased genome instability in Fanconi anemia cells." DNA Repair (Amst) 2(9): 1007-1013.

Bunting, S. F., Callen, E., Wong, N., Chen, H. T., Polato, F., Gunn, A., Bothmer, A., Feldhahn, N., Fernandez-Capetillo, O., Cao, L., Xu, X., Deng, C. X., Finkel, T., Nussenzweig, M., Stark, J. M. and Nussenzweig, A. (2010). "53BP1 inhibits homologous recombination in Brca1-deficient cells by blocking resection of DNA breaks." Cell 141(2): 243-254.

Buonomo, S. B., Wu, Y., Ferguson, D. and de Lange, T. (2009). "Mammalian Rif1 contributes to replication stress survival and homology-directed repair." J Cell Biol 187(3): 385-398.

Burkle, A., Chen, G., Kupper, J. H., Grube, K. and Zeller, W. J. (1993). "Increased poly(ADP-ribosyl)ation in intact cells by cisplatin treatment." Carcinogenesis 14(4): 559-561.

Callen, E., Di Virgilio, M., Kruhlak, M. J., Nieto-Soler, M., Wong, N., Chen, H. T., Faryabi, R. B., Polato, F., Santos, M., Starnes, L. M., Wesemann, D. R., Lee, J. E., Tubbs, A., Sleckman, B. P., Daniel, J. A., Ge, K., Alt, F. W., Fernandez-Capetillo, O., Nussenzweig, M. C. and Nussenzweig, A.

(2013). "53BP1 mediates productive and mutagenic DNA repair through distinct phosphoprotein interactions." Cell 153(6): 1266-1280.

Ceccaldi, R., Rondinelli, B. and D'Andrea, A. D. (2016). "Repair Pathway Choices and Consequences at the Double-Strand Break." Trends Cell Biol 26(1): 52-64.

Chabalier-Taste, C., Brichese, L., Racca, C., Canitrot, Y., Calsou, P. and Larminat, F. (2016). "Polo-like kinase 1 mediates BRCA1 phosphorylation and recruitment at DNA double-strand breaks." Oncotarget 7(3): 2269-2283.

Chan, S. H., Yu, A. M. and McVey, M. (2010). "Dual roles for DNA polymerase theta in alternative end-joining repair of double-strand breaks in Drosophila." PLoS Genet 6(7): e1001005.

Chang, H. H., Watanabe, G. and Lieber, M. R. (2015). "Unifying the DNA end-processing roles of the artemis nuclease: Ku-dependent artemis resection at blunt DNA ends." J Biol Chem 290(40): 24036-24050.

Chapman, J. D., Reuvers, A. P., Borsa, J. and Greenstock, C. L. (1973). "Chemical radioprotection and radiosensitization of mammalian cells growing in vitro." Radiat Res 56(2): 291-306.

Chapman JR, B. P., Vannier JB, Borel V, Steger M, Tomas-Loba A, Sartori AA, Adams IR, Batista FD, Boulton SJ. (2013). "RIF1 is essential for 53BP1-dependent nonhomologous end joining and suppression of DNA double-strand break resection." Mol.Cell 49(5): 858-871.

Chapman, J. R., Sossick, A. J., Boulton, S. J. and Jackson, S. P. (2012). "BRCA1-associated exclusion of 53BP1 from DNA damage sites underlies temporal control of DNA repair." J Cell Sci 125(Pt 15): 3529-3534.

Chen, Y., Farmer, A. A., Chen, C. F., Jones, D. C., Chen, P. L. and Lee, W. H. (1996). "BRCA1 is a 220-kDa nuclear phosphoprotein that is expressed and phosphorylated in a cell cycle-dependent manner." Cancer Res 56(14): 3168-3172.

Cheng, J., Yang, Y., Fang, J., Xiao, J., Zhu, T., Chen, F., Wang, P., Li, Z., Yang, H. and Xu, Y. (2013). "Structural insight into coordinated recognition of trimethylated histone H3 lysine 9 (H3K9me3) by the plant homeodomain (PHD) and tandem tudor domain (TTD) of UHRF1 (ubiquitin-like, containing PHD and RING finger domains, 1) protein." J Biol Chem 288(2): 1329-1339.

Chu, I. M., Hengst, L. and Slingerland, J. M. (2008). "The Cdk inhibitor p27 in human cancer: prognostic potential and relevance to anticancer therapy." Nat Rev Cancer 8(4): 253-267.

Citterio, E., Papait, R., Nicassio, F., Vecchi, M., Gomiero, P., Mantovani, R., Di Fiore, P. P. and Bonapace, I. M. (2004). "Np95 is a histone-binding protein endowed with ubiquitin ligase activity." Mol Cell Biol 24(6): 2526-2535.

Croke, M., Neumann, M. A., Grotsky, D. A., Kreienkamp, R., Yaddanapudi, S. C. and Gonzalo, S. (2013). "Differences in 53BP1 and BRCA1 regulation between cycling and non-cycling cells." Cell Cycle 12(23): 3629-3639.

Cruz-Garcia, A., Lopez-Saavedra, A. and Huertas, P. (2014). "BRCA1 accelerates CtIP-mediated DNA-end resection." Cell Rep 9(2): 451-459.

Cucinotta, F. A. and Durante, M. (2006). "Cancer risk from exposure to galactic cosmic rays: implications for space exploration by human beings." Lancet Oncol 7(5): 431-435.

Daley JM, S. P. (2014). "53BP1, BRCA1, and the choice between recombination and end joining at DNA double-strand breaks." Mol Cell Biol 34(8): 1380-1388.

Daley, J. M. and Sung, P. (2013). "RIF1 in DNA break repair pathway choice." Mol Cell 49(5): 840-841.

Davar, D., Beumer, J. H., Hamieh, L. and Tawbi, H. (2012). "Role of PARP inhibitors in cancer biology and therapy." Curr Med Chem 19(23): 3907-3921.

Deckbar, D., Jeggo, P. A. and Lobrich, M. (2011). "Understanding the limitations of radiation-induced cell cycle checkpoints." Crit Rev Biochem Mol Biol 46(4): 271-283.

Densham, R. M., Garvin, A. J., Stone, H. R., Strachan, J., Baldock, R. A., Daza-Martin, M., Fletcher, A., Blair-Reid, S., Beesley, J., Johal, B., Pearl, L. H., Neely, R., Keep, N. H., Watts, F. Z. and Morris, J. R. (2016). "Human BRCA1-BARD1 ubiquitin ligase activity counteracts chromatin barriers to DNA resection." Nat Struct Mol Biol 23(7): 647-655.

Di Virgilio M, C. E., Yamane A, Zhang W, Jankovic M, Gitlin AD, Feldhahn N, Resch W, Oliveira TY, Chait BT, Nussenzweig A, Casellas R, Robbiani DF, Nussenzweig MC. (2013). "Rif1 prevents resection of DNA breaks and promotes immunoglobulin class switching." science 339(6120): 711-715.

DiTullio, R. A., Jr., Mochan, T. A., Venere, M., Bartkova, J., Sehested, M., Bartek, J. and Halazonetis, T. D. (2002). "53BP1 functions in an ATM-dependent checkpoint pathway that is constitutively activated in human cancer." Nat Cell Biol 4(12): 998-1002.

Downs, J. A., Nussenzweig, M. C. and Nussenzweig, A. (2007). "Chromatin dynamics and the preservation of genetic information." Nature 447(7147): 951-958.

Durante, M., Bedford, J. S., Chen, D. J., Conrad, S., Cornforth, M. N., Natarajan, A. T., van Gent, D. C. and Obe, G. (2013). "From DNA damage to chromosome aberrations: joining the break." Mutat Res 756(1-2): 5-13.

Elkind, M. E. a. W., G. F. (1967). In vitro survival curves, in *The Radiobiology of Cultured Mammalian Cells.* .

Escribano-Diaz, C., Orthwein, A., Fradet-Turcotte, A., Xing, M., Young, J. T., Tkac, J., Cook, M. A., Rosebrock, A. P., Munro, M., Canny, M. D., Xu, D. and Durocher, D. (2013). "A cell cycle-dependent regulatory circuit composed of 53BP1-RIF1 and BRCA1-CtIP controls DNA repair pathway choice." Mol Cell 49(5): 872-883.

Evertts, A. G., Manning, A. L., Wang, X., Dyson, N. J., Garcia, B. A. and Coller, H. A. (2013). "H4K20 methylation regulates quiescence and chromatin compaction." Mol Biol Cell 24(19): 3025-3037.

Fattah, F., Lee, E. H., Weisensel, N., Wang, Y., Lichter, N. and Hendrickson, E. A. (2010). "Ku regulates the non-homologous end joining pathway choice of DNA double-strand break repair in human somatic cells." PLoS Genet 6(2): e1000855.

Feng, L., Fong, K. W., Wang, J., Wang, W. and Chen, J. (2013). "RIF1 counteracts BRCA1-mediated end resection during DNA repair." J Biol Chem 288(16): 11135-11143.

Feng, L., Li, N., Li, Y., Wang, J., Gao, M., Wang, W. and Chen, J. (2015). "Cell cycle-dependent inhibition of 53BP1 signaling by BRCA1." Cell Discov 1: 15019.

Ferguson, D. O., Sekiguchi, J. M., Chang, S., Frank, K. M., Gao, Y., DePinho, R. A. and Alt, F. W. (2000). "The nonhomologous end-joining pathway of DNA repair is required for genomic stability and the suppression of translocations." Proc Natl Acad Sci U S A 97(12): 6630-6633.

Fisher, A. E., Hochegger, H., Takeda, S. and Caldecott, K. W. (2007). "Poly(ADP-ribose) polymerase 1 accelerates single-strand break repair in concert with poly(ADP-ribose) glycohydrolase." Mol Cell Biol 27(15): 5597-5605.

Fonfria, E., Marshall, I. C., Benham, C. D., Boyfield, I., Brown, J. D., Hill, K., Hughes, J. P., Skaper, S. D. and McNulty, S. (2004). "TRPM2 channel opening in response to oxidative stress is dependent on activation of poly(ADP-ribose) polymerase." Br J Pharmacol 143(1): 186-192.

Fujimori, A., Matsuda, Y., Takemoto, Y., Hashimoto, Y., Kubo, E., Araki, R., Fukumura, R., Mita, K., Tatsumi, K. and Muto, M. (1998). "Cloning and mapping of Np95 gene which encodes a novel nuclear protein associated with cell proliferation." Mamm Genome 9(12): 1032-1035.

Goodarzi, A. A. and Jeggo, P. A. (2012). "The heterochromatic barrier to DNA double strand break repair: how to get the entry visa." Int J Mol Sci 13(9): 11844-11860.

Goodhead, D. T. (1994). "Initial events in the cellular effects of ionizing radiations: clustered damage in DNA." Int J Radiat Biol 65(1): 7-17.

Goodhead, D. T., Thacker, J. and Cox, R. (1993). "Weiss Lecture. Effects of radiations of different qualities on cells: molecular mechanisms of damage and repair." Int J Radiat Biol 63(5): 543-556.

Grabarz, A., Guirouilh-Barbat, J., Barascu, A., Pennarun, G., Genet, D., Rass, E., Germann, S. M., Bertrand, P., Hickson, I. D. and Lopez, B. S. (2013). "A role for BLM in double-strand break repair pathway choice: prevention of CtIP/Mre11-mediated alternative nonhomologous end-joining." Cell Rep 5(1): 21-28.

Gudas, J. M., Li, T., Nguyen, H., Jensen, D., Rauscher, F. J., 3rd and Cowan, K. H. (1996). "Cell cycle regulation of BRCA1 messenger RNA in human breast epithelial cells." Cell Growth Differ 7(6): 717-723.

Hada, M. and Georgakilas, A. G. (2008). "Formation of clustered DNA damage after high-LET irradiation: a review." J Radiat Res 49(3): 203-210.

Hall, E. J. a. G., A. J. (2012). Radiobiology for the radiologist., Lippincott Williams & Wilkins.

Hamada, N., Funayama, T., Wada, S., Sakashita, T., Kakizaki, T., Ni, M. and Kobayashi, Y. (2006). "LET-dependent survival of irradiated normal human fibroblasts and their descendents." Radiat Res 166(1 Pt 1): 24-30.

Hashimoto, H., Horton, J. R., Zhang, X., Bostick, M., Jacobsen, S. E. and Cheng, X. (2008). "The SRA domain of UHRF1 flips 5-methylcytosine out of the DNA helix." Nature 455(7214): 826-829.

Herrlitz, M. (2014). Elucidation of DNA methylation changes in response to ionizing radiation induced double strand breaks. Dissertation, TU Darmstadt.

Hidalgo, I., Herrera-Merchan, A., Ligos, J. M., Carramolino, L., Nunez, J., Martinez, F., Dominguez, O., Torres, M. and Gonzalez, S. (2012). "Ezh1 is required for hematopoietic stem cell maintenance and prevents senescence-like cell cycle arrest." Cell Stem Cell 11(5): 649-662.

Hirayama, R., Ito, A., Tomita, M., Tsukada, T., Yatagai, F., Noguchi, M., Matsumoto, Y., Kase, Y., Ando, K., Okayasu, R. and Furusawa, Y. (2009). "Contributions of direct and indirect actions in cell killing by high-LET radiations." Radiat Res 171(2): 212-218.

Huertas, P. (2010). "DNA resection in eukaryotes: deciding how to fix the break." Nat Struct Mol Biol 17(1): 11-16.

Iliakis, G. (1980). "Effects of beta-arabinofuranosyladenine on the growth and repair of potentially lethal damage in Ehrilch ascites tumor cells." Radiat Res 83(3): 537-552.

Iliakis, G. (2009). "Backup pathways of NHEJ in cells of higher eukaryotes: cell cycle dependence." Radiother Oncol 92(3): 310-315.

Iliakis, G., Murmann, T. and Soni, A. (2015). "Alternative end-joining repair pathways are the ultimate backup for abrogated classical non-homologous end-joining and homologous recombination repair: Implications for the formation of chromosome translocations." Mutat Res Genet Toxicol Environ Mutagen 793: 166-175.

Iliakis, G., Wang, H., Perrault, A. R., Boecker, W., Rosidi, B., Windhofer, F., Wu, W., Guan, J., Terzoudi, G. and Pantelias, G. (2004). "Mechanisms of DNA double strand break repair and chromosome aberration formation." Cytogenet Genome Res 104(1-4): 14-20.

Jackson, S. P. and Bartek, J. (2009). "The DNA-damage response in human biology and disease." Nature 461(7267): 1071-1078.

Jeanblanc, M., Mousli, M., Hopfner, R., Bathami, K., Martinet, N., Abbady, A. Q., Siffert, J. C., Mathieu, E., Muller, C. D. and Bronner, C. (2005). "The retinoblastoma gene and its product are targeted by ICBP90: a key mechanism in the G1/S transition during the cell cycle." Oncogene 24(49): 7337-7345.

Jenkins, Y., Markovtsov, V., Lang, W., Sharma, P., Pearsall, D., Warner, J., Franci, C., Huang, B., Huang, J., Yam, G. C., Vistan, J. P., Pali, E., Vialard, J., Janicot, M., Lorens, J. B., Payan, D. G. and Hitoshi, Y. (2005). "Critical role of the ubiquitin ligase activity of UHRF1, a nuclear RING finger protein, in tumor cell growth." Mol Biol Cell 16(12): 5621-5629.

Jenuwein, T. and Allis, C. D. (2001). "Translating the histone code." Science 293(5532): 1074-1080.

Jiang, G., Plo, I., Wang, T., Rahman, M., Cho, J. H., Yang, E., Lopez, B. S. and Xia, F. (2013). "BRCA1-Ku80 protein interaction enhances end-joining fidelity of chromosomal double-strand breaks in the G1 phase of the cell cycle." J Biol Chem 288(13): 8966-8976.

Jiang, Q. and Greenberg, R. A. (2015). "Deciphering the BRCA1 Tumor Suppressor Network." J Biol Chem 290(29): 17724-17732.

Kakarougkas, A., Ismail, A., Katsuki, Y., Freire, R., Shibata, A. and Jeggo, P. A. (2013). "Co-operation of BRCA1 and POH1 relieves the barriers posed by 53BP1 and RAP80 to resection." Nucleic Acids Res 41(22): 10298-10311.

Kakarougkas A, J. P. (2014). "DNA DSB repair pathway choice: an orchestrated handover mechanism." Br J Radiol. 87(1035): 1-8.

Karanja, K. K., Cox, S. W., Duxin, J. P., Stewart, S. A. and Campbell, J. L. (2012). "DNA2 and EXO1 in replication-coupled, homology-directed repair and in the interplay between HDR and the FA/BRCA network." Cell Cycle 11(21): 3983-3996.

Keijzers, G., Maynard, S., Shamanna, R. A., Rasmussen, L. J., Croteau, D. L. and Bohr, V. A. (2014). "The role of RecQ helicases in non-homologous end-joining." Crit Rev Biochem Mol Biol 49(6): 463-472.

Kraft, G. (1990). "The radiobiological and physical basis for radiotherapy with protons and heavier ions." Strahlenther Onkol 166(1): 10-13.

Kraft, G. (2007). Tumor Therapy with Heavy Ions, Verein zur Förderung der Tumortherapie mit schweren Ionen e.V.

Kramer, M., Scifoni, E., Walzlein, C. and Durante, M. (2012). "Ion beams in radiotherapy - from tracks to treatment planning." 1st Nano-Ibct Conference 2011 - Radiation Damage of Biomolecular Systems: Nanoscale Insights into Ion Beam Cancer Therapy 373.

Kramer, M., Weyrather, W. K. and Scholz, M. (2003). "The increased biological effectiveness of heavy charged particles: from radiobiology to treatment planning." Technol Cancer Res Treat 2(5): 427-436.

Kruger, I., Rothkamm, K. and Lobrich, M. (2004). "Enhanced fidelity for rejoining radiation-induced DNA double-strand breaks in the G2 phase of Chinese hamster ovary cells." Nucleic Acids Res 32(9): 2677-2684.

Kumar R., C. C. F. (2014). "RIF1: A novel regulatory factor for DNA replication and DNA damageresponse signaling." DNA Repair 15: 54-59.

Legesse-Miller, A., Raitman, I., Haley, E. M., Liao, A., Sun, L. L., Wang, D. J., Krishnan, N., Lemons, J. M., Suh, E. J., Johnson, E. L., Lund, B. A. and Coller, H. A. (2012). "Quiescent fibroblasts are protected from proteasome inhibition-mediated toxicity." Mol Biol Cell 23(18): 3566-3581.

Lemons, J. M., Feng, X. J., Bennett, B. D., Legesse-Miller, A., Johnson, E. L., Raitman, I., Pollina, E. A., Rabitz, H. A., Rabinowitz, J. D. and Coller, H. A. (2010). "Quiescent fibroblasts exhibit high metabolic activity." PLoS Biol 8(10): e1000514.

Li, L., Poon, H. Y., Hildebrandt, M. R., Monckton, E. A., Germain, D. R., Fahlman, R. P. and Godbout, R. (2017). "Role for RIF1-interacting partner DDX1 in BLM recruitment to DNA double-strand breaks." DNA Repair (Amst) 55: 47-63.

Li, X. and Heyer, W. D. (2008). "Homologous recombination in DNA repair and DNA damage tolerance." Cell Res 18(1): 99-113.

Li, Y., Reynolds, P., O'Neill, P. and Cucinotta, F. A. (2014). "Modeling damage complexity-dependent non-homologous end-joining repair pathway." PLoS One 9(2): e85816.

Lieber, M. R. (2010). "NHEJ and its backup pathways in chromosomal translocations." Nat Struct Mol Biol 17(4): 393-395.

Lilley, D. M. and White, M. F. (2001). "The junction-resolving enzymes." Nat Rev Mol Cell Biol 2(6): 433-443.

Little, J. B. (1969). "Repair of sub-lethal and potentially lethal radiation damage in plateau phase cultures of human cells." Nature 224(5221): 804-806.

Liu, C., Kawata, T., Shigematsu, N., Cucinotta, F., George, K., Saito, M., Uno, T., Isobe, K. and Ito, H. (2010). "A comparison of chromosome repair kinetics in G(0) and G(1) reveals that enhanced repair

fidelity under noncycling conditions accounts for increased potentially lethal damage repair." Radiat Res 174(5): 566-573.

Liu, C., Kawata, T., Zhou, G., Furusawa, Y., Kota, R., Kumabe, A., Sutani, S., Fukada, J., Mishima, M., Shigematsu, N., George, K. and Cucinotta, F. (2013). "Comparison of the repair of potentially lethal damage after low- and high-LET radiation exposure, assessed from the kinetics and fidelity of chromosome rejoining in normal human fibroblasts." J Radiat Res 54(6): 989-997.

Liu, H., Adler, A. S., Segal, E. and Chang, H. Y. (2007). "A transcriptional program mediating entry into cellular quiescence." PLoS Genet 3(6): e91.

Lobrich, M. and Jeggo, P. A. (2005). "Harmonising the response to DSBs: a new string in the ATM bow." DNA Repair (Amst) 4(7): 749-759.

Lobrich, M., Shibata, A., Beucher, A., Fisher, A., Ensminger, M., Goodarzi, A. A., Barton, O. and Jeggo, P. A. (2010). "gammaH2AX foci analysis for monitoring DNA double-strand break repair: strengths, limitations and optimization." Cell Cycle 9(4): 662-669.

Lorat, Y., Timm, S., Jakob, B., Taucher-Scholz, G. and Rube, C. E. (2016). "Clustered double-strand breaks in heterochromatin perturb DNA repair after high linear energy transfer irradiation." Radiother Oncol 121(1): 154-161.

Lowry, O. H., Rosebrough, N. J., Farr, A. L. and Randall, R. J. (1951). "Protein measurement with the Folin phenol reagent." J Biol Chem 193(1): 265-275.

Maeda, J., Bell, J. J., Genet, S. C., Fujii, Y., Genet, M. D., Brents, C. A., Genik, P. C. and Kato, T. A. (2014). "Potentially lethal damage repair in drug arrested G2-phase cells after radiation exposure." Radiat Res 182(4): 448-457.

Mansour, W. Y., Rhein, T. and Dahm-Daphi, J. (2010). "The alternative end-joining pathway for repair of DNA double-strand breaks requires PARP1 but is not dependent upon microhomologies." Nucleic Acids Res 38(18): 6065-6077.

Mao, Z., Bozzella, M., Seluanov, A. and Gorbunova, V. (2008). "DNA repair by nonhomologous end joining and homologous recombination during cell cycle in human cells." Cell Cycle 7(18): 2902-2906.

Misteli, T. and Soutoglou, E. (2009). "The emerging role of nuclear architecture in DNA repair and genome maintenance." Nat Rev Mol Cell Biol 10(4): 243-254.

Mladenov, E., Magin, S., Soni, A. and Iliakis, G. (2016). "DNA double-strand-break repair in higher eukaryotes and its role in genomic instability and cancer: Cell cycle and proliferation-dependent regulation." Semin Cancer Biol 37-38: 51-64.

Moynahan, M. E., Chiu, J. W., Koller, B. H. and Jasin, M. (1999). "Brca1 controls homology-directed DNA repair." Mol Cell 4(4): 511-518.

Mudbhary, R., Hoshida, Y., Chernyavskaya, Y., Jacob, V., Villanueva, A., Fiel, M. I., Chen, X., Kojima, K., Thung, S., Bronson, R. T., Lachenmayer, A., Revill, K., Alsinet, C., Sachidanandam, R., Desai, A., SenBanerjee, S., Ukomadu, C., Llovet, J. M. and Sadler, K. C. (2014). "UHRF1 overexpression drives DNA hypomethylation and hepatocellular carcinoma." Cancer Cell 25(2): 196-209.

Munshi, A., Hobbs, M. and Meyn, R. E. (2005). "Clonogenic cell survival assay." Methods Mol Med 110: 21-28.

Nakayama, J., Rice, J. C., Strahl, B. D., Allis, C. D. and Grewal, S. I. (2001). "Role of histone H3 lysine 9 methylation in epigenetic control of heterochromatin assembly." Science 292(5514): 110-113.

Nimonkar, A. V., Genschel, J., Kinoshita, E., Polaczek, P., Campbell, J. L., Wyman, C., Modrich, P. and Kowalczykowski, S. C. (2011). "BLM-DNA2-RPA-MRN and EXO1-BLM-RPA-MRN constitute two DNA end resection machineries for human DNA break repair." Genes Dev 25(4): 350-362.

Panier, S. and Boulton, S. J. (2014). "Double-strand break repair: 53BP1 comes into focus." Nat Rev Mol Cell Biol 15(1): 7-18.

Panier, S. and Durocher, D. (2013). "Push back to respond better: regulatory inhibition of the DNA double-strand break response." Nat Rev Mol Cell Biol 14(10): 661-672.

Parameswaran B, C. H., Lu Y, Coates J, Deng CX, Baer R, Lin HK, Li R, Paull TT, Hu Y. (2014). "Damage-induced BRCA1 phosphorylation by Chk2 contributes to the timing of end resection." Cell Cycle 14(3): 437-448.

Pardee, A. B. (1974). "A restriction point for control of normal animal cell proliferation." Proc Natl Acad Sci U S A 71(4): 1286-1290.

Paul, K., Wang, M., Mladenov, E., Bencsik-Theilen, A., Bednar, T., Wu, W., Arakawa, H. and Iliakis, G. (2013). "DNA ligases I and III cooperate in alternative non-homologous end-joining in vertebrates." PLoS One 8(3): e59505.

Peddi, P., Loftin, C. W., Dickey, J. S., Hair, J. M., Burns, K. J., Aziz, K., Francisco, D. C., Panayiotidis, M. I., Sedelnikova, O. A., Bonner, W. M., Winters, T. A. and Georgakilas, A. G. (2010). "DNA-PKcs deficiency leads to persistence of oxidatively induced clustered DNA lesions in human tumor cells." Free Radic Biol Med 48(10): 1435-1443.

Quennet, V., Beucher, A., Barton, O., Takeda, S. and Lobrich, M. (2011). "CtIP and MRN promote non-homologous end-joining of etoposide-induced DNA double-strand breaks in G1." Nucleic Acids Res 39(6): 2144-2152.

Riballo, E., Kuhne, M., Rief, N., Doherty, A., Smith, G. C., Recio, M. J., Reis, C., Dahm, K., Fricke, A., Krempler, A., Parker, A. R., Jackson, S. P., Gennery, A., Jeggo, P. A. and Lobrich, M. (2004). "A pathway of double-strand break rejoining dependent upon ATM, Artemis, and proteins locating to gamma-H2AX foci." Mol Cell 16(5): 715-724.

Rief, N. and Lobrich, M. (2002). "Efficient rejoining of radiation-induced DNA double-strand breaks in centromeric DNA of human cells." J Biol Chem 277(23): 20572-20582.

Rothkamm, K., Kruger, I., Thompson, L. H. and Lobrich, M. (2003). "Pathways of DNA double-strand break repair during the mammalian cell cycle." Mol Cell Biol 23(16): 5706-5715.

Roycroft, A. and Mayor, R. (2016). "Molecular basis of contact inhibition of locomotion." Cell Mol Life Sci 73(6): 1119-1130.

San Filippo, J., Sung, P. and Klein, H. (2008). "Mechanism of eukaryotic homologous recombination." Annu Rev Biochem 77: 229-257.

Sartori, A. A., Lukas, C., Coates, J., Mistrik, M., Fu, S., Bartek, J., Baer, R., Lukas, J. and Jackson, S. P. (2007). "Human CtIP promotes DNA end resection." Nature 450(7169): 509-514.

Schultz, M. (2008). " Rudolf Virchow. Emerging Infectious Diseases." 14(9): 1480-1481.

Shao, Z., Davis, A. J., Fattah, K. R., So, S., Sun, J., Lee, K. J., Harrison, L., Yang, J. and Chen, D. J. (2012). "Persistently bound Ku at DNA ends attenuates DNA end resection and homologous recombination." DNA Repair (Amst) 11(3): 310-316.

Shibata, A., Conrad, S., Birraux, J., Geuting, V., Barton, O., Ismail, A., Kakarougkas, A., Meek, K., Taucher-Scholz, G., Lobrich, M. and Jeggo, P. A. (2011). "Factors determining DNA double-strand break repair pathway choice in G2 phase." EMBO J 30(6): 1079-1092.

Shrivastav, M., De Haro, L. P. and Nickoloff, J. A. (2008). "Regulation of DNA double-strand break repair pathway choice." Cell Res 18(1): 134-147.

Silverman J, T. H., Buonomo SB, Eisenhaber F, de Lange T. (2004). "Human Rif1, ortholog of a yeast telomeric protein, is regulated by ATM and 53BP1 and functions in the S-phase checkpoint." Genes Dev. 18(17): 2108-2119.

Singh, S. K., Bednar, T., Zhang, L., Wu, W., Mladenov, E. and Iliakis, G. (2012). "Inhibition of B-NHEJ in plateau-phase cells is not a direct consequence of suppressed growth factor signaling." Int J Radiat Oncol Biol Phys 84(2): e237-243.

Singleton, B. K., Griffin, C. S. and Thacker, J. (2002). "Clustered DNA damage leads to complex genetic changes in irradiated human cells." Cancer Res 62(21): 6263-6269.

Soni, A., Siemann, M., Grabos, M., Murmann, T., Pantelias, G. E. and Iliakis, G. (2014). "Requirement for Parp-1 and DNA ligases 1 or 3 but not of Xrcc1 in chromosomal translocation formation by backup end joining." Nucleic Acids Res 42(10): 6380-6392.

Tauber, M. and Fischle, W. (2015). "Conserved linker regions and their regulation determine multiple chromatin-binding modes of UHRF1." Nucleus 6(2): 123-132.

Tian, Y., Paramasivam, M., Ghosal, G., Chen, D., Shen, X., Huang, Y., Akhter, S., Legerski, R., Chen, J., Seidman, M. M., Qin, J. and Li, L. (2015). "UHRF1 contributes to DNA damage repair as a lesion recognition factor and nuclease scaffold." Cell Rep 10(12): 1957-1966.

Tomimatsu, N., Mukherjee, B., Catherine Hardebeck, M., Ilcheva, M., Vanessa Camacho, C., Louise Harris, J., Porteus, M., Llorente, B., Khanna, K. K. and Burma, S. (2014). "Phosphorylation of EXO1 by CDKs 1 and 2 regulates DNA end resection and repair pathway choice." Nat Commun 5: 3561.

Tomimatsu, N., Mukherjee, B., Deland, K., Kurimasa, A., Bolderson, E., Khanna, K. K. and Burma, S. (2012). "Exo1 plays a major role in DNA end resection in humans and influences double-strand break repair and damage signaling decisions." DNA Repair (Amst) 11(4): 441-448.

Turner, B. M. (2007). "Defining an epigenetic code." Nat Cell Biol 9(1): 2-6.

Wang, C., Shen, J., Yang, Z., Chen, P., Zhao, B., Hu, W., Lan, W., Tong, X., Wu, H., Li, G. and Cao, C. (2011). "Structural basis for site-specific reading of unmodified R2 of histone H3 tail by UHRF1 PHD finger." Cell Res 21(9): 1379-1382.

Wang, F., Yang, Y. Z., Shi, C. Z., Zhang, P., Moyer, M. P., Zhang, H. Z., Zou, Y. and Qin, H. L. (2012). "UHRF1 promotes cell growth and metastasis through repression of p16(ink(4)a) in colorectal cancer." Ann Surg Oncol 19(8): 2753-2762.

Wang, H., Zeng, Z. C., Perrault, A. R., Cheng, X., Qin, W. and Iliakis, G. (2001). "Genetic evidence for the involvement of DNA ligase IV in the DNA-PK-dependent pathway of non-homologous end joining in mammalian cells." Nucleic Acids Res 29(8): 1653-1660.

Wang, M., Wu, W., Wu, W., Rosidi, B., Zhang, L., Wang, H. and Iliakis, G. (2006). "PARP-1 and Ku compete for repair of DNA double strand breaks by distinct NHEJ pathways." Nucleic Acids Res 34(21): 6170-6182.

Wang, X., Lu, G., Li, L., Yi, J., Yan, K., Wang, Y., Zhu, B., Kuang, J., Lin, M., Zhang, S. and Shao, G. (2014). "HUWE1 interacts with BRCA1 and promotes its degradation in the ubiquitin-proteasome pathway." Biochem Biophys Res Commun 444(3): 290-295.

Ward, J. F. (1988). "DNA damage produced by ionizing radiation in mammalian cells: identities, mechanisms of formation, and reparability." Prog Nucleic Acid Res Mol Biol 35: 95-125.

Ward, J. F. (1994). "The complexity of DNA damage: relevance to biological consequences." Int J Radiat Biol 66(5): 427-432.

Wei, L., Lan, L., Hong, Z., Yasui, A., Ishioka, C. and Chiba, N. (2008). "Rapid recruitment of BRCA1 to DNA double-strand breaks is dependent on its association with Ku80." Mol Cell Biol 28(24): 7380-7393.

West, S. C. (2003). "Molecular views of recombination proteins and their control." Nat Rev Mol Cell Biol 4(6): 435-445.

Weyrather, W. K. and Debus, J. (2003). "Particle beams for cancer therapy." Clin Oncol (R Coll Radiol) 15(1): S23-28.

Weyrather, W. K., Ritter, S., Scholz, M. and Kraft, G. (1999). "RBE for carbon track-segment irradiation in cell lines of differing repair capacity." Int J Radiat Biol 75(11): 1357-1364.

Willmore, E., de Caux, S., Sunter, N. J., Tilby, M. J., Jackson, G. H., Austin, C. A. and Durkacz, B. W. (2004). "A novel DNA-dependent protein kinase inhibitor, NU7026, potentiates the cytotoxicity of topoisomerase II poisons used in the treatment of leukemia." Blood 103(12): 4659-4665.

Wold, M. S. (1997). "Replication protein A: a heterotrimeric, single-stranded DNA-binding protein required for eukaryotic DNA metabolism." Annu Rev Biochem 66: 61-92.

Xu, D., Muniandy, P., Leo, E., Yin, J., Thangavel, S., Shen, X., Ii, M., Agama, K., Guo, R., Fox, D., 3rd, Meetei, A. R., Wilson, L., Nguyen, H., Weng, N. P., Brill, S. J., Li, L., Vindigni, A., Pommier, Y., Seidman, M. and Wang, W. (2010). "Rif1 provides a new DNA-binding interface for the Bloom syndrome complex to maintain normal replication." EMBO J 29(18): 3140-3155.

Yajima, H., Fujisawa, H., Nakajima, N. I., Hirakawa, H., Jeggo, P. A., Okayasu, R. and Fujimori, A. (2013). "The complexity of DNA double strand breaks is a critical factor enhancing end-resection." DNA Repair (Amst) 12(11): 936-946.

Yamazaki, S., Ishii, A., Kanoh, Y., Oda, M., Nishito, Y. and Masai, H. (2012). "Rif1 regulates the replication timing domains on the human genome." EMBO J 31(18): 3667-3677.

Yao, G. (2014). "Modelling mammalian cellular quiescence." Interface Focus 4(3): 20130074.

Zetterberg, A. and Larsson, O. (1985). "Kinetic analysis of regulatory events in G1 leading to proliferation or quiescence of Swiss 3T3 cells." Proc Natl Acad Sci U S A 82(16): 5365-5369.

Zhang, H. X., Liu, H. L., Chen, Y. L., Yang, X., Wang, P. F., Liu, T. Z., Deng, M., Qin, B., Correia, C., Lee, S., Kim, J., Sparks, M., Nair, A. A., Evans, D. L., Kalari, K. R., Zhang, P. M., Wang, L. W., You, Z. S., Kaufmann, S. H., Lou, Z. K. and Pei, H. D. (2016). "A cell cycle-dependent BRCA1-UHRF1 cascade regulates DNA double-strand break repair pathway choice." Nature Communications 7.

Zimmermann, M. and de Lange, T. (2014). "53BP1: pro choice in DNA repair." Trends Cell Biol 24(2): 108-117.

Zimmermann, M., Lottersberger, F., Buonomo, S. B., Sfeir, A. and de Lange, T. (2013). "53BP1 regulates DSB repair using Rif1 to control 5' end resection." Science 339(6120): 700-704.

Zou, L. and Elledge, S. J. (2003). "Sensing DNA damage through ATRIP recognition of RPA-ssDNA complexes." Science 300(5625): 1542-1548.

7. Appendix

7.1. Publications and contributions to scientific meetings

7.1.1. Publications

T. Syzonenko, B. Jakob, G. Becker, G. Taucher-Scholz, N. B. Averbeck (2017). BRCA1 is involved in resection of complex, heavy-ion induced DNA double-strand breaks in G1-phase cells. GSI, scientific report 2016

T. Syzonenko B. Jakob, G. Becker, M. Durante, G. Taucher-Scholz, N. B. Averbeck (2016). The role of RIF1 and BRCA1 in the resection of complex DNA double strand breaks after heavy ion irradiation. GSI, Scientific Report 2015

7.1.2. Contributions to scientific meetings

Oral presentation:

Annual Meeting of the GBS; Dresden (2015)

T. Syzonenko M. Durante, G. Taucher-Scholz, N. B. Averbeck “Complex DNA-Damage Response: Regulation of Resection of Double Strand Breaks (DSBs) Induced by Heavy-Ion Irradiation in G1-phase”

Poster presentation:

Annual Meeting of the GBS/ERRS; Essen (2017)

N.Averbeck, **T.Syzonenko**, E. Abdollahi, B. Jakob, G. Taucher-Scholz. „Proliferating versus quiescent cells: cell survival and repair of low- or high-LET radiation induced DNA double-strand breaks“

7.2. Lebenslauf

7.2.1. Persönliche Daten

Name	Tatyana Syzonenko
Geburtsdatum	17.07.1979
Geburtsort	Kiew

7.2.2. Universitäre und schulische Ausbildung

Seit 4/2014	Promotion an der Technischen Universität Darmstadt, Fachbereich Biologie, durchgeführt am GSI Helmholtzzentrum für Schwerionenforschung; Abteilung Biophysik
10/2003 - 12/2008	Studium der Biologie an der Technischen Universität Darmstadt mit externer Diplomarbeit im Clemens-Schöpf-Institut für Organische Chemie und Biochemie; FB Chemie TU Darmstadt; AG Prof. N. Dencher
9/1999 – 3/2003	Studium der Biologie an der Nationalen Universität in Kiew
6/1996	Abitur; Mittlere Reife in Kiew

7.2.3. Berufliche Erfahrung

9/2010 – 3/2014	Technische Assistentin im Institut für Tumorbiologie und experimentale Therapie, Georg-Speyer-Haus; AG Gentherapie
7/2009 – 8/2010	Wiss. Mitarbeiterin im Vascular Research Center; Universitätsklinikum Frankfurt a.M.
1/2009 – 6/2009	Wiss. Mitarbeiterin im Clemens-Schöpf-Institut für Organische Chemie und Biochemie; FB Chemie TU Darmstadt
10/1998 – 7/2002	Laborant im Bogatsch Institut für Physiologie; Nationale Universität in Kiew
10/1996 – 6/1997	Mitarbeiter der Statistikabteilung im städtischen onkologischen Zentrum in Kiew

7.3. Danksagung

Frau Prof. Dr. Gisela Taucher-Scholz möchte ich für die freundliche Überlassung des hochinteressanten Themas und die Bereitstellung des Arbeitsplatzes herzlich danken. Herrn Prof. Marco Durante möchte ich herzlich bedanken für die Übernahme des zweitens Gutachtens und die Unterstützung trotz weiter Entfernung. Ich danke den beiden für hilfreiche Unterstützung und viele anregende Diskussionen. Besonders bedanken will ich mich auch für die Freiheit, die ich während des gesamten Forschungsprojektes erfahren dürfte. Mein besonderer Dank gilt auch für Frau Dr. Nicole Averbeck. Jederzeit gewährte sie mir bei der Planung, Durchführung und Auswertung der vorliegenden Arbeit außerordentlich sachkundige, erfahrene und wertvolle Unterstützung. Ihre wegweisenden und kreativen Ideen haben wesentlich zum Erstellen der Arbeit beigetragen. Frau Dr. Anja Heselich danke ich für die zahlreichen konstruktiven und aufmunternden Gespräche und auch für eine professionelle Unterstützung bei den zahlreichen Auswertungen. Frau Gudrun Becker möchte ich herzlich für die technische und logistische Unterstützung bedanken und auch für ein tolles Betriebsklima, das sie immer schafft. Herrn Dr. Burkhard Jacob bedanke ich herzlich für das holen mich ins Team und eine durchgehende Unterstützung in zahlreichen Fragen. Ein besonderer Dank geht an Herrn Florian Braun für die sehr geduldige Unterstützung bei der Auswertung und dem Fitten der Überlebenskurven. Ich danke das ganze Strahlzeit-Team Rayees Khan, Wolfgang Becher, Christoph Sauter, Dr. Michael Scholz und Dr. Thomas Friedrich für die außerordentliche Arbeit am Tag und in der Nacht und Unterstützung in allen physikalischen und technischen Fragestellungen. Ich bedanke mich bei Frau Lotta Pack für eine außerordentliche Mitarbeit und Unterstützung jeglicher Art. Ein großes Dankeschön geht an alle meine Mitdoktoranden in der DNA Gruppe, der ganzen Biophysik Abteilung und GRK Mitglieder für Unterstützung und eine tolle Stimmung während dieser Zeit. Ich möchte mich herzlich bei Frau Maria Didonna-Schnellbächer bedanken für die Unterstützung in organisatorischen Fragen. Herzlich bedanken möchte ich mich bei Werkstudentinnen der DNA Gruppe Nadja Solomon, Kathrin Hadasch und Lisa Niederreiter für ihre Wertvolle Arbeit in Versorgung des Laborbedarfs. Ich bedanke mich bei der ganzen Biophysik Abteilung für eine schöne Zeit in GSI.

Natürlich bedanke ich mich bei allen meinen lieben Freunden und meiner Familie für die Ausdauer, Ruhe und Geduld, womit sie mir stets zur Seite standen und mich immer wieder aufgemuntert haben.

7.4. Ehrenwörtliche Erklärung

Ich erkläre hiermit ehrenwörtlich, dass ich die vorliegende Arbeit entsprechend den Regeln guter wissenschaftlicher Praxis selbstständig und ohne unzulässige Hilfe Dritter angefertigt habe.
Sämtliche aus fremden Quellen direkt oder indirekt übernommenen Gedanken sowie sämtliche von Anderen direkt oder indirekt übernommenen Daten, Techniken und Materialien sind als solche kenntlich gemacht. Die Arbeit wurde bisher bei keiner anderen Hochschule zu Prüfungszwecken eingereicht.

Darmstadt, den 29.09.2017

.....
Tatyana Syzonenko